

The Physicochemical and Systems Level Implications of using CO₂ as a Working Fluid in Hydraulically Fractured Shale Gas Wells

A Dissertation

Presented to

the faculty of the School of Engineering and

Applied Science

University of Virginia

in partial fulfillment

of the requirements for the degree

Doctor of Philosophy

by

Rodney F. Wilkins III

August 2018

APPROVAL SHEET

This Dissertation
is submitted in partial fulfillment of the requirements
for the degree of
Doctor of Philosophy

Author Signature:  _____

This Dissertation has been read and approved by the
examining committee:

Advisor: Andres Clarens

Committee Member: Lisa Peterson

Committee Member: James Smith

Committee Member: Rider Foley

Committee Member: David Green

Committee Member: Mike Plampin

Accepted for the School of Engineering and Applied Science:



Craig H. Benson, School of Engineering and Applied Science

August 2018

**The Physicochemical and Systems Level
Implications of using CO₂ as a Working Fluid in
Hydraulically Fractured Shale Gas Wells**

A Dissertation

Presented to
the faculty of the School of Engineering and Applied Science
University of Virginia

In Partial Fulfillment
of the requirements for the Degree
Doctor of Philosophy (Civil and Environmental Engineering)

by
Rodney F. Wilkins III
August 2018

Abstract

The rapid growth of natural gas production from unconventional gas shale formations over the past decade has changed the US energy landscape dramatically. This growth has been enabled by directional horizontal drilling and hydraulic fracturing technologies, which allow engineers to access larger portions of a host rock and improve its permeability. The most effective hydraulic fracturing operations use millions of gallons of water at each wellhead. Even though much of this water is returned and must be treated, the majority remains trapped within the target formation. The fate of these large volumes of water and its impact on gas production are still poorly understood. This work seeks to answer critical questions concerning the fate of water in unconventional shale wells and to understand how the design of these fluids might be engineered to improve production, reduce wastewater generation, or both. The role of fluid-solid interfacial properties in these processes is studied in depth and the possible role for non-aqueous alternatives, specifically carbon dioxide is explored. Finally, the system-level environmental impacts of switching to waterless fracturing operations are quantified using a life cycle assessment framework.

To better understand the fate of water during fracturing operations, a Marcellus shale core sample from the Marcellus Shale Energy and Environment Laboratory (MSEEL) experimental well in West Virginia was characterized to understand its pore structure, mineralogy, and interfacial characteristics. Its wettability to synthetic fracturing fluid and CH_4 was measured at high temperatures and pressures. These results were then used to simulate water imbibition and gas production flow dynamics in a hydraulically fractured shale well using the TOUGH2 code. The results suggest that water imbibition increases 125% as contact angle decreases from 85 to 5 degrees, while the water produced/imbibed fraction decreases 73%. Using the measured interfacial properties, gas production rates were simulated for the MSEEL well with good agreement between

field data and simulation results. Exploring different fracture spacing scenarios in the model and comparing results with field data reveals information about fracture area otherwise not available. These findings provide new insight into the fate of water in fracturing operations and could inform improved design of hydraulic fracturing fluids.

While our experiments and modeling suggest that the properties of fracturing fluids had a small impact on natural gas production, most estimates suggest that only 15-25% of the gas originally in these well is actually produced. This inefficiency could be tied to the geomechanics of fractures or it could be tied to the presence of natural gas liquids, which are common in many regions of the Marcellus and other shale plays. To help elucidate the role that capillary forces might have in regions with higher proportions of natural gas liquids (NGL's), experiments and modeling were performed on the MSEEL core using different fluid pairs. Contact angles for slickwater in propane and a propane/methane mixture were measured confirming shale likely becomes hydrophobic as NGL concentration and pressure increase, impacting capillary forces. As a non-aqueous alternative, CO₂ is miscible with CH₄ which reduced the role of capillary forces in mass transport. CO₂ is also thought to increase fracture complexity, which could increase the fracture area and gas production rates. Model simulations with CO₂ confirmed fracture complexity increases gas production 133% in addition to an increase of 33% if NGL's are present. Results further show CO₂ fracturing has the potential to sequester up to 1×10^7 kg CO₂ per well. These data are assimilated to provide the first geospatially explicit data of CO₂ fracturing and storage potential for the Marcellus region.

To quantify the impact of hydraulic fracturing on the environment, water resources, and energy consumption, a Life Cycle Analysis (LCA) model was developed to analyze key impacts for a typical gas well in the Marcellus shale. This analysis compared the impacts of fracking for

three scenarios: (1) a base-case well fracked with water-based (slickwater) fluids, (2) a base-case well fracked with CO₂ using current data, and (3) a forward looking CO₂ outlook scenario using parameters which assume key advances in these processes. The impact on energy (MJ), greenhouse gas emissions (GHG in CO₂ equivalents), and water consumption (m³) was measured for each scenario for the functional unit of lifetime energy production (GJ natural gas). LCA results show CO₂ based fluids have the potential to reduce GHG emissions by 400% and water consumption by 80% compared with conventional water-based fluids. However, these are offset by a 44% increase in net energy consumption, pointing to the need to reduce CO₂ transport and processing energy requirements while pursuing improved processes to increase natural gas recovery.

Acknowledgements

I want to first express my appreciation for the time and patience of my committee and the commitment of my advisor to this rather unusual endeavor:

Dr. Lisa Peterson, Chair

Dr. David Green

Dr. Rider Foley

Dr. Jim Smith

Dr. Mike Plampin

Dr. Andres Clarens, Advisor

Without the able support and encouragement of the following this truly would not have been possible. You now also have a degree in patience. Words cannot express my gratitude, and how much I will miss you all. And, I will look forward with great anticipation of hearing your future successes.

Bo Liang

Dan Plattenberger

Anne Menefee

Sarah "Gussy" Gustitus

Special mention goes to David Thomas, the most extraordinary, and again patient IT expert alive on the planet. I owe you David, call me. And, Farrah Dang for artistic talents, it was a joy to meet.

For the commitment and selflessness of my wife, Melissa, during my 5 year absence (here we go again), I am indebted. Time to start on a 10 year list. Now what are you going to do with me ?

For the encouragement of my children, John, Chad & Maggie, Kate and Brandon Fulk, and Trey, I owe you time that you have not had. For the encouragement of grandchildren, Vivi Wilkins and Ainsley Fulk, I look forward to your future and hope to watch you grow.

And finally, for originally giving me the desire to learn, listening to all those questions, and subsequent years of quiet encouragement, I dedicate this work to my father

Rodney F. Wilkins Jr.

Table of Contents

Chapter 1: Introduction	1
1.1. Background	1
1.2. Problem Statement	3
1.3. Research Objective and Summary of Dissertation.....	5
1.3.1. Research Objective	5
1.3.2. Summary of Dissertation	6
Chapter 2: The impact of interfacial properties on fluid fate and transport in hydraulic fracturing of unconventional gas wells	9
2.1. Introduction	9
2.2. Materials & methods	17
2.2.1. Sample preparation	17
2.2.2. Contact angle and interfacial tension experiments	17
2.2.3. Mercury intrusion porosimetry	20
2.2.4. Residual gas and water saturations	21
2.2.5. Total organic carbon	21
2.2.6. Transport modeling	23
2.2.7. Integration of experimental and modeling work	25
2.3. Results and discussion.....	26
2.3.1. Experimental characterization of shale core	26
2.3.2. Model results	32
2.3.2.1. Baseline wettability model	32
2.3.2.2. Model sensitivity to wettability	34
2.3.2.3. Model sensitivity to residual liquid and gas saturations	38
2.3.2.4. Model sensitivity to rock chemistry	40
2.3.2.5. Model sensitivity to rock fracture spacing.....	41
2.3.2.6. Upscaling and benchmarking of modeling results.....	42
2.4. Conclusions	44
Chapter 3: Estimating the CO ₂ Fracturing and Storage Potential of Marcellus Shale Wells Based on Physicochemical Properties	46
3.1. Introduction	46
3.2. Methods.....	50
3.2.1. Experimental Measures	50

3.2.2.	Modeled Measures	51
3.2.3.	Literature Measures	54
3.3.	Results and Discussion.....	55
3.3.1.	Interfacial Properties	55
3.3.2.	TOUGH2 model fracture complexity/roughness impact on EUR	58
3.3.3.	Comparison of interfacial impacts on EUR	60
3.3.4.	Mapping CO ₂ potential for increased gas EUR and CO ₂ sequestration	61
3.3.4.1.	Gas production potential (EUR) mapping for CO ₂ fracturing.....	62
3.3.4.2.	CO ₂ sequestration mapping for CO ₂ fracturing.....	62
3.4.	Conclusions.....	63
Chapter 4: Environmental life cycle analysis of water and CO ₂ -based fracturing fluids used in unconventional gas production		66
4.1.	Introduction.....	66
4.2.	Methods.....	70
4.2.1.	System boundaries and functional unit	70
4.2.2.	Scenario development	71
4.2.3.	Production performance	71
4.2.4.	Fluid sourcing	72
4.2.5.	Blending and fracturing	74
4.2.6.	Flowback and production	74
4.2.7.	Allocation	76
4.2.8.	Life cycle modeling and impact assessment	77
4.3.	Results and discussion.....	78
4.3.1.	Life cycle burdens	78
4.3.2.	Key impact drivers	80
4.3.3.	Environmental implications	81
4.3.4.	Social factors	83
4.3.5.	Outlook for CO ₂	84
Chapter 5: Conclusions		86
5.1.	Conclusions.....	86
5.1.1.	Water fate and transport	87
5.1.2.	Use of CO ₂ as a fracturing fluid and storage potential in shale formations	88
5.1.3.	Life cycle comparison of slickwater and CO ₂ impacts on water, energy consumption, and GHG emissions	89
5.2.	Future work.....	90

5.2.1. Experimental interfacial measures for natural gas liquids (NGLs) with methane on alternate surfaces and conditions	90
5.2.2. Model post-fracturing CO ₂ injection in a Marcellus well	91
5.2.3. Experimental water imbibition in surface soils	91

List of Tables

Table 2-1: Model parameters and boundary conditions used in the TOUGH2 simulations.....	24
Table 2-2: Impact of contact angle on imbibition and produced fluids in shale at 8MPa	35
Table 2-3: Water imbibition and production data for high/low S_{lr} and S_{gr} parameters modeled	39
Table 2-4: Water imbibed in shale, coal, and quartz based on contact angles.	41
Table 3-1: TOUGH2 Model parameters and boundary conditions	53
Table 4-1: Summary of major input parameters. Stochastic inputs modeled as uniform or triangular distributions are reported as the median or likely values respectively followed by the ranges considered here.	77

List of Figures

Figure 1-1: Cross section of hydraulically fractured directional drilled horizontal shale gas well. (Al Granberg, earthtimes.org).....	2
Figure 1-2: Marcellus wellhead showing support equipment for drilling and fracturing multiple wells at a single well site.	3
Figure 1-3: Flowchart for dissertation	6
Figure 2-1: Hydraulically fractured horizontal shale gas well showing modeled grid volume and the corresponding process steps, pressures, and time scales. Induced and natural fractures are modeled as shown.	10
Figure 2-2: Contact angle and interfacial tension experimental schematic	19
Figure 2-3: Imbibition (top) and drainage (gas production) (bottom) processes for (i) coal, (ii) shale, and (iii) quartz flowpaths in shale with different contact angles noted, illustrating relative saturations for each scenario. It is important to note the effect of previous imbibition or drainage steps and residual saturations on the residual saturation of subsequent process steps.	22
Figure 2-4: Workflow for developing model inputs from experimental data. Simulations are built to test sensitivity to interfacial and matrix variables and provide a final match for model geometry with specific Marcellus well data.	26
Figure 2-5: Static contact angles for coal (72.3% TOC), shale (3.1% TOC) and quartz (0% TOC) for 0.1% polyacrylamide (PAM) drops on initially dry, DI water wet, and 0.1% PAM wet surfaces. Measurements were taken at 70°C and 20MPa and all surfaces were prepared dry to 1-10 µm surface roughness to preserve the chemical integrity of the organic surfaces.	27

Figure 2-6: Dynamic contact angles for shale/coal/quartz for 0.1% PAM drops on initially dry or initially 0.1% PAM wet surfaces measured at 70C, 20MPa. Advancing (dry) and receding (wet) angle conditions chosen to reflect imbibition/drainage conditions. 29

Figure 2-7: Marcellus shale MIP data curves: (a) Pc-Sw, (b) Pore volume-pore diameter, and (c) Pc-pore diameter 31

Figure 2-8: Baseline saturation and pressure data for Shale (8MPa backpressure, 24 MPa reservoir pressure) for (a) forced imbibition (fracturing or injection), (b) natural imbibition (shut-in), and (c) production (gas and water). 33

Figure 2-9: Sensitivity of water produced/imbibed fraction to static contact angle. For reference, the initial 0.1% PAM wet and dry conditions on baseline shale are shown. 35

Figure 2-10: Saturation and pressure for standard, low, and high contact angle on shale (8MPa). The standard contact angle scenario (advancing $\Theta = 83.1^\circ$, receding $\Theta = 13.3^\circ$) is included for comparison..... 36

Figure 2-11: Pc-Sw curves showing the theoretical response of shale for (1) initial saturation, (2) forced imbibition (non-equilibrium), (3) natural imbibition (near equilibrium), (4a) production (drainage) and (4b) counter-current imbibition. 39

Figure 2-12: Sensitivity of H2O produced/imbibed fraction to well backpressure from 4-16 MPa at fracture face for 1 m (natural and induced fractures) and 10m (induced fractures only) grid simulations. These correspond to 2 m and 20 m fracture spacing respectively..... 42

Figure 3-1: Map showing the transition from wet to dry gas in the Marcellus (MCOB PSU)..... 47

Figure 3-2: Hydraulically fractured horizontal shale gas well modeled for additional fracture complexity, both resulting from fracturing fluid interfacial properties. 48

Figure 3-3: Marcellus shale gas well isopressure map (AAPG Marcellus Wiki)..... 54

Figure 3-4: Marcellus shale formation thickness isopach map (EIA) 55

Figure 3-5: Static contact angle for 0.1% PAM in methane, propane, and a 95/5 mixture of methane/propane on Marcellus shale at 70C and pressures representing reservoir and well conditions. This shows contact angle on shale increasing with NGL concentration..... 57

Figure 3-6: Static contact angle for 0.1% PAM in methane, propane and a 95/5 mixture on Marcellus shale and coal (72% TOC) as a surrogate for organic carbon pathways in shale. While contact angle is higher in coal as expected, the NGL Cx number appears to have less impact than on shale..... 58

Figure 3-7: Impact of increased contact angle on shale for PAM (H₂O) in propane (C₃H₈) below compared with the contact angle in methane (CH₄) above. Above 90 degrees propane becomes the wetting phase and capillary forces reverse, reducing the imbibition of PAM..... 58

Figure 3-8: Fracture complexity and fracturing fluid impacts on EUR showing an increase in gas production with increasing fracture complexity. 60

Figure 3-9: Flowchart for mapping natural gas production increase and CO₂ sequestration potential from CO₂ fracturing. 61

Figure 3-10: Forced imbibition water (left) and CO₂ saturation (right) plots in shale showing increased penetration depth and saturation of CO₂. This depth is an important consideration if CO₂ preferentially sorbs to displace CH₄..... 63

Figure 3-11: CO₂ required to fracture the base fracture (10m) and complex fracture (1m) scenarios in Marcellus shale at 70 °C, 45MPa, and produced and sequestered CO₂ quantities for both scenarios. This indicates roughly half the CO₂ required to frack shale is sequestered..... 63

Figure 4-1: Process flow diagram and system boundaries encompassing the life cycles of water and CO₂-based fracturing fluids. Processes and flows in blue indicate a water frac and green indicates a CO₂ frac scenario. 73

Figure 4-2: Concentration profile of CO₂ and CH₄ returned during flowback, separation, and production following well completions with liquid CO₂. 76

Figure 4-3: Life cycle energy use, greenhouse gas emissions, and consumptive water use associated with the production of a functional unit of energy (1 GJ) from a Marcellus shale gas well under three fracturing fluid scenarios. 79

Figure 4-4: Tornado plots revealing the sensitivity of each impact to stochastic model inputs for three fracturing fluid scenarios. Centerlines represent the base case, while light and dark bars consider variations of ±10% of input distributions. 81

List of Abbreviations

CA – Contact angle

EUR – Estimated ultimate recovery

MIP – Mercury intrusion porosimetry

NGL – Natural gas liquids PIF – Performance improvement factor

S_{lr} – Saturation, liquid residual

S_{gr} – Saturation, gas residual

S_{wr} – Saturation, water residual

S_{wi} – Saturation, water initial

S_{ls} – Saturation, liquid saturation

TOC – Total organic carbon

Θ - Contact angle

\emptyset – Porosity

γ – Interfacial Tension

K – Permeability

K_r – Relative Permeability

P_c – Capillary Pressure

σ_{sg} – Solid-gas interfacial tension

σ_{sl} – Solid-liquid interfacial tension

σ_{lg} – Liquid-gas interfacial tension

Chapter 1: **Introduction**

1.1. Background

The rapid growth of unconventional shale gas resources is attributed to recent developments in hydraulic fracturing using water-based “slickwater” fluids and directional horizontal drilling (Figure 1-1). Natural gas has become the second-largest energy source in the U.S. (behind petroleum liquids), with 50% now sourced from low-permeability shale. The Marcellus shale centered on West Virginia/Pennsylvania/New York is the largest of these fields, providing the majority of domestic shale gas. The extraction company, Range Resources combined slickwater (or simply “water”) with horizontal drilling in 2005 in the Marcellus, in the first commercially successful shale gas development. Slickwater, primarily composed of water and 0.01-1.0% polyacrylamide (PAM), allows the high pump flowrates necessary to build adequate pressure and fracture shale. Horizontal drilling allows well tubulars to precisely access the gas-storing horizontal shale strata, and further extend up to 2 km into these narrow formations (10-300 m thick). This horizontal tubular is perforated by explosive charge at designated intervals, typically 10-30m, allowing both water to penetrate and fracture shale and gas to flow back to the wellhead. Hydraulic fracturing (fracking) provides higher permeability pathways to release trapped gas, and horizontal drilling provides strategic access for multiple fractures over the length of this horizontal.

Fracking is a complex process, and for purposes of this work is described as three basic steps: (1) forced imbibition, or the high pressure injection of water into shale via well tubulars to generate primary vertical fractures, (2) natural imbibition, also known as “shut-in”, when high pressure pumping ceases and the injected and well fluids seek equilibrium to optimize production, and (3) production, as the wellhead is opened to the pipeline, reversing flow to produce gas. The time required for each step is important when evaluating the fluid transport and fate processes; forced imbibition typically requires 2-4 hours, natural imbibition is normally 5-15 days up to

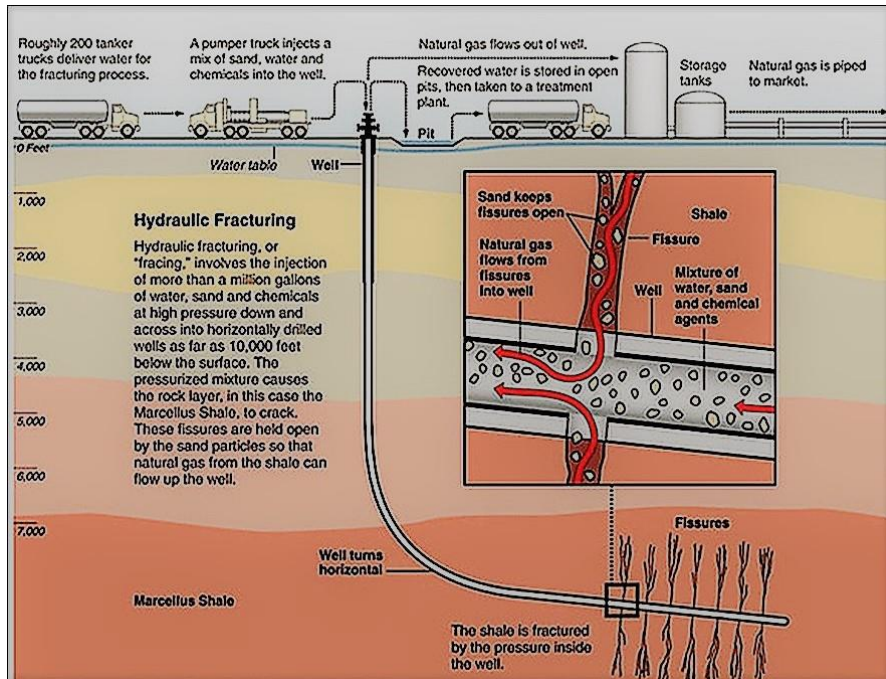


Figure 1-1: Cross section of hydraulically fractured directional drilled horizontal shale gas well. (Al Granberg, earthtimes.org)

months, and the production lifetime is assumed to be 30 years. Hydraulic fracturing typically requires in excess of 5 million gallons of water which must be sourced and transported by tanker or constructed pipelines from wells and/or surface sources. Water must be stored at the wellhead in lined reservoirs or tanks, and provision for water flowing back from the well to be treated for discharge or stored for fracking adjacent wells. The well site must initially support drilling equipment, followed by trucks and equipment to provide pumps, additives, proppant (sand), and fluid separation systems (Figure 1-2). At the beginning of production the flowback fluid is predominantly water, transitioning to mostly gas over a period of days. This water must be separated, stored, and discharged or re-injected in an additional well. Decreasing volumes of water continue to be produced over the well lifetime, with ongoing fluid handling processes on a smaller scale.



Figure 1-2: Marcellus wellhead showing support equipment for drilling and fracturing multiple wells at a single well site.

1.2. Problem Statement

In spite of the apparent success of fractured shale gas development, the fate of large volumes of water lost in the process and the inability to recover a large fraction of original gas in place (OGIP) are important and potentially related questions remaining to be answered. Less than half of the water injected in fracturing Marcellus shale flows back to the surface, typically 7-15%, with the balance lost or trapped in the reservoir (King, 2012a; Singh, 2016). Consumption of millions of gallons of fresh water raises local resource concerns, requires disruptive pipeline construction or trucking of water, and ultimately disposal of flow-back water. While flowback water is increasingly recycled to fracture adjacent wells, treatment of water containing additives (biocides, acids, and surfactants) and high salt content requires special facilities and discharge is an environmental concern for local residents (Hayes, 2009; Rowan et al., 2011). Leak-off into

drinking water aquifers and seismic risks associated with wastewater injection wells are additional concerns addressed in previous work (Flewelling and Sharma, 2014; Mauter and Palmer, 2014; Myers, 2012; Walsh and Zoback, 2015).

Estimated ultimate gas recovery rates (EUR), or the fraction of OGIP produced over the well lifetime are typically 15-25% in gas shales (Ribeiro and Sharma, 2013a). The majority of gas remains trapped in the shale, either poorly accessed by induced (hydraulic) and natural fractures or by capillary forces between water, gas, and shale (Cheng, 2012; O'Malley et al., 2016). Capillary trapping is the result of competitive interfacial forces leading to high negative pressure in the wetting phase which resists flow from small pores. This capillary pressure is defined by Young-Laplace in terms of pore size and interfacial fluid-solid properties:

$$P_c = \frac{2\sigma\cos\theta}{r}$$

Where P_c is capillary pressure, σ is interfacial tension, θ is contact angle, r is pore radius.

From this it is evident that nanoscale pores dominant in gas shales lead to high capillary pressures (P_c). This negative pressure imbibe water to successively smaller pores, and presents a large pressure differential which resists advective (multiphase Darcy) flow of gas or water. In sum, water is assumed to imbibe in the rock matrix at capillary pressures sufficient to permanently isolate and trap regions of gas in shale. The lack of interfacial data for methane, slickwater and shale and a poor understanding of the impacts of interfacial properties on water and gas trapping in shale are significant challenges which remain to be answered. Alternatives to water-based fracking fluids include dense phase super critical CO₂ (scCO₂, or simply CO₂ hereafter), which is miscible with methane (the primary component in natural gas) and thus lacking P_c . Few fracking jobs have been completed with CO₂ due to cost, supply logistics, separation equipment, and the lack of data supporting the impact on gas production (Pei et al., 2015). Nevertheless, CO₂ provides

promising benefits by eliminating water source/discharge concerns, and the potential to permanently sequester CO₂ in shale.

1.3. Research Objective and Summary of Dissertation

1.3.1. Research Objective

The objectives of this work are to (1) quantitatively compare the effect of hydraulic fracturing fluid on energy and environmental impacts, (2) determine key missing interfacial parameters for hydraulic fracturing fluids at reservoir conditions, and (3) develop the fundamental understanding of the impact of these interfacial properties on the fate and transport of water, and the production of natural gas, in a hydraulically fractured shale gas well. The ultimate goal is to develop models to predict gas and fracture fluid production in a typical Marcellus shale gas well from the interfacial properties of alternative fracturing fluids, including CO₂.

Producing gas from low-permeability shale was commercially inconceivable until the last decade. While impressive advances have been made in that time, the high cost of developing trial wells and the extended production lifespan hinder consideration of unproven methods. Further complex hydraulic fracturing processes are difficult to analyze due to extreme spatial and temporal scales involved, and industry efforts are focused on economic recovery. Paradoxically, the sudden abundance of shale gas is a major factor in current low energy prices which restrains capital for further development. As a result, in spite of common assumptions, important questions remain unanswered: What is the system level impact of hydraulic fracturing on environmental measures and the net efficiency of energy production? How might slickwater-shale interfacial properties be altered to optimize water consumption, in addition to other properties such as proppant transport, and upfront costs? Can interfacial frac fluid properties be modified to increase gas recovery,

particularly considering miscible fluids such as CO₂ and the properties of other natural gas liquids (NGL's) in addition to methane? And finally, what data is lacking to facilitate these analyses, particularly fluid-solid parameters at real reservoir conditions?

1.3.2. Summary of Dissertation

This dissertation is composed of five chapters to address the objectives and research questions above, as shown in the flowchart (Figure 1-3).

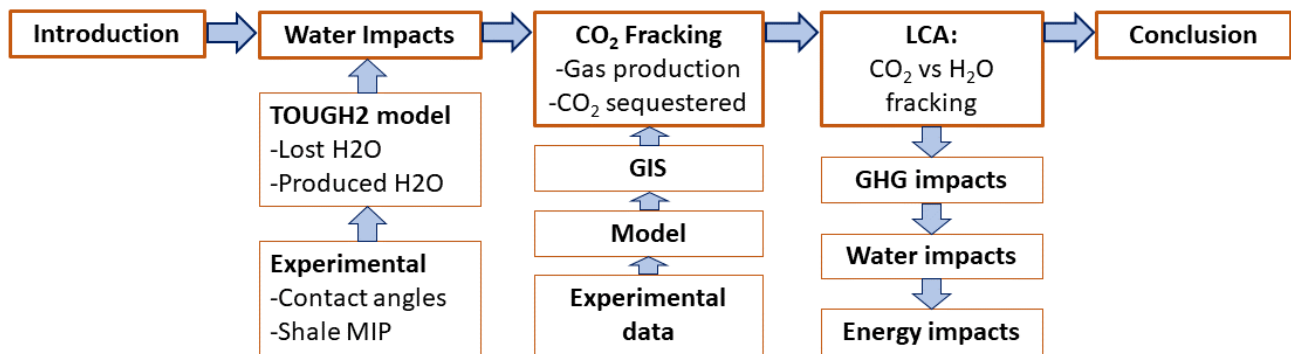


Figure 1-3: Flowchart for dissertation

Chapter 1 provides the technical background for this dissertation, a summary of the broad research questions in this field, and defines the scope and primary objective of this work.

Chapter 2 seeks to first provide interfacial inputs for a water/gas/shale system which are currently unavailable. Experimental advancing and receding contact angle and interfacial tension will be determined at Marcellus shale representative pressure and temperature. Further measures will supply primary shale capillary pressure-liquid saturation (Pc-Sw) data using mercury intrusion porosimetry (MIP), and shale total organic carbon (TOC) using carbon analysis. To develop a better understanding of how these interfacial properties impact water and gas flow in shale, we built a 1D model simulating these flows for a typical Marcellus shale gas well using a proven and

readily available numerical simulation platform (TOUGH2 EOS7C) (Lawrence Berkeley National Laboratory). To extend the predictive capabilities of this model we will scale the model inputs to allow interfacial properties, system pressure, and fracture geometry as simulation variables. The results from these simulations will be analyzed to provide a better understanding of the fate of fracking fluids in shale, assess the sensitivity of the model as a predictive tool, and provide well-scale results for comparison with Marcellus field data.

Chapter 3 investigates the potential for using CO₂ as a fracking fluid, building on the previous simulation for comparison with current slickwater processes. Our model builds on recent research for CO₂ fracture complexity combined with our TOUGH2 EOS7C model. Further experimental interfacial data is provided to explore the impact of propane at reservoir conditions, a surrogate for potential liquid-phase components in natural gas. This work provides gas production data for CO₂ fracturing.

Chapter 4 investigates the life cycle burdens for water, greenhouse gas (GHG) emissions, and energy production in the Marcellus shale to better understand the impact of frack fluid alternatives. Using a life cycle analysis model, three frack fluid scenarios are developed based on MJ energy as a functional unit including: (1) a base-case analysis corresponding to a state-of-the-art slickwater fracking process, (2) a conservative CO₂ fracking alternative derived from best available field data, and (3) a forward-looking CO₂ scenario applying hypothetical inputs based primarily on potential gas production. This chapter is based on our article published in ES&T on November 4, 2016.

Chapter 5 connects the experimental and modeling results with the LCA scenarios and summarizes those findings. In particular, the opportunity for interfacial solutions to address water issues revealed in the LCA, and data for CO₂ fracturing to evaluate the hypothetical LCA scenarios.

Additional research is proposed which builds on the understanding gained from the research described, aiming to reduce the environmental impacts of hydraulic fracturing and increase the efficiency of natural gas production.

Chapter 2: **The impact of interfacial properties on fluid fate and transport in hydraulic fracturing of unconventional gas wells**

2.1. Introduction

Technological breakthroughs in hydraulic fracturing and horizontal drilling techniques have contributed to the rapid growth in production of oil and gas from unconventional formations (King, 2012a). Completing a shale gas well proceeds via several steps. First a well is drilled and perforations are placed in the wellbore at predetermined intervals. Second fracturing fluids are pumped at high pressure into the shale through these perforations in the wellbore. The well is then “shut in” in the third step to allow injected proppant (typically sand) to settle into fracture openings. Finally, the well is opened and flow is reversed to remove process water and begin gas production. Most wells are large enough that this process is repeated several times (in stages) where certain sections are isolated from the rest of the well to ensure uniform fracturing throughout the formation. Figure 2-1 provides a schematic representation of (a) forced imbibition (b) natural imbibition and (c) production and the ways in which it impacts fluid flow.

After a well is completed, most of the water that was injected (typically between 70-80%) remains trapped in the source rock (King, 2012b; Singh, 2016). Recent work suggests that these fracturing fluids are trapped via capillary forces within the fracture network and bulk rock (Figure 2-1) (Cheng, 2012; Ghanbari and Dehghanpour, 2016; O'Malley et al., 2016). This trapping is thought to contribute to the low estimated recovery rates (EUR) of most nonconventional formations which are estimated to be on the order of 15-25%. (Ribeiro and Sharma, 2013b). Despite these pressing issues, frac fluid process development has largely focused on cost due to the volumes required and optimizing proppant delivery to impact the fracture network structure and improve the effective permeability of the formation (Gaurav et al., 2012).

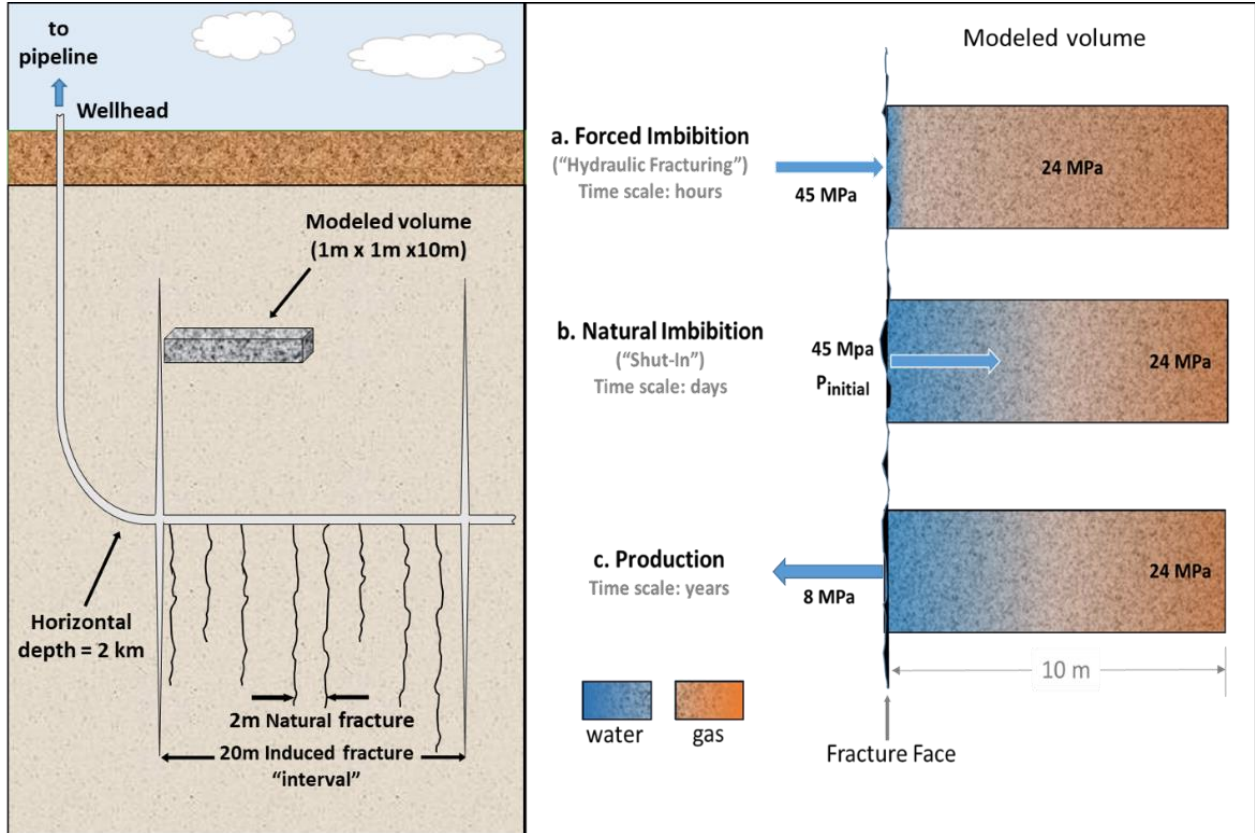


Figure 2-1: Hydraulically fractured horizontal shale gas well showing modeled grid volume and the corresponding process steps, pressures, and time scales. Induced and natural fractures are modeled as shown.

The permeability of a fractured shale depends largely on the network of induced and natural fractures in the rock. Natural fractures are typically aligned vertically and spaced every 0.4 – 2m in the Marcellus Shale (Engelder, 2012a), and Marder et al. conclude up to 60 fractures may be generated at each frac perforation (Marder et al., 2015). Natural fractures aligned horizontally are thought to be less common and are frequently sealed by lithostatic forces (Gale and Holder, 2010; Gale et al., 2014; Kanfar et al., 2013; Marder et al., 2015; Patzek et al., 2013). Within the network of natural and induced fractures, microfractures may develop on the surface of the rock. These microfractures, which are on the order of several mm in length and several microns in width,

typically develop because of the shrink and swell stresses in shale after exposure to frac fluids (Apaydin et al., 2012; Chakraborty et al., 2017; Dehghanpour et al., 2013; Gale et al., 2014; Kumar et al., 2016).

This fracture network has a nominal volume that is not insignificant and it has been suggested that this is the ultimate source for much of the water injected during well completion. But recent work suggests that the fracture network itself holds only a small fraction of the total water volume that remains trapped after injection (O'Malley et al., 2016). O'Malley and colleagues used a computational Discrete Fracture Network (DFN) fracture geometry model for large fractures and a statistical model for small fractures, to estimate that the vast majority (<90%) of the water penetrates a few mm into the bulk rock where it remains trapped. In fact, any water remaining in fractures will continue to imbibe into shale at the fracture face, further depleting water in fractures over time. Sharma et al. (2013) suggest this makes it unlikely fractures retain water during gas production, except in specific scenarios where fracture bottoms may actually fill with water because of gravity.

Different processes will govern fluid flow as it moves from the wellbore (characteristic length of centimeters) into the fracture networks (millimeters), into microfractures (micrometers), and finally into the bulk rock (where average pores are tens of nanometers in diameter). Continuum flow in the fractures and larger pores can be modeled as Darcy flow with a relative permeability (K_r) term added to address the permeability reduction typical of multiphase flows, which are driven by a systems-level pressure differential. Capillary forces dominate imbibition in smaller pore spaces according to the Young-Laplace relationship:

$$P_c = \frac{2\sigma\cos\theta}{r}$$

Where P_c is the capillary pressure, σ is the interfacial tension, Θ is the contact angle, and r is the radius. Contact angle and interfacial tension are determined by the forces between fluid-solid and fluid-fluid interfaces respectively. The wetting phase (typically water in shale) is imbibed or drawn into smaller pores by increasing capillary pressure or retained in those pores by P_c and prevented from draining. This results in a static equilibrium over time, requiring system pressure sufficient to overcome P_c to initiate flow into these smaller pores. The size and distribution of pore sizes in shale is typically reported using capillary pressure-water saturation (P_c - S_w) curves. Gas and water saturations are important and must be known for the fluid-solid system to define boundaries for the P_c - S_w curve. Diffusion must also be included in flow analysis, and “slip flow” from the Klinkenberg effect is significant for the smallest pores ($\sim 10^{-9}$ m) (Li and Sultan, 2017). Gas may also desorb from shale surfaces as pressure drops in the reservoir, contributing as much as 22% to production (Yu and Sepehrnoori, 2014; Yu et al., 2016).

Measuring capillary imbibition of fracturing fluids into the microfractures and nanopores of the shale has relied on experimental results and analytical relationships. Engelder et al. reported that water imbibed 4.9 cm in Marcellus shale core after 2.9 hours at atmospheric pressures and temperature (Engelder et al., 2014). Al-Bazali et al. (2009) suggests that osmosis (Al-Bazali et al., 2009; Roshan et al., 2016), differential process pressures, and interfacial properties is necessary when investigating fluid-shale interactions. Pagels et al. similarly found water imbibing 3 cm in 3 days in a nanodarcy shale sample (Pagels et al., 2012). Analytical attempts to explain capillary imbibition include early work by Lucas (1918), Washburn (1921), and Handy (1960), which provide solutions for imbibition distance in porous media as a function of the square root of time (\sqrt{t}). Makhanov et al. (2014) point out the difficulty of defining a system constant required for different porous media and missing factors such as process pressure differentials. Hybrid

approaches combine an early-time \sqrt{t} function with late-time scaling functions to estimate imbibition over time (March et al., 2016). While these methods provide interesting information on capillary imbibition, they cannot capture the impact of complex fracturing processes nor water-shale interfacial properties at reservoir conditions.

The chemical and physical structure of shale is highly heterogeneous, which impacts the ways fluids move through it. Most gas shales typically contain organic carbon-rich zones called kerogen, which are hydrophobic, and inorganic mineral phases, which are largely hydrophilic. Importantly, much of the rock permeability exists in the organic-rich hydrophobic zone. Several groups have attempted to establish cause-and-effect relationships between shale composition and fluid flow, Dehghanpour et al. (2012) found imbibition decreases with increasing quartz content. Water imbibition was found to decrease with increasing TOC in low pressure experiments by Zhou et al. (2014; 2016). Interfacial data for the specific minerals in shale pores is needed to resolve the conflicting results from these studies, and to further investigate the impact of flow path mineralogy in shale on imbibition of water (Gao and Hu, 2016).

Fracturing fluid chemistry will impact its capillary flow in shale formations. Using Marcellus shale samples, Roychaudhuri et al. (2013) showed that fluorocarbon surfactants increase the contact angle on samples and subsequently reducing imbibition. Makhanov et al. (2014; 2012) suggest anionic surfactants reduce imbibition by reducing surface tension. Mirchi et al. (2015) also focus on contact angles with surfactant solutions in oil/shale systems at reservoir conditions. The results indicate that surfactant types and concentrations may be used to modify contact angle, but sample preparation with liquid may have caused pre-wetting. Although focused on gas production in sandstone, Naik et al. (2015) also proposes to optimize wettability by surfactants, reducing water blocking which leads to an increase in gas relative permeability. Yethiraj et al. (2013) question

whether gas-shale interactions can be modified by manipulating interfacial properties. Despite a need to model interactions between supercritical fluids and nanoscale shale surfaces under in situ conditions, most work to date has relied on empirical relationships based on hypothetical materials and fluids, lacking characterized shale samples and interfacial data for fracturing fluids (Cole et al., 2013).

Birdsell et al. (2015b) propose an imbibition rate parameter derived from limited (Byrnes, 2011) shale capillary pressure-water saturation (Pc-Sw) data, based on the McWhorter and Sunada analytical solution for two phase flows (McWhorter and Sunada, 1990). While relative permeability hysteresis is claimed, this approach relies on scanning curves using only drainage Pc-Sw data, while noting the lack of sufficient relative permeability data to evaluate that assumption. Their imbibition results for the Marcellus estimate 15%-34% of the frac fluid is imbibed through a 5-day shut-in period. They further note the lack of shale capillary data needed to predict capillary pressure for multiphase flow modeling. Pagels et al. (2012) propose an analytical “fluid retention ratio” to predict the drainage of a wetting fluid from shale (Pagels et al., 2012). Capillary entry pressures, or the pressure required to overcome capillary pressure in a given system, are compared to show how surfactants may reduce the amount of fluid retained (drainage) in a fractured well. The authors perform centrifuge experiments to derive contact angles experimentally, noting the difficulty of directly measuring advancing or receding contact angles in shales and the need to measure interfacial parameters specific to mineralogy. Edwards et al. (2017a) developed a Darcy flow model in Matlab that demonstrates how most of the imbibed water fraction is contained in the shale matrix, not fractures. While providing interesting results, experimental and analytical approaches are best suited to investigate specific conditions and variables. Multistep fracturing

processes and changing conditions within a nanoscale pore structure pose significant challenges for isolated attempts to simulate flows in gas shale (Edwards et al., 2017b),(Hyman et al., 2016).

Numerical simulations are ultimately required to overcome the limited ability of experimental work and analytical models to model the complex flow physics and heterogeneous matrix of shale. These simulators must be capable of iteratively solving equations of state and governing flow equations for the fluids and shale matrix chosen. Commercial simulations, such as one used by Yu et al. (2016) in a thorough analysis of gas transport, focus on optimizing gas recovery and often lack transparency with respect to the underlying physics required for research. Calderon et al. (2015) provide an excellent overview of reservoir modeling and simulation methods from the literature, noting each comes with tradeoffs. As recent editorials have addressed, a lack of code verification or availability reduces the utility of these methods in further research (Nature Editors, 2018). Four numerical codes for H₂O/CO₂/CH₄ flow modeling in deep gas wells were compared and validated (CHEMTOUGH by Industrial Research Ltd, GEM by Computer Modeling Group, SIMUSCOPP by Institut Francais du Petrole, and TOUGH2/EOS7C by Lawrence Berkeley National Lab) (Oldenburg et al., 2003). Tested under different pressures and gas/aqueous phase conditions, TOUGH2/EOS7C was the preferred match in all but high pressure aqueous solutions where gas fractions were overestimated. Birdsell et al. (2015a) used one of these codes, Finite Element Heat and Mass (FEHM), to model vertical migration of tracers in shale, and noted that imbibition will affect flowback and produced fluid volumes although actual volumes were not determined. There is a need for research models such as this using validated simulation codes with characterized shale properties and in situ fluid parameters to investigate gas and water flows in the Marcellus. Once more, this lack of data currently limits the design of

alternative frac fluid processes that may significantly improve gas recovery and reduce environmental impacts linked to fracturing fluids (Middleton et al., 2017).

Building off the recent experimental and modeling studies outlined above, this work seeks to address several critical questions: How do interfacial properties impact imbibition volume and penetration of fracturing fluid in shale? How do formation conditions and fracturing fluid delivery characteristics impact fracturing fluid fate? How might we better design fracturing fluids to increase gas production and loss of fluid to the environment? To answer these questions, we developed a model using TOUGH2/EOS7C, a validated and readily available numerical simulator to investigate the impact of interfacial properties on fluid flow in low permeability shale (Keating et al., 2013; Nature Editors, 2018; Oldenburg et al., 2002; Pruess, 1991; Pruess et al., 2004; Pruess, 2004). Experimental interfacial and contact angle measures using slickwater, and characterization of a Marcellus shale core sample using Mercury Intrusion Porosimetry (MIP) and TOC analysis will provide model inputs not currently available. This data is used to determine system-specific capillary pressure, relative permeability, and fluid saturations for flow simulations in shale and specific flowpaths within shale (organic carbon and mineral). Three primary process steps are modeled sequentially to reveal the impact of each step on water imbibition and trapping. In summary, these results provide important water-shale properties, illustrate the application of an accessible, proven simulation code appropriate for modeling multiphase flow in low permeability shale, and show water penetration, trapping, and production from a Marcellus shale gas well as a function of interfacial properties. This work gives new insights for predicting water flows in shale, and designing fluid systems to minimize environmental impacts by strategically trapping or releasing hydraulic fracturing fluids from wells.

2.2. Materials & methods

2.2.1. Sample preparation

Samples of shale core, coal and quartz were prepared for measuring static and dynamic contact angles on the mineral surface. A Marcellus Shale core sample (2283m depth) from the Marcellus Shale Energy and Environmental Laboratory (MSEEL) well in Monongalia County, WV was provided by National Energy Technology Laboratory (NETL) (Morgantown WV). Quartz crystals were obtained from Ward's Natural Science, and coal with 72% measured total organic carbon (TOC) from a local supplier. All samples were cleaved and flat faces selected for final dry lapping using 180/320/600 grit silicon carbide abrasive paper. Initial samples were inspected using a Zygo Newview 7300 non-contact profilometer, and a consistent lapping procedure yielded a 1-10 micron surface finish. Exposure to any fluids prior to contact angle measures will alter results and this difference will vary with surface chemistry. Thus, the use of fluids in sample preparation must be avoided unless strategically reflecting the process conditions desired.

2.2.2. Contact angle and interfacial tension experiments

A high pressure view cell was used to perform three-phase (methane-fracturing fluid-mineral) contact angle measurements (Jessop and Leitner, 2008) A schematic of the experimental setup is shown in Figure 2-2 Pressure in the view cell could be controlled up to 20 MPa and temperature could be adjusted up to 70°C. Heating tape and a shielded Omega K-thermocouple were used to control temperature in the vessel. Temperature was continuously recorded and controlled using National Instruments CompactDAQ modules and Labview software. Solid samples were loaded into the view cell using a Teflon stage to secure the sample at a fixed elevation. All tubing and fixtures in the system were 0.030 ID stainless steel (HIP). Fracturing

fluid was injected from above the sample surface for static or dynamic contact angle experiments. Fluid droplet images were captured through sapphire windows in the cell using an AVT Guppy NIR CCD camera with 6x zoom 18-108mm lens.

Methane was used as the continuous phase as provided (99.995% certified purity bottle gas) and injected at controlled pressure to the view cell using a Teledyne ISCO 500HP syringe pump suited for flammable gases. Because this experiment used flammable gases at high pressures, it required protective shields and ventilation. To simulate fracturing fluid chemistry, 5-6M molecular weight PAM (#92560 Sigma Aldrich) was blended with DI water in proportions of 0.01/0.1/1.0% by weight. Sample viscosity was measured using a Brookfield DVE viscometer for these samples (1.57, 4.23, and 360 cP respectively) the 0.1% PAM solution was selected to match reported slickwater viscosity (2-5 cP). Other common additives such as biocides are used in low concentrations and are not expected to impact results. Surfactants are not only operator-specific, and are purposefully excluded from our experimental fluid to provide a clear baseline condition. Fluids were injected into the pressure chamber using a High Pressure Equipment model #62-6-10 manual syringe pump, after initially pressurizing and purging the system three times with methane. Following a final fill with CH₄, the system was allowed to reach experimental temperature and pressure, and equilibrate for one hour.

Interfacial tension of CH₄-PAM/H₂O was measured by first capturing pendant drop images then using ImageJ image processing software using Bashforth-Adams fits for the Young-Laplace equation (Stalder et al., 2010) for axisymmetric drop shape analysis. Interfacial tension for 0.1% PAM in methane at 70C/20MPa is measured as 59.0 +/- 6.3mN/m, similar to water (60.3 +/- 4.3 mN/m) measured under the same conditions. Both static and dynamic contact angles for the three-phase system were similarly measured on captured sessile drop images using ImageJ image

processing software with the Dropsnake (Stalder et al., 2006) plugin for axisymmetric drop shape analysis. The manual syringe pump provided a means of initially advancing the drop interface, then withdrawing fluid and receding the interface via the injection tube in the drop. Contact angle was measured simultaneously on both sides of drops and averaged to minimize the effect of gravity. Advancing/receding contact angles were measured at different intervals to provide data for a specific drop width normalized to the maximum width. Receding angle data is challenging to measure due to extremely low angles for all samples. When these data were plotted, an inflection point in the angle/drop width curve was observed. We used dynamic contact angle to fit the imbibition and drainage process conditions modeled by capillary pressure-saturation curves for shale. In some experiments the sample surface was pre-wetted with fracturing fluid to simulate the conditions that would exist during the drainage stage of well completion. Together these provide true Pc-Sw parameters defining the primary hysteretic conditions in the imbibition-drainage

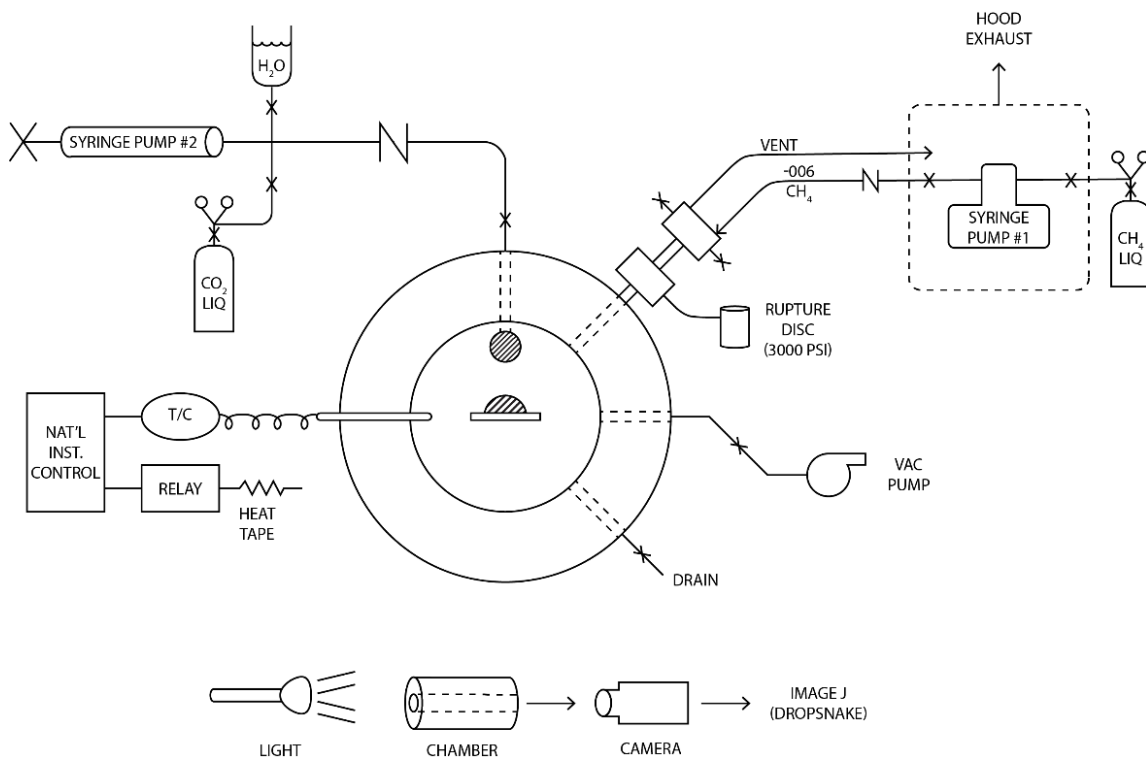


Figure 2-2: Contact angle and interfacial tension experimental schematic

process. Contact angle hysteresis is also a function of surface physical and chemical heterogeneity, adding uncertainty to contact angle measures.

2.2.3. Mercury intrusion porosimetry

Mercury Intrusion Porosimetry (MIP) measurements were carried out (Autopore IV 9500 mercury porosimeter, Poro Technology (Kingwood TX)) to obtain the characteristic capillary pressure-saturation (P_c - S_w) data for our samples. Non-wetting mercury is forced into the shale sample by an incremental increase in pressure and then the process is reversed. By measuring the flow during this process (termed intrusion and extrusion based on the corresponding flow of the wetting vapor phase) P_c - S_w data is derived for a porous sample. These data can then be interpreted using the Young-Laplace equation to obtain data about the pore size distribution of the sample. Note that MIP data below 20-30 MPa is commonly assumed to result from surface conformance and blank (compressibility) effects and therefore low pressure data for larger pores is excluded (Hudson et al., 2012). Using SEM we observed pores larger than 1 μm in cleaved Marcellus samples, but assume these are likely inaccessible from work by Clarkson et al. (2012; 2016) using SANS, nitrogen and CO_2 sorption, and MIP. MIP results for our samples are provided in the Supporting Information document.

Our work investigates the effect of interfacial forces for different fluid/solid conditions. Using MIP data requires scaling the P_c - S_w data for fluids other than mercury using the Leverett J-function (Leverett, 1941):

$$J(S_w) = \frac{P_c}{\gamma \cos \theta} \left[\frac{K}{\phi} \right]^{0.5}$$

Where γ is interfacial tension, θ is contact angle, K is permeability, and ϕ is porosity.

The J-function is a characteristic function for a given porous sample, from which we scale P_c from measures of interfacial tension and contact angle for our methane-fluid-shale system. This relationship allows us to further explore sensitivity for new slickwater formulations with hypothetical interfacial inputs, and assumed flowpaths in shale that are either mineral (i.e., quartz), organic (i.e., kerogen), or a composite.

2.2.4. Residual gas and water saturations

Residual saturations for gas (S_{gr}) and water (S_{lr} or S_{wr}) are also needed to model relative permeability, and we derived those using contact angle data (discussion in Appendix A) (Mohammadmoradi and Kantzas, 2018). These correlations are an extension of reported experimental correlations for other fluid-solid systems (Bethel and Calhoun, 1953) and boundary conditions reported for gas shales (Blunt, 1997; Byrnes, 2005b; Engelder et al., 2014; Naar et al., 1962; Tanino and Blunt, 2013). Figure 2-3 qualitatively shows the impact of contact angle in chemically different flow path surfaces on residual saturations. The sequence of imbibition and drainage processes affects these residual saturations of gas and water. In particular, the residual gas trapped at the start of drainage affects residual water and gas saturations remaining after drainage is complete.

2.2.5. Total organic carbon

Total organic carbon (TOC) was measured for both shale and coal samples to provide baseline information to be used in projecting contact angle measures from shales of differing organic fractions and potential organic carbon pore spaces (Balashov et al., 2015; Kang et al., 2011). Duplicate measures were performed using a Carlo Erba Flash 2000 CHN analyzer and a Shimadzu SSM5000A indicating TOC for our Marcellus shale sample is 3.2%, and 72% for coal

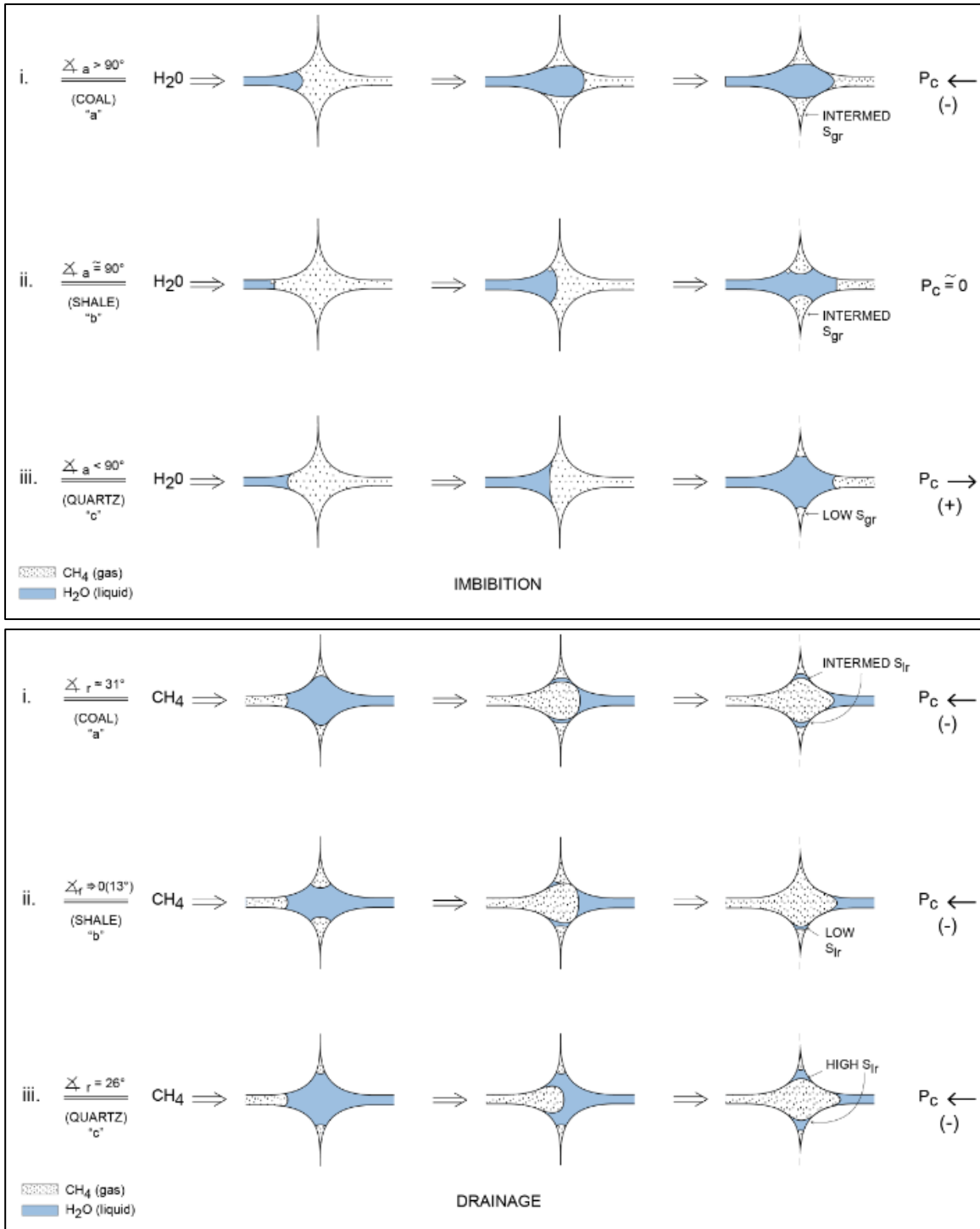


Figure 2-3: Imbibition (top) and drainage (gas production) (bottom) processes for (i) coal, (ii) shale, and (iii) quartz flowpaths in shale with different contact angles noted, illustrating relative saturations for each scenario. It is important to note the effect of previous imbibition or drainage steps and residual saturations on the residual saturation of subsequent process steps.

(see Appendix A). Industry log data for the Monongalia WV region our shale sample was sourced predicts 5.7% TOC for comparison (Appendix A).

2.2.6. Transport modeling

TOUGH2 with the equation of state (EOS) module EOS7C was used to simulate multiphase flow. This code can model flow of water, methane, and carbon dioxide using an extended Darcy governing equation to include relative permeability, and the Peng-Robinson EOS. We investigated the impact of interfacial properties in these simulations using our experimental data to scale MIP Pc data for the van Genuchten-Mualem (VG-M) relative permeability model (Ren et al., 2016; Van Genuchten, 1980). Our MIP data curve is fitted to VG-M by P_o (entry pressure) and m (pore size distribution), providing key model parameters for each specific fluid-shale scenario.

Our modeling domain was established based on the architecture of a typical horizontal wellbore in the Marcellus Shale. Hydraulically fractured horizontal shale gas wells are characterized by vertical fractures induced at designed intervals, and our 1D model is based on the flow from the shale matrix for 1m^2 of fracture area. We assume a typical induced fracture spacing of 20 m for the Marcellus and model flow from the midpoint between fractures (interference zone) horizontally to the fracture face (10 m), as shown for this base-case scenario in Figure 2-1. An additional simulation for potential natural fractures is modeled for 1 m horizontally, based on 2 m fracture spacing. These two scenarios were selected to illustrate the impact of changing the fracture surface/shale volume ratio and interfacial properties in combination. The characteristic fracture symmetry allows upscaling the model output to estimate full well impacts by post-processing the model output in an excel file we developed which is available in the Supporting Information.

Primary model parameters and boundary conditions are given in Table 2-1. Both fracture scenarios are spatially discretized from 1 mm grid blocks near the fracture face to incrementally

larger grid blocks at the opposing no-flow boundary (midpoint between fractures). Fine discretization near the fracture face reflects the limited penetration of water expected, and more extreme process pressure changes in this region. The fracture face boundary block is assigned a large volume to act as either a source of water in imbibition, or a sink for gas and water during production. Flow between this boundary block and the adjacent block is integrated for water and methane in both liquid and gas phases using RStudio following post-processing with the TOUGH2 EXT module. The opposing no-flow boundary block is assigned a small volume ($E-10 \text{ m}^3$) and width to determine pressure and saturation at the midpoint between fractures.

Table 2-1: Model parameters and boundary conditions used in the TOUGH2 simulations

Parameter	Symbol	Units	Value	Source
Rock Porosity	\emptyset	%	0.10	Dobson et al. (2014)
Relative Permeability (horizontal)	K_{rx}	m^2	4.4E-21	Dobson et al. (2014)
Relative Permeability (vertical)	K_{rz}	m^2	1.6E-21	Dobson et al. (2014)
VG-M (forced/natural/product)	m		0.30/0.43/0.55	MIP data fit
Initial water saturation	S_{wi}	%	0.05	Engelder (2014)
Residual water saturation	S_{wr}	%	0-0.3	Byrnes (2005)
Residual gas saturation	S_{gr}	%	0-0.475	Naar et al. 1962
Liquid saturation	S_{ls}	%	1.01	Engelder (2014)
Hydraulic fracturing pressure		Pa	4.5E7	Field Report
Formation pore pressure		Pa	2.4E7	Dobson et al. (2014)

Each scenario requires simulating three progressive process steps: (1) Forced imbibition representing high pressure water injection in fracturing (2 hours), (2) natural imbibition when injection ends and the well is shut-in (14 days), and (3) production of gas and water as the well is reopened and flow reverses (30 years). Saturation and pressure conditions at the conclusion of each step are used as inputs for the following step. As a transitional process, natural imbibition

assumes the volume of the fracture face boundary block is equal to the fracture volume proportioned to the area of the modeled frac face (1 m^2), and the VG parameters (P_o and m) as the mean of the forced and produced parameter values. Simulation time discretization is relative to the process step duration, ranging from $1-10^5$ seconds.

Scenarios are first modeled to investigate the primary role of interfacial properties in the fate and transport of water in shale using both measured and hypothetical contact angles. These scenarios use gas and water saturations theoretically derived from contact angle data, and sensitivity of the model was tested for a range of S_{Ir} and S_{gr} values to address uncertainty in these key parameters. This analysis is next extended to scenarios for coal and quartz as surrogates for flow paths in shale which are either organic carbon or mineral surfaces, again using experimental contact angle measures. Recognizing the interdependence between process conditions and interfacial properties, further simulations were performed at different pressures for both fracture models (the combined pipeline and flowing bottomhole pressures at the fracture face).

2.2.7. Integration of experimental and modeling work

The experimental data was integrated with the model as shown in Figure 2-4. Interfacial data were used to derive parameters for saturation, pressure, and relative permeability relationships. These in turn were used as model inputs in water flow simulations which strategically test how these interfacial properties impact the penetration, saturation, and water flow volumes in gas shales.

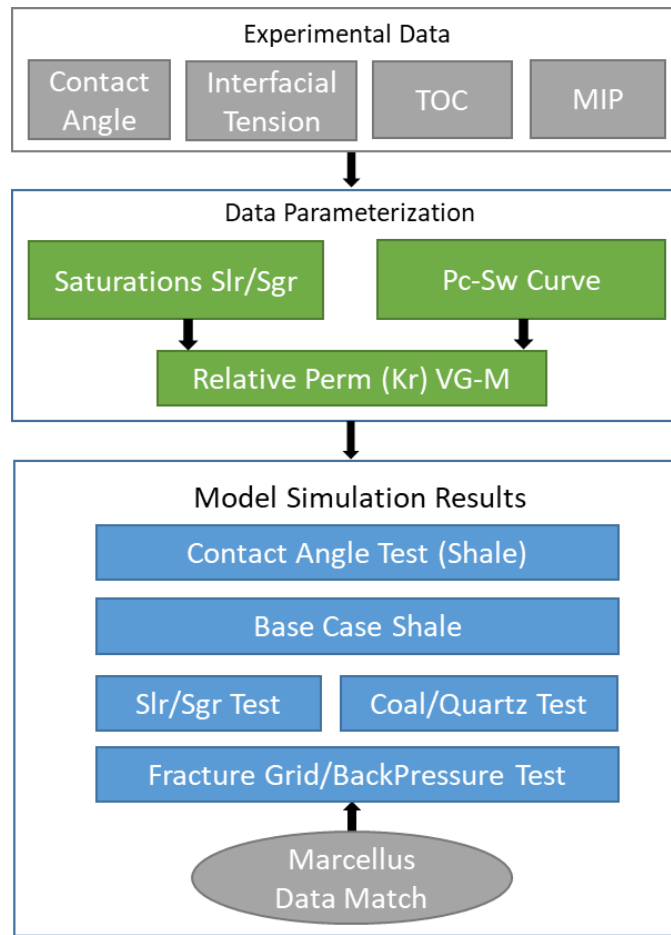


Figure 2-4: Workflow for developing model inputs from experimental data. Simulations are built to test sensitivity to interfacial and matrix variables and provide a final match for model geometry with specific Marcellus well data.

2.3. Results and discussion

Shale core from a Marcellus shale gas well (MSEEL well MIP3H) in Monongalia County, WV was used to perform experimental characterization of interfacial properties. The sample was taken at a depth of 2283 m.

2.3.1. Experimental characterization of shale core

Experimental results of static contact angle measurements on coal, shale, and quartz are presented in Figure 2-5 for three initial conditions: dry, pre-wetted with DI water, and pre-wetted

with 0.1% PAM. Se. All contact angle measurements were made with sessile 0.1% PAM drops at conditions representative of a Marcellus shale well (70°C; 20 MPa) with methane as the continuous phase. Coal was selected to provide model of the wettability conditions within the organic kerogen fraction of the shale matrix (Balashov et al., 2015). This organic component of the shale matrix has high porosity and contains much of the sorbed methane and is likely not represented by using an averaged wettability for the bulk shale sample.

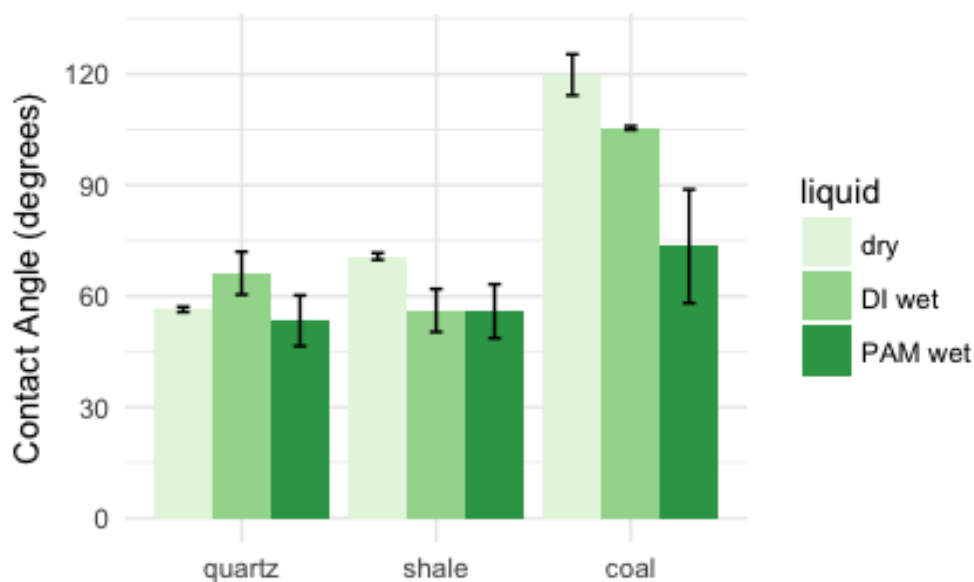


Figure 2-5: Static contact angles for coal (72.3% TOC), shale (3.1% TOC) and quartz (0% TOC) for 0.1% polyacrylamide (PAM) drops on initially dry, DI water wet, and 0.1% PAM wet surfaces. Measurements were taken at 70°C and 20MPa and all surfaces were prepared dry to 1-10 μm surface roughness to preserve the chemical integrity of the organic surfaces.

The results show that coal (TOC 72.3%) is non-wetting to PAM when dry or pre-wetted with water. But it does show a significant drop in contact angle when pre-wetted with a PAM solution. Quartz was used as a surrogate to represent the inorganic component of the shale matrix. It was found to be somewhat wetting for all initial conditions and was not affected by pre-wetting. Bonn et al. (2009) and others have reported that contact angles on composite surfaces reflect the major component if greater than 70%. Thus the similarity of the shale and quartz contact angle is

expected due to the low TOC (3% as measured) and high quartz (10-60%.) (Boyce and Carr, 2009) fraction in Marcellus shale. Coal and shale are more heterogeneous physically and chemically than quartz, which is reflected by both greater hysteresis between wet and dry measures, and more uncertainty in the dry contact angle measures (Bonn et al., 2009).

Dynamic advancing and receding contact angles were also measured and those results are reported in Figure 2-6. The advancing contact angles are useful to represent the forced imbibition conditions during which the water invades an initially dry shale. The Marcellus may initially be at sub-irreducible water saturation which means the shale contains less water than expected for the conditions.(Byrnes, 2011; Engelder et al., 2014; King, 2012b) Once a pore is filled with water, it may drain into an adjacent pore, which is represented by the receding contact angle (shown in Figure 2-6). There is good agreement between static and dynamic contact angle for coal (high contact angle) to quartz (low contact angle), with advancing contact angle slightly higher than static contact angle, and receding contact angle much lower than static contact angle. The relationship between dry static and advancing angle measures is expected because the static drop advances slowly as it attempts to spread on the surface. Heterogeneity in coal and shale contributes to the greater uncertainty in dry advancing angles from stick-slip flow, as the wetting bubble encounters and overcomes discontinuities in the surface. The variability in our receding angle results was quite low for pre-wetted samples, as surface heterogeneities are obscured by the wetting surface film as water recedes. While receding contact angle is often assumed to be zero, we observed an inflection point in these data when contact angle is plotted as a function of the receding distance. This angle is reported in Figure 2-6, as we assumed lower angles to be an artifact of removing water from the surface by suction from the injection tubing.

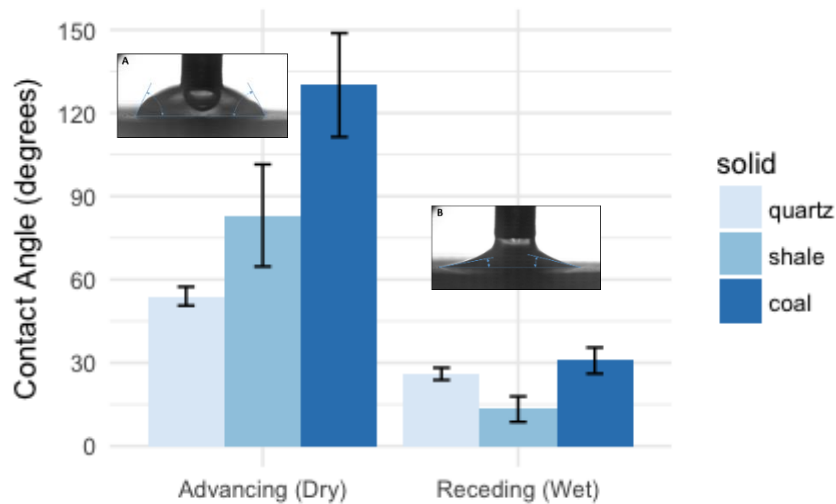


Figure 2-6: Dynamic contact angles for shale/coal/quartz for 0.1% PAM drops on initially dry or initially 0.1% PAM wet surfaces measured at 70C, 20MPa. Advancing (dry) and receding (wet) angle conditions chosen to reflect imbibition/drainage conditions.

The MIP characterization of the core sample is provided in Figure 2-7. Figure 2-7a are the Pc-Sw data for the sample. Data collected at pressures below approximately 0.3 MPa was assumed to be filling surface roughness and is not included in the final analysis. Over 50% of the total pore volume is contained in pores less than 10 nm in diameter (Figure 2-7b) which matters because Pc is high in these small pores (Figure 2-7c). Scaled Pc-Sw curves are fitted using the van Genuchten-Mualem (VG-M) model to supply relative permeability-saturation parameters.(Van Genuchten, 1980) Fitting VG-M requires a constant (m) representing pore size distribution for the shale sample (Figure 5a). The lack of reported MIP data for Marcellus shale at reservoir depths has led to the use of correlations for these constants (Dobson and Houseworth, 2014) or simplified analysis using only the drainage curve data (i.e., production data in our models). We calculated all parameters from full drainage and imbibition MIP data, using the advancing/receding contact angle data for

imbibition/drainage (production) respectively. Fitting data with VG-M also requires water and gas residual saturations (S_{lr} and S_{gr}) which are largely unknown. S_{lr} is reported in the range of 0-30% and S_{gr} as 50% of the initial gas saturation (Engelder et al., 2014). Using these reported ranges and those determined experimentally results based on our interfacial data, we projected values for S_{lr} and S_{gr} to systematically fit the VG-M model (see SI). Full Pc-Sw data sets are available in the supporting information, along with Pc-Sw curves for modeled scenarios scaled (Leverett, 1941) from this data, fluid interfacial properties, and saturation endpoints for water and gas.

The MIP data provide insight into the role of interfacial forces during water imbibition and drainage during the fracturing process. Capillary pressure is lower on the MIP imbibition curve, dropping abruptly as S_w increases. During forced imbibition (fracturing) high water saturations develop near the fracture face as high pressure flow fills large pores dominated by Darcy flow and capillary pressure fills small pores with the higher Pc. In sum, the capillary pressure difference between these Pc-Sw imbibition-drainage curves illustrates that once water invades a pore a much greater pressure will be required to drain this water from that pore. This effect, termed hysteresis, is amplified when capillary pressure is scaled for the modeled frac fluids by the difference between advancing and receding contact angles. If the difference between formation pressure, and either fracture or producing wellhead pressure is insufficient to overcome this capillary pressure, water will remain trapped in the pore. The initial sub-irreducible water saturation in shale provides a significant volume of nanoscale pores near the frac face for water to invade at high Pc, as seen in the MIP pore volume distribution (Figure 2-7b).

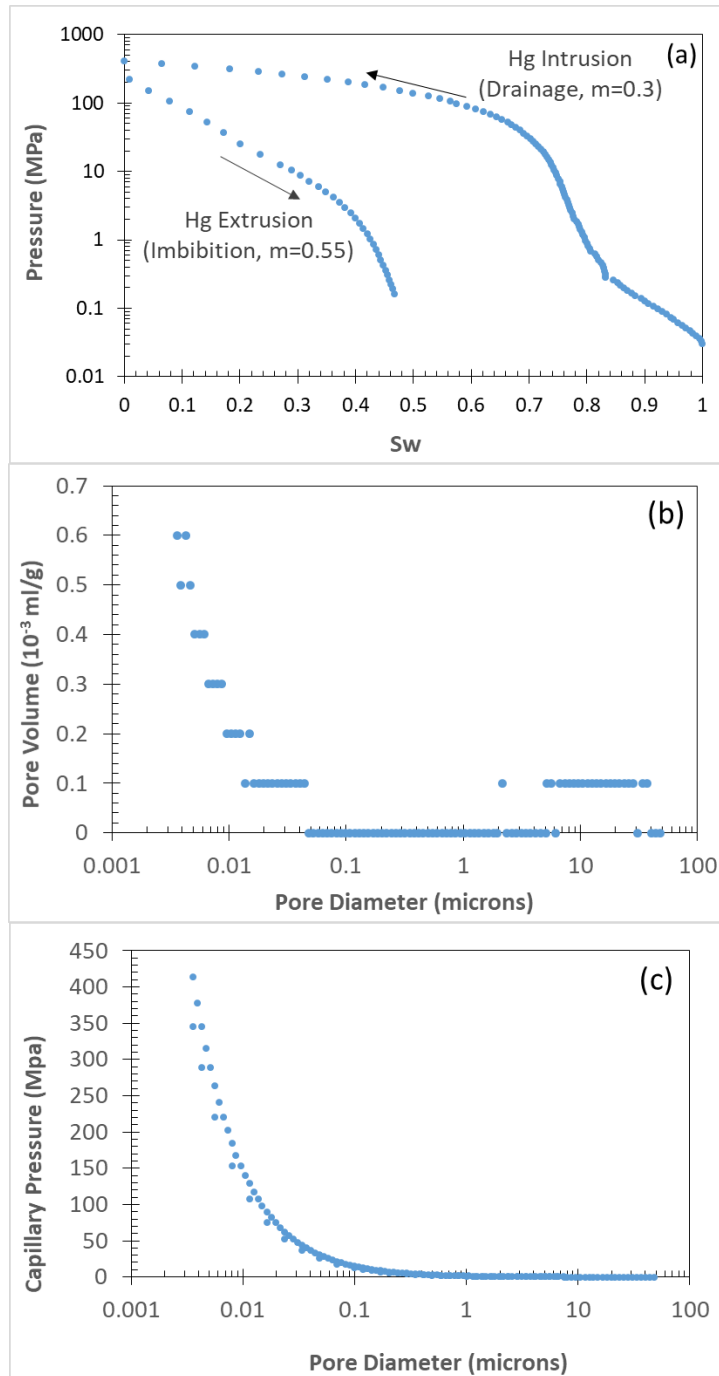


Figure 2-7: Marcellus shale MIP data curves: (a) Pc-Sw, (b) Pore volume-pore diameter, and (c) Pc-pore diameter

2.3.2. Model results

TOUGH2 was used to model water imbibition and drainage using the experimental data described above as inputs. Several measures of water transport were output from the model including the absolute volume crossing the fracture face, penetration depth from the face, and saturation within the shale. Together these measures provide a comprehensive picture of how interfacial properties impact water flows in fracturing processes.

2.3.2.1. Baseline wettability model

For a baseline wettability condition (advancing $\theta = 83.1^\circ$, receding $\theta = 13.3^\circ$) with a 0.1% PAM solution at 70°C and 20MPa, fracturing fluid flux across the fracture surface was found to be 0.369, 0.709, and -0.25 kg/m² for forced imbibition (fracturing), natural imbibition (shut in) and production, respectively. These steps vary considerably in duration so after normalizing for time, the results are 4.4E0, 5.1E-2, and -2.3E-5 kg/m²day for the respective processes. Interestingly, the water continues to invade the shale even during the production phase of the well lifecycle. The water imbibition front was estimated to be 7, 19, and 55 mm for forced imbibition, natural imbibition and production, respectively, within the 50-150mm range often cited (Byrnes, 2011). Forced and natural imbibition together constitute only 0.1% of process time, yet water penetrates 35% of the total imbibed distance in that time. This suggests Darcy flow is important in early processes, whereas counter-current imbibition velocity during production is governed by wetting velocity (Berg, 2010; Bonn et al., 2009; March et al., 2016). Water in fractures is also available to maintain imbibition in early processes, and low contact angle during counter-current imbibition increases the force required for spreading from Young's equation (Bonn et al., 2009):

$$\sigma_{sg} = \sigma_{sl} + \sigma_{lg} \cos\theta$$

Simulation results are visualized in Figure 2-8, which shows the water saturation and the pressure profile as a function of distance from the fracture face for the three stages of the well lifecycle. Note the different characteristic time steps used for each stage. During fracturing (Figure 2-8a) a large induced pressure in the fracture drives fracturing fluid into the face of the shale and increases the pressure above its pre-fracture condition. During the shut in period where natural imbibition takes pace (Figure 2-8b), the fracturing fluid continues to invade as the fracture face pressure declines to reach equilibrium with the reservoir pressure (24 MPa). After the well is opened to produce gas (Figure 2-8c), the pressure in the fracture is chosen as 8 MPa based on estimates of flowing bottomhole pressure in the Marcellus (Edwards et al., 2017b).

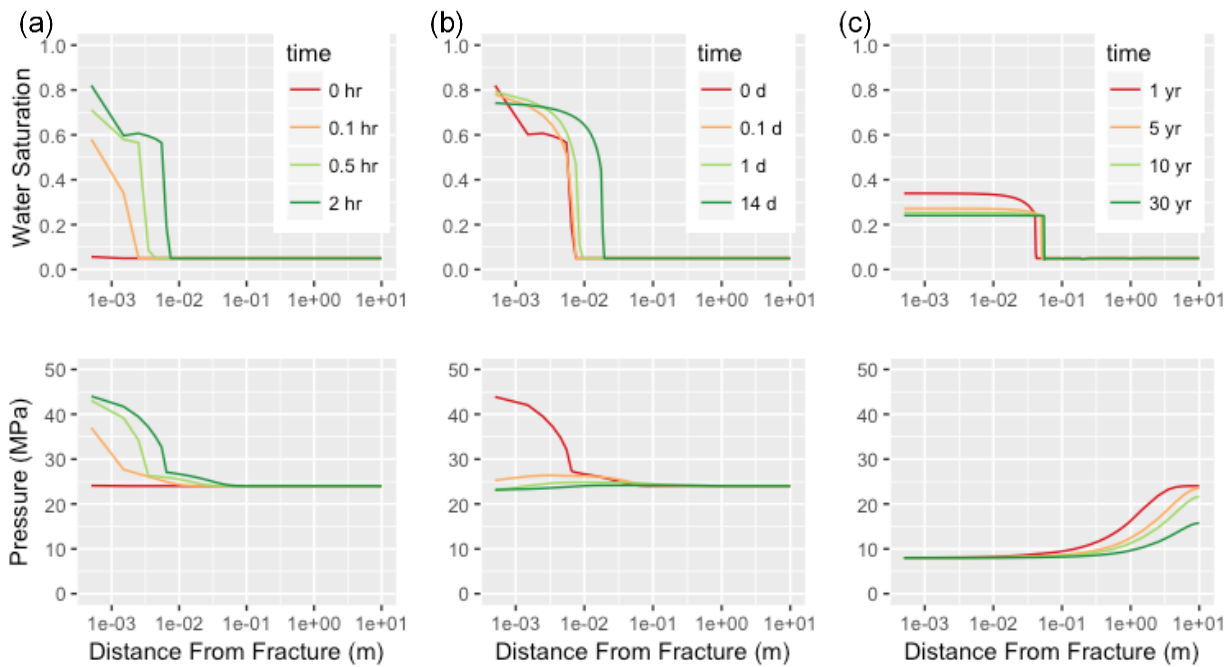


Figure 2-8: Baseline saturation and pressure data for Shale (8MPa backpressure, 24 MPa reservoir pressure) for (a) forced imbibition (fracturing or injection), (b) natural imbibition (shut-in), and (c) production (gas and water).

During this period, water imbibes deeper into the shale in counter-current flow during production, penetrating an additional 36mm from the frac face after 30 years of simulated production. This represents 66% of total penetration depth into shale while 23% of the water

volume is flowing in the opposite direction. Water saturation at the face drops during this time period due to both the ongoing imbibition under local capillary pressure in pores and Darcy flow from shale to fracture. In this system modeled with a fracture-fracture spacing of 20 m (thus 10 m depth from each fracture to a common midpoint), interference between fractures occurs in 416 days. At that time, the maximum reservoir pressure begins to drop but remains above the modeled fracture pressure in more than 90% of the reservoir at the end of production. Comparing process steps in this simulation with the same respective steps in the contact angle sensitivity test above, the flow results match expectations for a given contact angle.

2.3.2.2. **Model sensitivity to wettability**

The TOUGH2 model was then re-run using wettability conditions that range from highly wetting ($\theta = 5^\circ$) to nearly non-wetting ($\theta = 85^\circ$) to explore the full range interfacial conditions. A range of static contact angles was selected and the modeling results are presented in Table 2-2. The data suggest that fracturing fluid imbibed volume is somewhat insensitive to contact angle during forced imbibition. During shut in (natural imbibition), the imbibed volume is high at low to intermediate contact angles but decreases significantly at higher contact angle values. Taken together, the total amount of fracturing fluid imbibed into the shale is high at low to intermediate contact angles but drops significantly as the fluids become less wetting. During production, the amount of water that is generated from the shale increases steadily with contact angle. Interestingly our model suggests that gas production is insensitive to fracturing fluid contact angles. We hypothesize that during natural imbibition, the fracturing fluid drains out of the larger pores clearing the way for CH₄ to flow during production.

Table 2-2: Impact of contact angle on imbibition and produced fluids in shale at 8MPa

Contact Angle	degrees	Std (83.1/13.3)	5	39.7	57.2	71.7	85
Forced Imbib	kg/m ²	0.369	0.26	0.273	0.302	0.325	0.377
Natural Imbib	kg/m ²	0.709	0.795	0.706	0.661	0.332	0.092
Total Imbib	kg/m ²	1.078	1.055	0.979	0.963	0.657	0.469
Produced H ₂ O	kg/m ²	0.250	0.27	0.272	0.37	0.43	0.4
Produced CH ₄	kg/m ²	58.06	62.2	62.2	62.3	62.5	62.23

These results suggest that fracturing fluids can be designed to manage the fate of water during fracturing operations. Figure 2-9 shows the ratio of fracturing fluid produced to imbibed over a range of contact angles. The synthetic fracturing fluid tested here (0.1% PAM) exhibits a contact angle that would result in a ratio of produced to imbibed water of approximately 35%. Much higher water recoveries are theoretically possible for fracturing fluids that are designed to be less wetting of the shale surface. (Blake and De Coninck, 2004) Such developments would need to take into consideration the wetting of proppants and wellbore materials but these results provide insight into the sensitivity of fracturing fluid design and its fate in these wells.

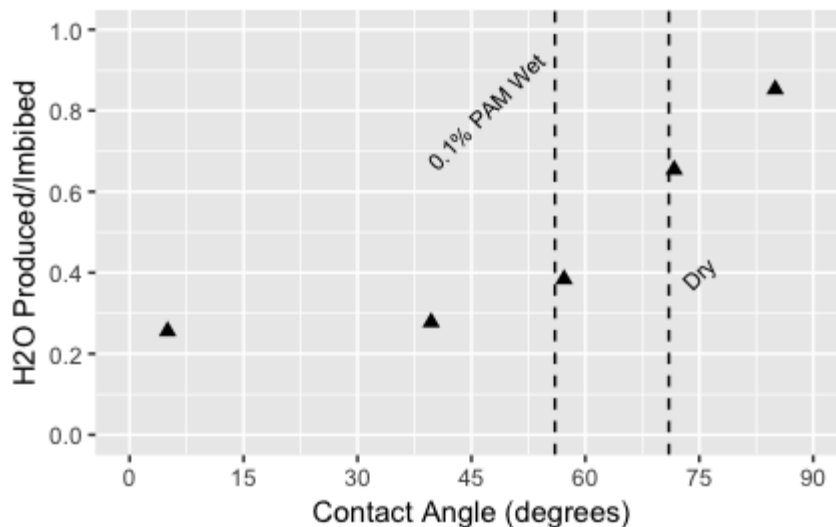


Figure 2-9: Sensitivity of water produced/imbibed fraction to static contact angle. For reference, the initial 0.1% PAM wet and dry conditions on baseline shale are shown.

In the same way that fracturing fluid wettability impacts imbibed water, it influences penetration into the bulk shale rock. Figure 2-10 shows model output of fracturing fluid penetration for three wettability conditions. The standard case is the same baseline wettability condition modeled above (advancing $\theta = 83.1^\circ$, receding $\theta = 13.3^\circ$). A “low” contact angle condition was selected in which a static contact angle of 5° was selected for both advancing and receding conditions and a “high” contact angle condition was selected in which a static contact angle of 85° was selected for both advancing and receding conditions.

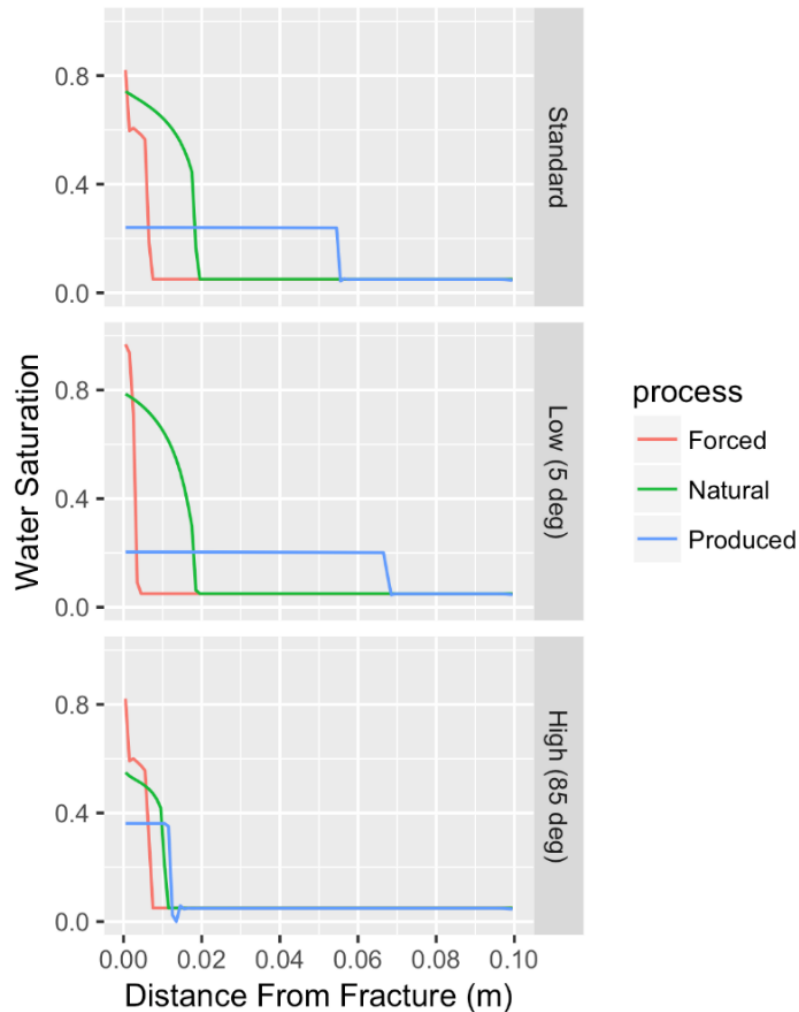


Figure 2-10: Saturation and pressure for standard, low, and high contact angle on shale (8MPa). The standard contact angle scenario (advancing $\Theta = 83.1^\circ$, receding $\Theta = 13.3^\circ$) is included for comparison.

The model results suggest that the low contact angle fracturing fluids penetrate much more deeply into the shale (69 mm during production) when compared to the high contact angle fluids (12 mm). Counterintuitively, this water front advances 38% less during forced imbibition with lower contact angle, as the more wetting conditions lead to higher water saturations close to the face of the fracture. Based on the Young-Laplace equation, lower contact angle increases the capillary pressure for a given pore radius, and consequently increases the ability of the fluid to invade, fill, and remain trapped in larger pores. When the fracture network is overpressurized (using fracturing fluid) with respect to the bulk rock, a high contact angle fluid will be forced through larger pores which lack the capillary pressure necessary to trap this fluid. Once the driving force of fracturing pressure is removed during natural imbibition, capillary pressure in the low-contact angle process dominates and penetration distance increases. Capillary pressure continues to drive further water penetration when flow is reversed to begin gas production. This counter-current flow is due to capillary pressures which are greater than the system pressure, continuing to drive water into lower saturation regions in shale with small, unfilled pores. It should be noted that these limited penetrations in shale indicate a low risk for significant frac fluid migration in the absence of actual fractures.

Figure 2-10 illustrates how shale near the frac face remains at water saturations approaching 1 with low CA, when the fracture is over pressurized with water supplied during hydraulic fracturing (forced imbibition). During the natural fracturing that follows, water continues to imbibe from fractures into the shale matrix, maintaining this elevated saturation with low CA. Water saturation at the fracture face decreases during production, as water continues to imbibe by capillary forces deeper into the formation. At higher contact angles, capillary pressure is insufficient to trap water in larger pores, and water is drained from shale during production,

producing water and reducing the saturation near the face. In addition, saturation is reduced at the fracture face more by counter-current capillary forces in production for low-CA processes than by the reduction caused by flow from the shale matrix to fractures driven by pressure differential.

In sum, the impact of both capillary pressure and process pressure must be considered to understand water transport in hydraulic fracturing (Figure 2-1). These pressures act in concert with, or opposition to each other, depending on location in the shale matrix. As a result, counter-flows may be occurring at the same time (such as during production), with Darcy flow favoring large pores with high relative permeability, and capillary imbibition favoring small pores with high capillary pressure. While the direction of Darcy flow is apparent from process pressure, capillary imbibition simply seeks smaller pores regardless of direction. During forced and natural imbibition, as Darcy flow is occurring in larger pores, capillary imbibition is simultaneously draining water to adjacent smaller pores. While apparently enabling flow in a single direction, capillary imbibition is simply taking water supplied by Darcy flow and distributing this water to small adjacent pores regardless of direction. Our model results show the impact of both process and capillary pressure on fluid flow, and thus illustrate the importance of interfacial properties in determining frac fluid flows. As shown, contact angle determines the balance between flow induced by process pressure and capillary forces in shale.

2.3.2.3. **Model sensitivity to residual liquid and gas saturations**

Figure 2-11 illustrates the ways in which the P_c - S_w curves for a gas shale would behave: (1-2) initially low saturation and later oversaturated during forced imbibition at high pressure; (2) during natural imbibition; and (2-3) when the system seeks equilibrium as water imbibes from large pores into successive smaller pores with higher P_c . During production (4a) water drains from large pores with insufficient P_c to resist the system pressure which is driving gas toward the frac

face. Simultaneous counter-current imbibition (4b) continues as water imbibes small pores with sufficient P_c to offset the system pressure differential. These combined flows lead the system to approach the residual water saturation, S_{lr} . The difference between these imbibition-drainage curves is the cumulative effect of pore size distribution (m) and wettability (contact angle Θ) as shown.

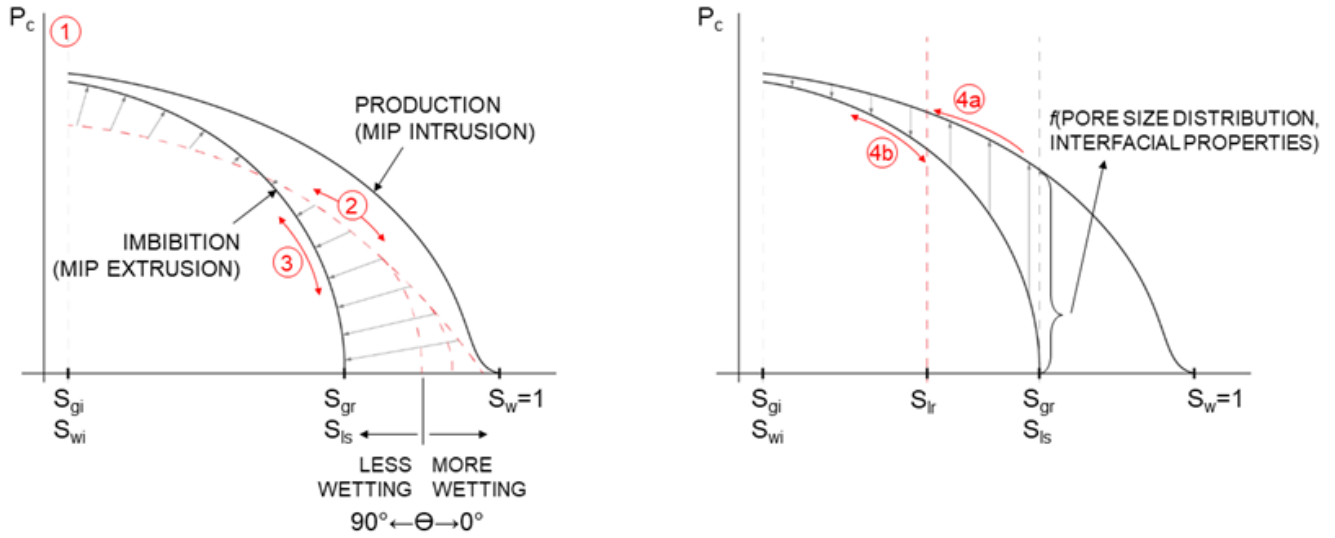


Figure 2-11: P_c - S_w curves showing the theoretical response of shale for (1) initial saturation, (2) forced imbibition (non-equilibrium), (3) natural imbibition (near equilibrium), (4a) production (drainage) and (4b) counter-current imbibition.

Table 2-3: Water imbibition and production data for high/low S_{lr} and S_{gr} parameters modeled

	LOW $S_{gr} = 0$	HI $S_{gr} = 0.475$	LOW $S_{lr} = 0$	HI $S_{lr} = 0.3$
Forced imbib	0.511	0.383	0.269	0.369
Natural imbib	0.717	0.505	0.775	0.675
Produced H₂O	0.01	0.31	0.26	0.27
Produced CH₄	2.49	62.13	59.32	62.45
H₂O Prod/Imbib	0.008	0.349	0.249	0.259

From Table 2-3, the final water saturation (S_{lr}) has a relatively low impact on overall imbibition of water. This is expected as capillary pressure is less sensitive to saturation at low water saturations as seen in these curves (Figures 2-7 and 2-11). Thus the change in residual water saturation has little impact on imbibition. In contrast, imbibition is significantly affected by S_{gr} for all process steps, resulting in high water retention at low residual gas saturation. Gas production is also greatly affected by S_{gr} as gas relative permeability is reduced at high water saturations. With the lack of in situ residual saturation data, this analysis shows the risk from assumed values in modeling. Recognizing the connection between these saturations and interfacial properties, we developed relationships providing residual saturations from experimental contact angle measures for modeling (Appendix A). With increased wettability (low contact angle) these relationships show reduced residual gas and water saturations.

2.3.2.4. **Model sensitivity to rock chemistry**

Simulations were performed assuming the fluid flow path in shale is dominated by either organic carbon (Balashov et al., 2015; Kang et al., 2011) or mineral surfaces, here represented by quartz as the primary mineral constituent in shale. Contact angle data specific to these flowpath chemistries are the basis for model inputs, and the results in Table 2-4 are consistent with the contact angle sensitivity results (Figure 2-9, and Table 2-2) indicating greater forced imbibition in higher contact angle systems, more natural imbibition with low CA, and water production relatively insensitive at the consistently low contact angle values shown here. It must be noted that the coal contact angle was reduced to 89 degrees in the model as TOUGH2 EOS7C is not capable of simulating the negative capillary pressure resulting from $\theta > 90^\circ$. Since water capillary pressure approaches zero at $\theta = 90^\circ$ the resulting low capillary forces have little effect on water transport.

However, the shift in water and gas saturations will change relative permeabilities, impacting Darcy flows. As a result, water flow in an organic carbon flowpath is expected to be more dependent on process pressures, with little capillary imbibition.

Table 2-4: Water imbibed in shale, coal, and quartz based on contact angles.

Process		Shale (83°/13°)	Coal (130°/31°)	Quartz (54°/26°)
Forced Imbib	kg/m ²	0.369	0.362	0.299
Natural Imbib	kg/m ²	0.709	0.558	0.656
Produced H2O	kg/m ²	0.25	0.25	0.25
H2O Prod/Imbib	kg/kg	0.232	0.272	0.262

2.3.2.5. Model sensitivity to rock fracture spacing

The exact spacing of natural fractures in shale formations is thought to play a significant role in gas production. Figure 2-12 shows the estimated ratio of produced to imbibed water for a range of well backpressures for two representative fracture spacings. The 10m model is based on induced fractures spaced 20m with no natural fractures, and the 1m model assumes natural fractures spaced 2m apart. The modeling results show much greater sensitivity to backpressure for the 10m model. The extended length and greater volume of the 10m grid provides a pressure reservoir to maintain pressure over the total production time. Interference with adjacent fractures occurs in just 31 days in the 1m model compared with 416 days in the 10m model, both at 8MPa backpressure. Reservoir pressure is depleted in approximately 3 years with the 1 m model due to this interference, whereas residual reservoir pressure still exists in the 10m model after 30 years. Lacking formation pressure to produce water over extended time in the 1 m model, additional water is imbibed by capillary forces and trapped, leading to lower produced water fractions.(Bažant et al., 2014) Well backpressure changes over time primarily as a function of pipeline pressure and well flowrate. This analysis reveals additional variables to consider in

determining the transport of water over the lifetime of a shale gas well. In practice, producers will control backpressure at the wellhead, and this shows the impact of those processes on water transport.

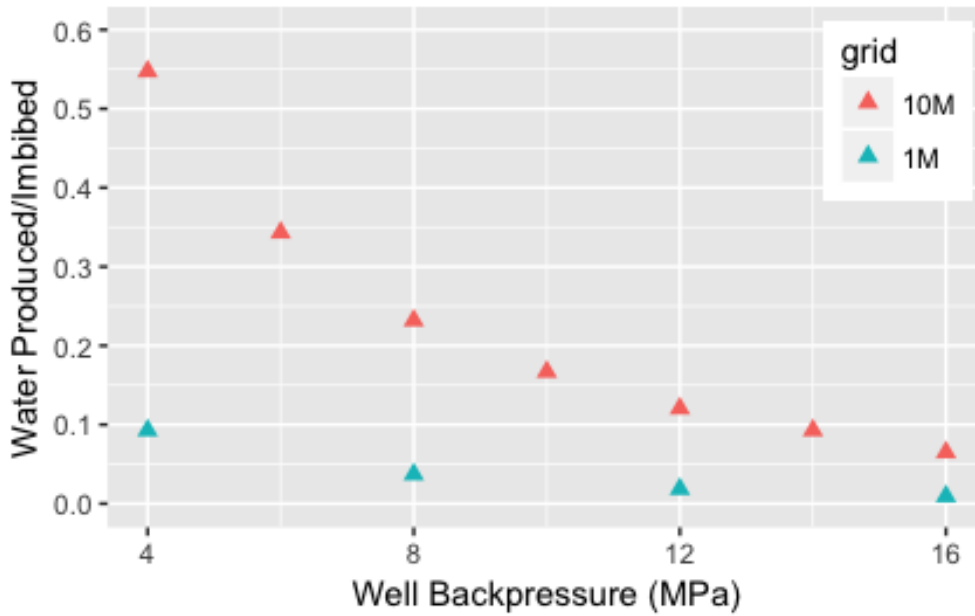


Figure 2-12: Sensitivity of H₂O produced/imbibed fraction to well backpressure from 4-16 MPa at fracture face for 1 m (natural and induced fractures) and 10m (induced fractures only) grid simulations. These correspond to 2 m and 20 m fracture spacing respectively.

2.3.2.6. Upscaling and benchmarking of modeling results

At the nominal backpressure of 8 MPa, upscaled simulation results (Appendix A) yields gas EUR of 2.85 and 3.49 BCF for 1 m and 10 m models, respectively, compared with the weighted average Marcellus EUR of 4.35 BCF. Aggregated Marcellus data for two counties (Fayette and Greene Counties, PA) adjacent to the well site we modeled report average EUR's of 2.33 and 3.91 BCF, supporting our EUR values (Swindell, 2015). Integrating our model over six years of production provides a detailed comparison with the MSEEL wellhead modeled. We estimate 1.49 BCF of gas is produced for 10m and 2.84 BCF for 1m models, closely matching field data reporting

EUR's of 2.26 and 1.15 BCF. The fraction of injected water which is produced for the fractured well (baseline scenario, 8MPa backpressure) ranges from 8% for the 1M to 33% for 10m simulations. The natural fracture system was scaled for both 5 and 50 micron fractures due to the lack of data, with the produced fraction only varying from 7% to 9%. In sum, field data generally validates the model based on expected gas EUR and produced/injected water fractions. Our data for 1m (natural and induced fractures) and 10m (induced fractures only) suggests the presence of natural fractures may help us understand questions surrounding the variation in reported produced water fractions. While lacking field data to fully support imbibed and produced water volumes estimates, fracture scaling may be necessary to match data and give insight into the real fracture surface area.

We recognize no model captures all the physical mechanisms potentially impacting multiphase flows and complex process conditions in nanoscale shale. Hysteresis is addressed using both imbibition and drainage MIP data with advancing and receding contact angle measures to show the effects of surface heterogeneity and wetting history. Fully hysteretic simulations (Ren et al., 2016) may include Pc-Sw scanning curves which model both drainage and imbibition capillary pressure at a given saturation, although thermal effects may overshadow hysteresis in pores smaller than 100nm (De Gennes, 1985). Sorption could also be included, particularly for gas analyses using supercritical fracturing fluids, but is not expected to change results focused on interfacial properties of slickwater fluids. (Yu et al., 2016) TOUGH2 EOS7C is valid for Darcy flow and Fickian diffusion, recognizing continuum fluid mechanics is valid to the transitional flow regime defined by Knudsen number, $Kn = 0.1-1.0$ in nanoscale shale pores (Gensterblum et al., 2015). The inclusion of slip flow in this model (Roy et al., 2003) makes this work valid to 5 molecular diameters (Bocquet and Charlaix, 2010) or approximately 2 nm (Vincent et al., 2016). Some

parameters for modeling unconventional formations simply do not exist. We provide missing interfacial measures and propose methods to estimate residual saturations for the benefit of and consideration by other researchers.

2.4. Conclusions

This work provides new insights into the role of interfacial processes on multiphase (e.g., fracturing fluid, methane) flow in gas shale formations. Experimental data on contact angle, interfacial tension, and pore-size distribution are reported for a core from the MSEEL site in West Virginia, USA as well as for other representative minerals that help us understand the role of solid chemistry on flow processes. Modeling results obtained using the TOUGH2/EOS7C code are used to simulate multiphase flow behavior at the well scale and the results are benchmarked to field data showing significant agreement. This analysis resulted in a number of important conclusions:

- Most of the water that is injected during fracturing operations remains trapped in the first few centimeters of bulk shale adjacent to the fracture face and the volume of water and the distance it imbibes into the rock is impacted strongly by the wettability of the fracturing fluid.
- At low to intermediate wettability values, the correlation is modest but at higher contact angles, which would be expected in organic-rich kerogen pores, an increase in contact angle will significantly decrease the amount of fracturing fluid that remains trapped in the bulk rock.
- Interfacial processes play an especially important role during natural imbibition (well shut in) suggesting that fracturing fluid wettability should be considered along with the traditional variables (e.g., time and pressure) that are used to design well shut in periods.

- Capillary forces change in the presence or absence of Darcy flow and with water saturation. As a result, time and spatial discretization will affect model results.
- The contact angle data and the simulations show that flow path mineralogy will impact water imbibition/production. This may become important in organic-rich kerogen pores where the fracturing fluid may achieve non-wetting conditions (e.g., $\theta > 90^\circ$), which create negative P_c conditions. Understanding these dynamics requires additional knowledge of in situ flow conditions and further modeling of this switch in flow dynamics.
- The movement of fracturing fluid through the shale matrix is more sensitive to residual gas saturation than it is to residual liquid saturation so additional data on the former is needed to support future modeling efforts.
- Upscaling these results is strongly dependent on assumptions about the structure of natural fractures in the bulk shale rock.
- Natural gas production does not appear to be sensitive to fracturing fluid wettability. While these surprising results warrant further investigation, it is possible that the models reflect processes in which spatial conditions (gas relative permeability primarily) are offsetting.
- Improved pore connectivity data for shale is needed to understand the extent small pores may block larger pores by capillary forces. While high pressure processes enable Darcy flow to penetrate deeper and transport water to access small pores, this may simply increase capillary blocking of gas which resides beyond those small pores.
- The limited penetration of fracturing fluid in shale results in little risk for fluid migration outside the formation except through actual fractures.

Chapter 3: **Estimating the CO₂ Fracturing and Storage Potential of Marcellus Shale Wells Based on Physicochemical Properties**

3.1. Introduction

Natural gas production from shale formations is leading the current surge in domestic energy production (U.S. Energy Information Association, 2015) due to hydraulic fracturing with water-based “slickwater” fluids horizontal directional drilling. Nevertheless, the estimated ultimate recovery (EUR) of gas from these formations is thought to be less than 25%. (Ribeiro and Sharma, 2013b) This raises serious questions regarding the sustainability of these processes from both environmental and economic viewpoints, and the lost opportunity to produce remaining gas. The low EUR’s in gas shales are commonly attributed to capillary blocking of gas by water-based slickwater fracturing (frac) fluids (Middleton, 2013). Capillary blocking is a function of shale pore size and the wettability of slickwater on shale, increasing in smaller pores and in systems with lower fluid-solid contact angle. Shale gas wells in the Marcellus with high natural gas liquid (NGL) concentrations (“wet gas”) are reported to be more sensitive to capillary blocking from water-based fracturing. As interfacial properties impact capillary blocking and potentially even the fracture matrix in shale, modifying aqueous frac fluids or using miscible alternatives such as supercritical CO₂ (scCO₂, or CO₂ hereafter) are important considerations in natural gas production systems.

The map in Figure 3-1 shows the Marcellus transition from dry gas with low NGL levels remaining in produced gas, and wet gas with increased levels of NGL’s (MCOR PSU,). NGL’s are valuable and therefore economically attractive to separate in areas such as the panhandle of West Virginia with processing plants nearby. The nominal composition of wet gas in the Marcellus is methane (76.8%) with the addition of NGL’s including ethane (12.6%), propane (6.1%), and

minor fractions of other complex hydrocarbon liquids (Lawrence Berkeley National Laboratory,). The presence of these NGL's will affect the interfacial contact angle of slickwater on shale, and therefore capillary blocking in a water-based frac process. Capillary blocking results from capillary pressure (P_c) trapping water in small pores, defined by Young-Laplace as a function of contact angle (Berg, 2010). Contact angle is also predicted to increase with carbon number making capillary blocking more sensitive to specific NGL's (Bertrand et al., 2002; Zeppieri et al., 2001). Similarly, reservoirs with increasing concentrations of NGL's may be expected to exhibit greater gas trapping from slickwater (water) as a result of increased capillary pressures. The concern for low gas recovery using slickwater in high NGL wells appears to be confirmed by interfacial physics.

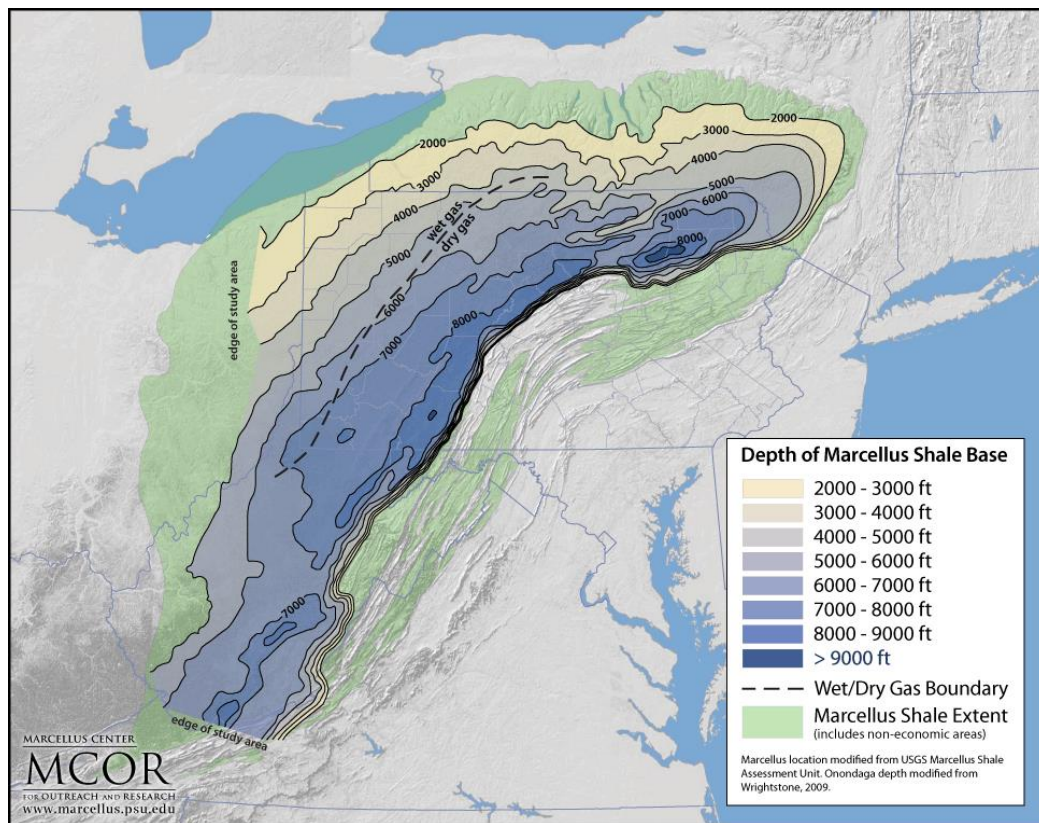


Figure 3-1: Map showing the transition from wet to dry gas in the Marcellus (MCOR PSU)

In addition to eliminating capillary issues, CO₂ fracturing has gained interest from recent research focused on the impact of interfacial properties in generating fracture complexity (Gan et al., 2015), concluding fluids with low or no interfacial tension create fractures at lower pressure. Alpern et al. (2012) show this reduced fracture pressure corresponds with lower molecular weight fracture fluids. Carbon dioxide (CO₂) is assumed to be miscible with NGL's at reservoir pressures thus eliminating capillary blocking (Hamdi and Awang, 2014), and reports confirm the generation of more complex fractures with greater surface roughness fracturing with CO₂, as shown in Figure 3-2 (Ishida et al., 2012; Li et al., 2016; Zhang et al., 2016)). The impact of fracture complexity and roughness on gas production in shale is unknown, and including these factors in modeling gas production with CO₂ frac fluids has not been done.

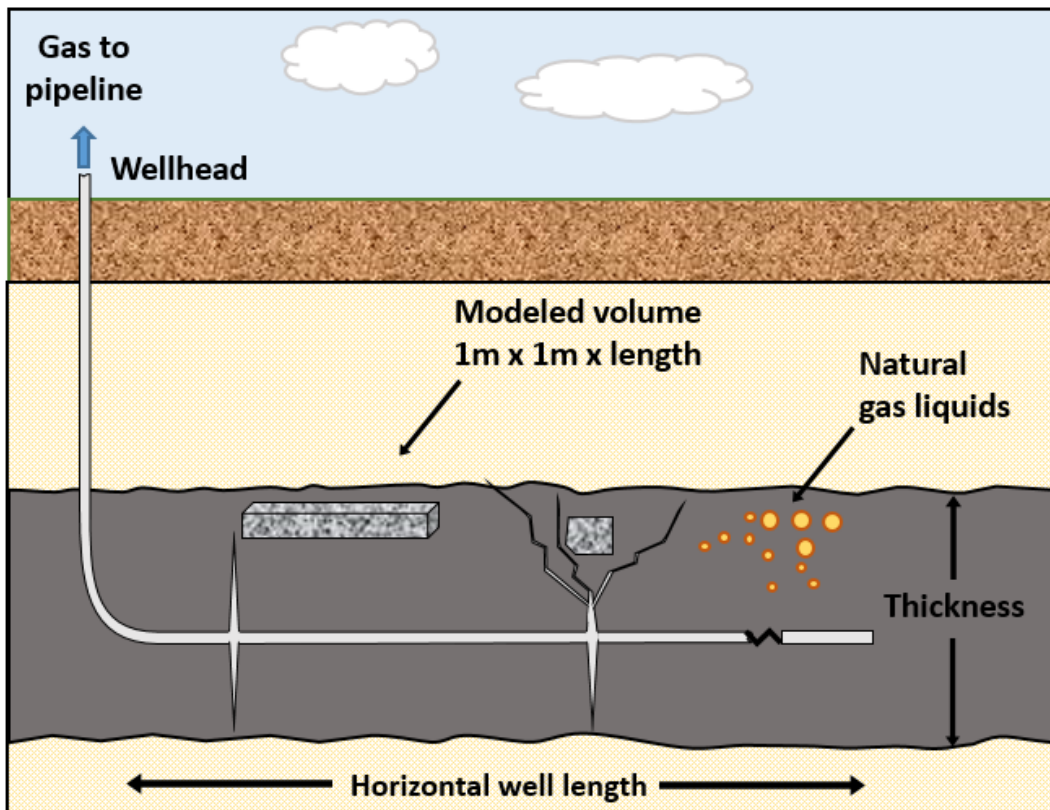


Figure 3-2: Hydraulically fractured horizontal shale gas well modeled for additional fracture complexity, both resulting from fracturing fluid interfacial properties.

Gaining an understanding of the potential for CO₂ fracturing from pilot wells is similarly limited, primarily due to the economic cost of pilot projects and poor CO₂ supply infrastructure. Field tests with CO₂ in the Montney in Canada and Devonian formation in Kentucky yielded mixed results, and these wells are not representative of advanced horizontal wells in low permeability shale such as the Marcellus. As a result, there is a need for analysis and data projecting the impact of CO₂ fracturing which considers the potential interfacial and fracture complexity advantages. CO₂ fracturing simulations providing gas production predictions which also consider other factors such as NGL concentrations, TOC, and sequestration potential for strategically locating these wells, will provide a valuable incentive for producers.

Important questions remain unanswered by these studies: Do NGL's increase capillary blocking in shale as a result of interfacial properties when compared with dry gas wells (predominantly methane)? If reduced contact angle, or ultimately miscible CO₂ processes result in fracture complexity and surface roughness, what is the contribution from each to gas production? Can we support projections for the potential for CO₂ as a fracturing fluid from these properties, and subsequently CO₂ sequestration (Middleton et al., 2015a)? We seek to answer these questions by (1) measuring and comparing contact angle for water in NGL's and methane at reservoir conditions, and (2) modeling the impact of both fracture geometry and frac fluid properties in a gas production simulation using TOUGH2-EOS7C, and (3) use model data for CO₂ and GIS data to predict conditions and locations in the Marcellus best suited for both CO₂ fracturing and sequestration. In sum, this work provides new insight for the impact of NGL's in Marcellus shale gas production and the opportunity for CO₂ as a frac fluid.

3.2. Methods

This work provides experimental interfacial data for typical Marcellus shale reservoir conditions and processes, in addition to capillary pressure-saturation (P_c - S_w) data for a Marcellus shale core sample. A flow simulation for CO_2 is performed to assess the impact of interfacial properties on natural gas production and the potential for CO_2 sequestration. Simulation results are combined with GIS data to map the potential for gas EUR increase and CO_2 sequestration potential for specific wells or regions.

3.2.1. Experimental Measures

Marcellus shale core samples (NETL Morgantown WV) were prepared for contact angle (CA) experiments using 180/320/600 grit silicon carbide abrasive paper (dry) to a 1-10 micron surface finish. As a surrogate for organic carbon pores and throats in shale (Balashov et al., 2015; Kang et al., 2011), coal samples were similarly prepared. A AVT Guppy NIR CCD camera with 6x zoom 18-108 lens was used to capture droplet images in a high pressure view cell. The cell is purged and filled with either methane (CH_4 , 99.995% purity) or propane (99.5%) and pressurized to 20 MPa using a Teledyne ISCO 500HP syringe pump suited for flammable gases. To simulate a wet gas (significant NGL fraction) with a nominal 5% propane fraction described above, a mixed phase fluid is also used for further experiments. This required first filling the chamber to 19 MPa with methane, then a final fill with propane to 20 MPa (assuming propane is miscible in $scCH_4$ and thus the ideal gas law and Dalton's law applies). A basic slickwater fluid composed of 0.1% polyacrylamide (PAM, 5-6M molecular weight) in DI water is injected by manual syringe pump for contact angle measures. Interfacial tension of PAM/ H_2O in both propane and methane was determined from pendant drop images using ImageJ image processing software with the Goutte Pendante plug-in to fit the Bashforth-Adams axisymmetric drop shape equation. Static contact

angles were similarly measured on captured sessile drop images using ImageJ image software with the Dropsnake plugin.

Mercury Intrusion Porosimetry (MIP) provides capillary pressure-saturation (P_c - S_w) data required for modeling multiphase flow in porous media such as the Marcellus shale. P_c - S_w data is derived by forcing non-wetting mercury into the shale sample by an incremental increase in pressure, then releasing pressure to allow mercury to drain from the shale pores. Mercury volume is measured for each pressure increment during this process (termed intrusion and extrusion based on the corresponding flow of the wetting vapor phase) to determine the characteristic P_c - S_w data curve for this sample. From Young-Laplace and MIP pressure data, pore size data is also obtained.(Hudson et al., 2012) Using an Autopore IV 9500 mercury porosimeter, Poro Technology (Kingwood TX) provided MIP data for our shale sample. Using SEM we observed pores larger than 1 μm in cleaved Marcellus samples, but assume these are inaccessible from work by Clarkson et al. (2012) using SANS, nitrogen and CO_2 sorption, and MIP.(Clarkson et al., 2012) Our work investigates the effect of interfacial forces for different fluid/solid conditions. Using MIP data requires scaling the P_c - S_w data for fluids other than mercury using the Leverett J-function (Leverett, 1941) with interfacial tension (γ), contact angle (θ), permeability (K), and porosity (ϕ):

$$J(S_w) = \frac{P_c}{\gamma \cos \theta} \left[\frac{K}{\phi} \right]^{0.5}$$

The J-function is a characteristic function for a given porous sample, from which we scale P_c from experimental measures of interfacial tension and contact angle for our fluid-solid system.

3.2.2. Modeled Measures

TOUGH2 with equation of state (EOS) module EOS7C was used to simulate multiphase flow in low permeability Marcellus shale. In combination, these numerically model flow of water,

methane, and carbon dioxide using an extended Darcy governing equation to include relative permeability, and Peng-Robinson EOS. We investigate the impact of interfacial properties in these simulations using our experimental data to scale MIP Pc data for the van Genuchten-Mualem (VG-M) relative permeability model. (Van Genuchten, 1980) Our MIP data curve is fitted to VG-M by P_o (entry pressure) and m (pore size distribution), providing key model parameters for each specific slickwater-shale scenario. Residual saturations for gas (S_{gr}) and water (S_{lr} or S_{wr}) are also required to model relative permeability, and lacking this data we developed hypothetical correlations based on contact angle (Appendix A). These correlations are an extension of reported experimental correlations for other fluid-solid systems (Bethel and Calhoun, 1953) and boundary conditions reported for gas shales (Byrnes, 2005a; Engelder et al., 2014; Naar et al., 1962).

Hydraulically fractured horizontal shale gas wells are characterized by vertical fractures induced at designated intervals (Figure 3-2) (Gale and Holder, 2010; Gale et al., 2014). Our 1D model is based on the flow from the shale matrix for a fracture face area of 1m^2 for the base-scenario assuming smooth fractures. The overall fracture geometry is modeled by a typical induced fracture spacing of 20 m for the Marcellus and flow from the midpoint between fractures (interference zone) horizontally to the fracture face (10 m). This characteristic fracture symmetry allows upscaling the model output to estimate full well impacts in a subsequent excel model (Appendix A). Complex fractures and fracture face roughness increase the effective surface area at the fracture face. Macroscale fracture complexity is modeled in a 1m flow simulation (2m fracture spacing) to investigate the impact of the decreased flow path length.

The model details largely follow those in chapter 2. Primary model parameters and boundary conditions are given in Table 3-1. Fracture scenarios are spatially discretized beginning with 1 mm grid blocks near the fracture face to incrementally larger grid blocks at the opposing

no-flow boundary (midpoint between fractures). The fracture face boundary block is assigned a volume of $E98 \text{ m}^3$ to act as either a source of fracture fluid in imbibition, or a sink during production. Flow between this boundary block and the adjacent block is integrated for methane in both liquid and gas phases using RStudio following post-processing with the TOUGH2 EXT module. The opposing no-flow boundary block is assigned a small volume ($E-10 \text{ m}^3$) and width.

Table 3-1: TOUGH2 Model parameters and boundary conditions

Parameter	Symbol	Units	Value	Source
Rock Porosity	\emptyset		0.10	Dobson et al. (2014)
Relative Permeability (horizontal)	K_{rx}	m^2	4.4E-21	Dobson et al. (2014)
Relative Permeability (vertical)	K_{rz}	m^2	1.6E-21	Dobson et al. (2014)
VG-M (forced/natural/product)	m		0.30/0.43/0.55	MIP data fit
Initial water saturation	S_{wi}		0.05	Engelder (2014)
Residual water saturation	S_{wr}		0-0.3	Byrnes (2005)
Residual gas saturation	S_{gr}		0-.475	Naar et al. 1962
Liquid saturation	S_{ls}		1.01	Engelder (2014)
Hydraulic fracturing pressure		Pa	4.5E7	Field Report
Formation pore pressure		Pa	2.4E7	Dobson et al. (2014)

Each scenario requires simulating three progressive process steps: (1) Forced imbibition representing high pressure injection of water or CO_2 in fracturing (2 hours), (2) natural imbibition when injection ends and the well is shut-in (14 days), and (3) production of gas as the well is reopened and flow reverses (30 years). Saturation and pressure conditions at the conclusion of each step are used as inputs for the following step. As a transitional process, natural imbibition assumes the volume of the fracture face boundary block is equal to the fracture volume proportioned to the area of the modeled frac face), and the VG-M parameters (P_o and m) as the mean of the forced and produced parameter values. Simulation time discretization is relative to the process step duration, ranging from $1-10^5$ seconds.

3.2.3. Literature Measures

Marcellus parameter maps for GIS analysis are shown in Figures 3-1, 3-3, 3-4, and 3-5. Using empirical relationships proposed below, flow model outputs for natural gas and CO₂, and these mapped parameters, the potential for increased gas EUR and CO₂ sequestration is calculated and for mapping:

$$EUR\ Potential\ (CO_2\ Frac) = (model\ EUR) * (thickness) * (1.33 * NGL\%) * (TOC\%) * (Reservoir\ pressure\ \%)$$

$$CO_2\ Sequestration = (model\ CO_2\ sequestered) * (thickness) * (TOC\%) * (horizontal\ length)$$

Well horizontal length may be applied to either relationship to analyze a specific well, or the model well coverage area may be used to determine the total production or sequestration for a region of wells. Aggregate horizontal well length data for this purpose is available from PADEP and other sources for specific counties (Swindell, 2015).

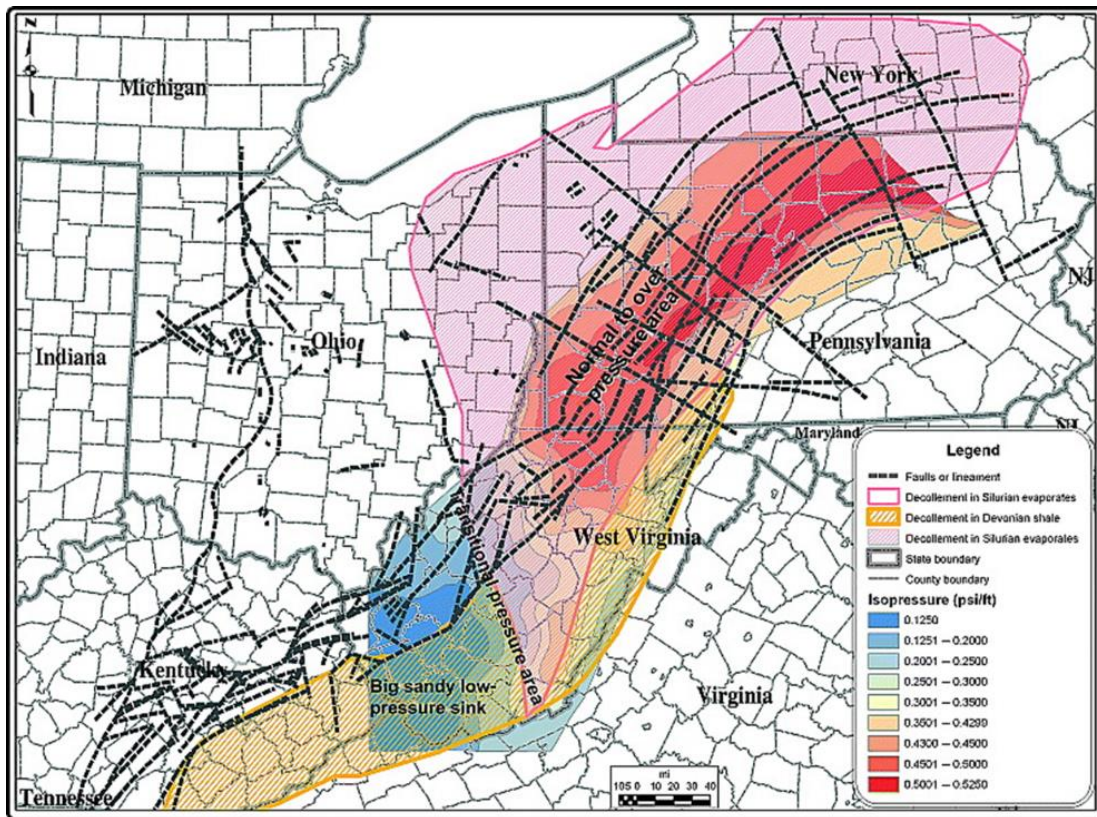


Figure 3-3: Marcellus shale gas well isopressure map (AAPG Marcellus Wiki)

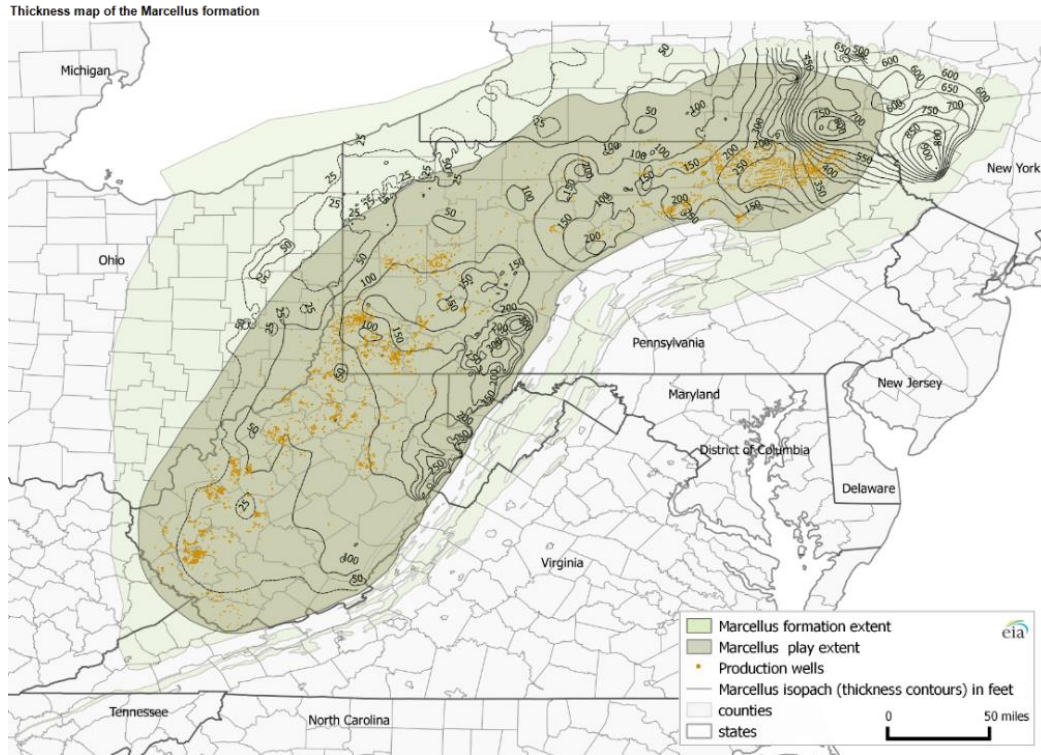


Figure 3-4: Marcellus shale formation thickness isopach map (EIA)

3.3. Results and Discussion

3.3.1. Interfacial Properties

With interfacial tension (IFT) between propane and methane in shale, the more wetting component could block flow due to capillary pressure at the interface of the two fluids. To investigate IFT, we first determined the phases of each at expected reservoir conditions (70 °C, 4-20 MPa). Propane exists as a liquid at these conditions above 2.6 MPa (NIST Webbook), while CH₄ will be supercritical above 4.6 MPa, both within the range modeled. The miscibility of propane in methane was further confirmed experimentally from 4-20 MPa (including the CH₄ gas-supercritical transition), precluding the likelihood of separate component phases existing in shale. This lack of interfacial tension eliminates the potential for capillary pressure trapping between these hydrocarbons. Other NGL's such as butane and pentane are present in lower amounts in the

Marcellus and are similarly expected to be miscible with methane. While existing in higher concentrations (12%), ethane is a gas at reservoir conditions. Since there is no IFT between propane and methane in natural gas, we next investigated how NGL's affect the CA of slickwater (0.1% PAM) on shale using propane as a surrogate for other NGL's.

Results for static contact angle measures for 0.1% PAM in propane, methane, and a nominal 5% propane/95% methane mix on Marcellus shale are given in Figure 3-6, indicating propane contact is significantly higher than methane at all pressures as expected for hydrocarbons with higher carbon (C_x) number (Balashov et al., 2015; Kang et al., 2011). Similarly other higher C_x hydrocarbons are expected to exhibit even higher contact angles. If contact exceeds 90 degrees PAM is no longer the wetting phase, and as shown in Figure 3-7 propane may prevent PAM from entering small pores. The effect of pressure on contact angle is important to consider during production, as this change in wetting phase as the formation pressure drops will alter the transport mechanisms for hydrocarbons as they become non-wetting. Water will begin to imbibe (counter-current) into small pores, and displace hydrocarbons from solid surfaces. The propane-methane mixture contact angle is between the angles for the pure components, and increases with pressure similar to the individual components. While we did not find a significant increase in gas production with contact angle in previous simulations, increasing contact angle greatly reduced the (imbibed) frac fluid volume required and increased the produced/imbibed frac fluid fraction. Thus, these

results indicate propane does potentially reduce the frac fluid required, and returns a higher fraction of frac fluid for recycling or treatment.

Coal as a surrogate for organic carbon pathways in shale is compared with shale in Figure 3-8. Propane is shown to have slight effect on the contact angle of 0.1% PAM on coal. The addition of other NGL's is expected to increase the measured CA by the combined effect of increasing C_x and concentration. The hydrophobic nature of these fluid combinations raises important questions for methane production, using earlier modeling results for the inverse system with hydrophilic (low CA) shale. Those previous results showed high imbibition of the wetting phase (water in that

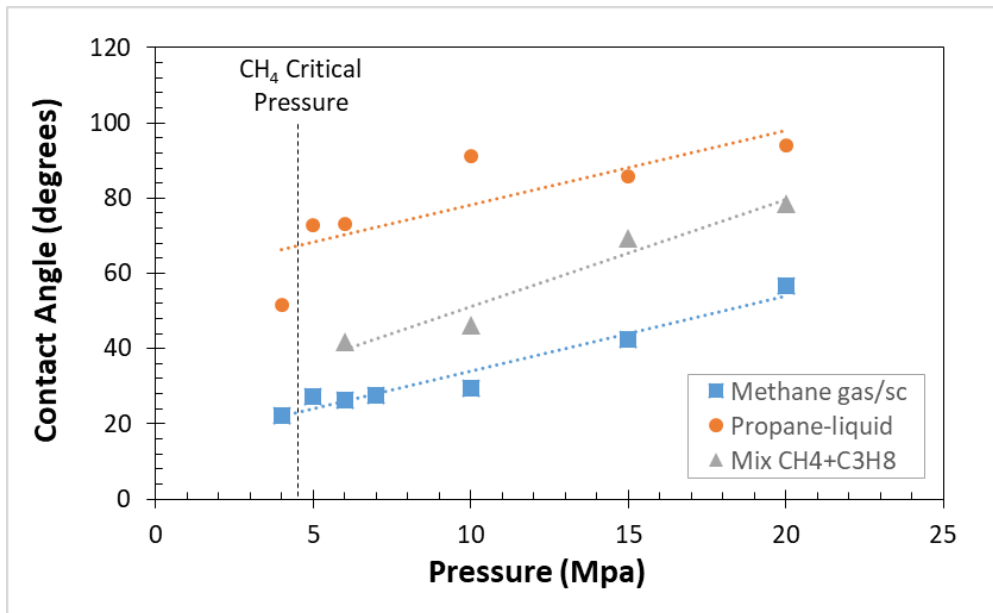


Figure 3-5: Static contact angle for 0.1% PAM in methane, propane, and a 95/5 mixture of methane/propane on Marcellus shale at 70C and pressures representing reservoir and well conditions. This shows contact angle on shale increasing with NGL concentration.

scenario), and increased retention of that phase once imbibed in shale. Now, if shale flowpaths are largely organic carbon as reported, these results infer a hydrocarbon wetting phase (180 degrees minus measured PAM CA) and similarly increased retention of these hydrocarbons (reduced

production of gas). Increased wettability of NGL's on organic carbon will amplify this effect further and reduce natural gas production.

3.3.2. TOUGH2 model fracture complexity/roughness impact on EUR

The two fracture scenarios in Figure 2 were modeled in TOUGH2 EOS7C, for roughness and complexity in separate simulations. These simulations test the potential impact of interfacial experimental results by other researchers previously discussed. Roughness (Figure 3-2b) was

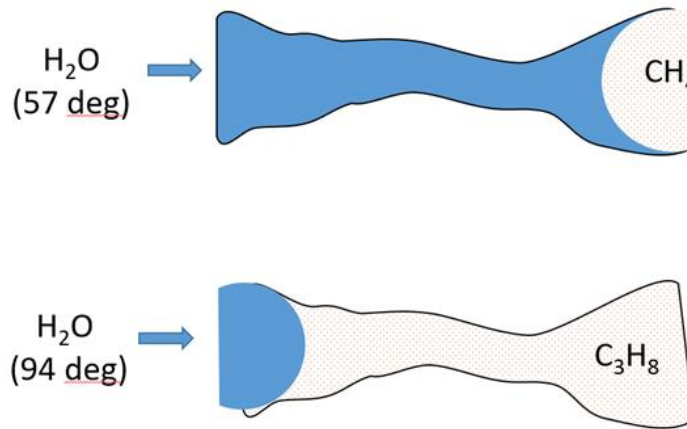


Figure 3-6: Static contact angle for 0.1% PAM in methane, propane and a 95/5 mixture on Marcellus shale and coal (72% TOC) as a surrogate for organic carbon pathways in shale. While contact angle is higher in coal as expected, the NGL Cx number appears to have less impact than on shale.

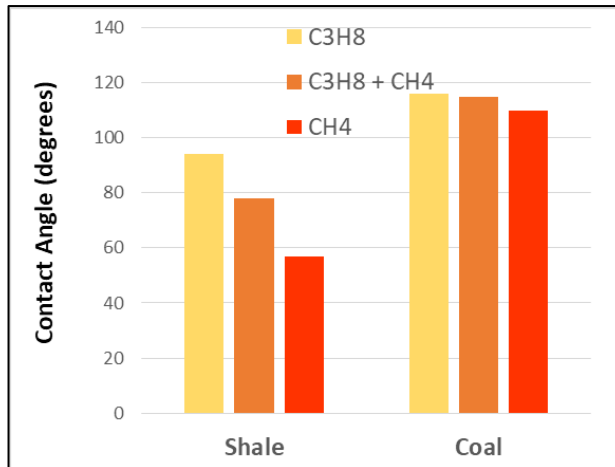


Figure 3-7: Impact of increased contact angle on shale for PAM (H₂O) in propane (C₃H₈) below compared with the contact angle in methane (CH₄) above. Above 90 degrees propane becomes the wetting phase and capillary forces reverse, reducing the imbibition of PAM.

simulated by increasing the surface area at the fracture face 200% with no change in volume, and resulted in no significant change in methane production. With horizontal permeability 3x vertical permeability, penetration of frac fluid and the effect on gas production is unchanged at each point on the frac face, with expected results. While outside the scope of this study, Jia et al. (2018) do report increased fracture permeability from dislodged grains at the frac face propping fractures more effectively.

Fracture complexity is the generation of branched fracture structures and is modeled with a reduced flow distance (or volume) using the same 1m^2 of frac face area from other simulations. From previous studies of natural fracture spacing, and the likely scenario that this increased fracture complexity will follow the natural fracture geometry, this was modeled as a 2m fracture spacing (1m simulation flow distance). Others have numerically and experimentally found increased fracture complexity using CO_2 frac fluid, concluding a similar fracture spacing of 1.9m (Liu et al., 2018; Zhang et al., 2017). Estimated ultimate recovery (EUR) of gas in a 0.1% PAM (slickwater) system for the base (10m) and complex (1m) fracture scenarios are shown in Figure 3-9. These results indicate an 80% increase in EUR due to fracture complexity assuming a slickwater fracture. Modeling the same physical system using CO_2 as the frac fluid in both base and complex fracture scenarios yields a 109% increase in EUR (Figure 3-9).

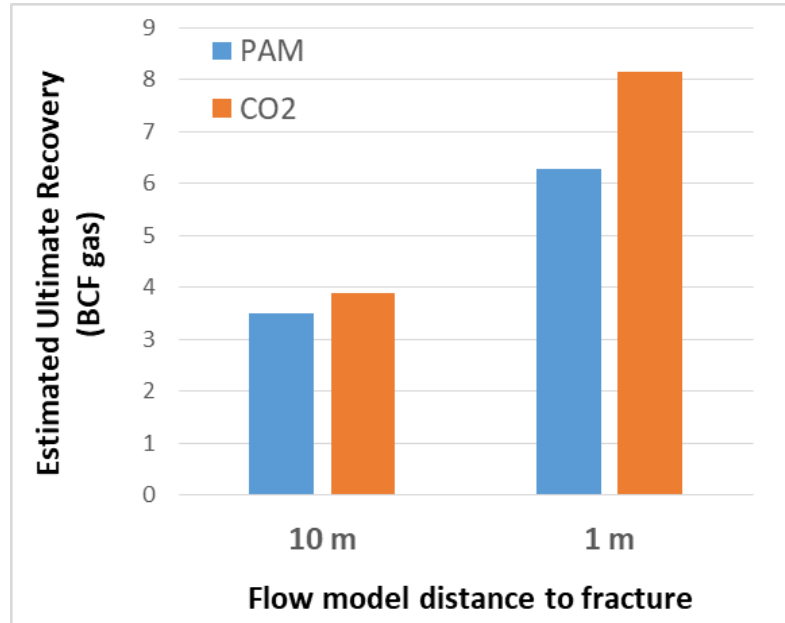


Figure 3-8: Fracture complexity and fracturing fluid impacts on EUR showing an increase in gas production with increasing fracture complexity.

3.3.3. Comparison of interfacial impacts on EUR

This analysis considers interfacial impacts on natural gas production in Marcellus shale (1) resulting from the inherent natural gas composition and shale mineralogy, (2) due to induced fracture complexity, and (3) as a result of CO₂ frac fluids.

First, recognizing the presence of NGL's with different C_x and varying concentration, we extend our slickwater model results to NGL's in organic carbon pathways (coal) as previously discussed. Using those results for a 52 degree CA variation (57-5) degrees, we assume a similar decrease (65-13 degrees) in this natural system. From this output, the produced/imbibed fluid ratio decreases 33%. This drop in production corresponds to the largest change in EUR anticipated from the full range of NGL components and concentrations. Second, from model simulations fracture complexity contributes 80-109% increase in EUR, for PAM and CO₂ processes respectively.

Third, CO₂ frac fluids alone increase EUR 12% in a 10m fracture base scenario, and 30% in the 1m complex fracture scenario.

From this analysis, the presence of NGL's in natural gas potentially reduces EUR. Thus, this variation in natural gas chemistry is a consideration to determine the potential impact of frac fluid interfacial properties. The most extreme change in interfacial properties will result from using CO₂ as a frac fluid, as no IFT will exist in this system with methane. Therefore using CO₂ as a surrogate for the optimal frac fluid (no capillary blocking), results in a 12% increase in EUR for the base-case 10m model. This suggests the maximum impact for CO₂ fracturing will occur in a wet-gas region (high NGL's) increasing EUR and additional 33%, for a total of 45% improvement in gas production. Further, increased fracture complexity from optimized interfacial properties (CO₂ in our scenario) is projected to provide nominally 2x more increase in EUR. Considering the EUR increase for the 1m scenario, CO₂ fracturing is projected to increase EUR from 133-166% compared with slickwater fracturing.

3.3.4. Mapping CO₂ potential for increased gas EUR and CO₂ sequestration

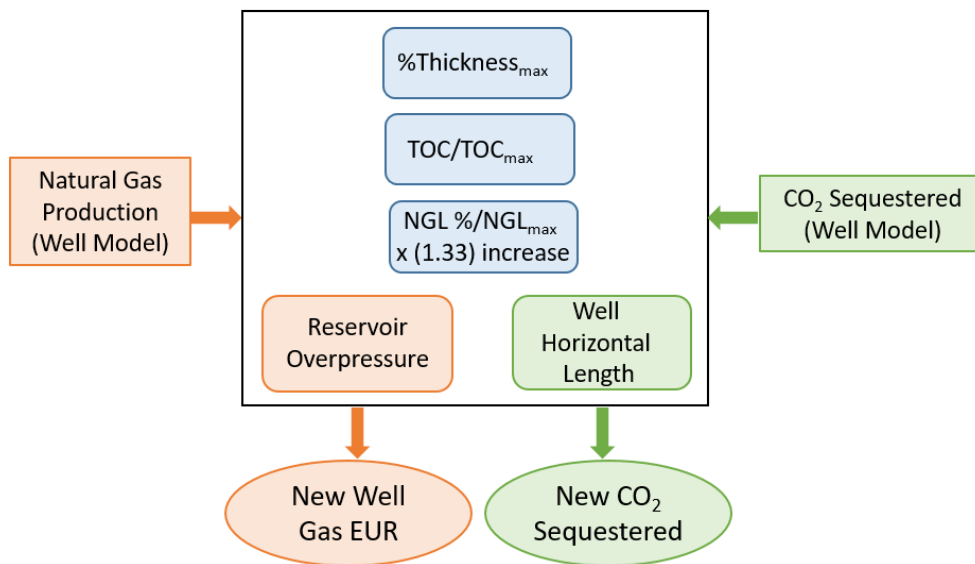


Figure 3-9: Flowchart for mapping natural gas production increase and CO₂ sequestration potential from CO₂ fracturing.

3.3.4.1. Gas production potential (EUR) mapping for CO₂ fracturing

Building on the model for CO₂ fracturing, I propose applying the output from this simulation to map the potential increase in natural gas production by combining Marcellus GIS data with natural gas production data from our model. The proposed method is shown in Figure 3-10 and will require geospatial shale thickness, reservoir pressure, TOC as a surrogate for porosity, and the NGL fraction to build this predictive mapping. The baseline gas production for a CO₂ fractured well (Figure 3-9) is used to provide the primary data, and includes the option for fracture complexity. This work will provide strategic direction for locating and producing shale gas wells with the maximum impact on production.

3.3.4.2. CO₂ sequestration mapping for CO₂ fracturing

CO₂ sequestration data from the TOUGH2 simulation using CO₂ fracturing fluid is shown in Figure 3-12. These results indicate over half of the injected CO₂ is sequestered in both the base 10m and complex fracture 1m scenarios, and results are approximately scaled with fracture surface area. Compared with slickwater fracturing, Figure 3-11 illustrates CO₂ penetration into shale is 3x that of slickwater during forced imbibition (i.e. 25mm vs 8mm), increasing to 10x by diffusion during natural imbibition (200mm vs 19mm). Nevertheless even CO₂ penetration is limited and does not reach the extreme no-flow boundary during imbibition for either the 1m or 10m model scenarios. During production the reservoir pressure drop at the 1m no-flow boundary occurs earlier than in the 10m scenario, leading to some incremental difference in the produced/sequestered CO₂ scaling between fracture scenarios. As a result, the basic difference between CO₂ scenarios is the access to the shale volume gained in the complex (1m) fracture scenario. Modifying the process step durations and pressures will also impact the ratio of produced/sequestered CO₂ and change the absolute quantities.

This data may be incorporated into a future model from which the CO₂ sequestration potential for a given well may be predicted from key parameters, using the methodology shown in Figure 3-10. Combining Marcellus shale GIS data with the model output will allow development of a system to map the CO₂ sequestration potential for specific or large regions of this formation.

3.4. Conclusions

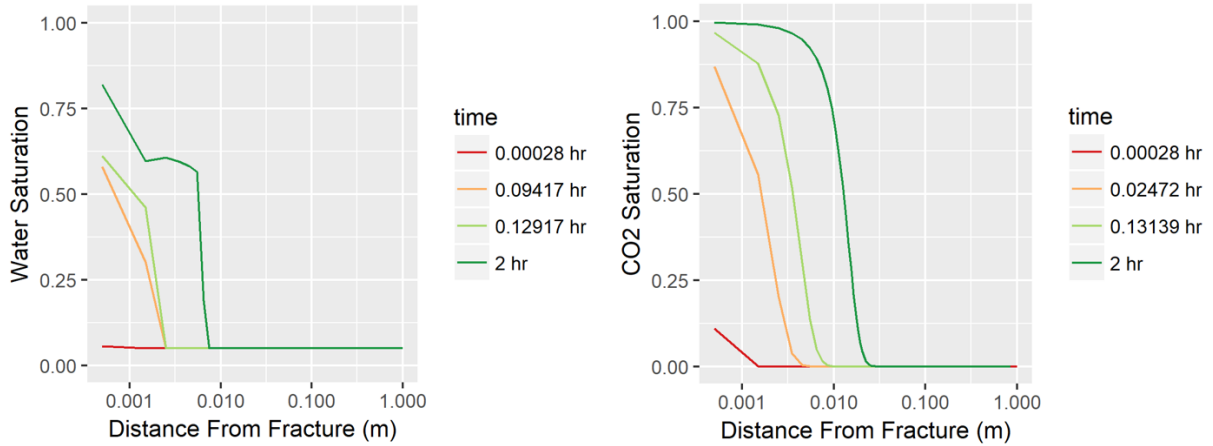


Figure 3-10: Forced imbibition water (left) and CO₂ saturation (right) plots in shale showing increased penetration depth and saturation of CO₂. This depth is an important consideration if CO₂ preferentially sorbs to displace CH₄.

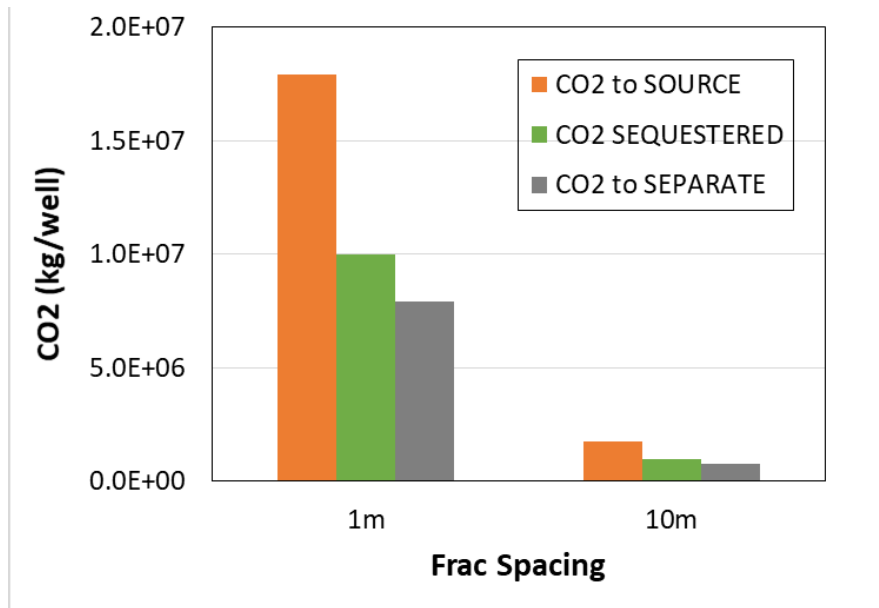


Figure 3-11: CO₂ required to fracture the base fracture (10m) and complex fracture (1m) scenarios in Marcellus shale at 70 °C, 45MPa, and produced and sequestered CO₂ quantities for both scenarios. This indicates roughly half the CO₂ required to frack shale is sequestered.

Interfacial properties impact the consumption and production of fracturing fluids significantly, with little impact on actual gas production in our model using methane as a surrogate for natural gas. However increasing NGL concentration, and the CA change with pressure will result in a system which is actually hydrocarbon wetting at different times in the fracturing/production process. This hypothesis indicates reduced gas production may occur in shales with high NGL concentrations due to gas preferentially sorbing on the shale surface. The dependence of CA on pressure further shows the complexity of this mechanism, as the system wettability for water or gas changes during production as pressure drops. This effect is initially local, extending globally in the shale matrix over time. Thus the concentration and chemistry of NGL's is an important consideration in analyzing gas production in these systems. Fracturing with CO₂ reduces these interfacial impacts which are most pronounced in high NGL gas reservoirs, such as the northwest region of the Marcellus. This work also expands on other research showing potential fracture complexity using CO₂, and shows the potential benefit otherwise not recognized in modeling. We provide insights useful for understanding the conditions under which CO₂ will provide the greatest increase in gas production and potential for CO₂ sequestration. These results question current estimates of the CO₂ sequestration potential of spent gas wells which are based on gas production processes using slickwater, and do not include the impact of added fracture complexity from CO₂ fracturing. This work indicates fracturing with CO₂ in a typical Marcellus shale gas well potentially sequesters 9.76E5-9.98E6 kgCO₂, depending on fracture complexity. Earlier work estimated CO₂ sequestration from field reports and LCA analysis to range from an expected value of 2.73E6 to a forward looking projection of 5.08E6 kgCO₂ (Wilkins et al., 2016). These values closely match within the range of fracture complexity projected. By combining model outputs for gas production and geospatial data for the Marcellus, future mapping may point

to regions most attractive for CO₂ fracturing to produce gas. Similar mapping for CO₂ sequestration potential is also made possible by this model, applying GIS data with the baseline CO₂ sequestration simulation data.

Chapter 4: **Environmental life cycle analysis of water and CO₂-based fracturing fluids used in unconventional gas production**

**Reprinted with permission from Wilkins R, Menefee AH, Clarens AF. Environmental life cycle analysis of water and CO₂-based fracturing fluids used in unconventional gas production. Environ Sci Technol 2016;50:13134-41. Copyright 2016 American Chemical Society.

4.1. Introduction

Over the past decade, energy systems in the United States have been revolutionized by the rapid growth of oil and gas production from unconventional reservoirs (DOE, 2009). Tight shale formations are characterized by low permeability and have only recently emerged as economically viable sources of hydrocarbons through advances in directional drilling coupled with high-volume hydraulic fracturing techniques (Rodriguez and Soeder, 2015). Conventional fracturing fluids consist primarily of fresh or recycled water because this is what is typically available in large volumes and at low cost. The other principal component in hydraulic fracturing fluids is proppant, typically silica sand, that is used to maintain fractures once the fluid is retracted (Gaurav et al., 2012). Chemical additives include surfactants that are used to modify viscosity and surface tension, acids to prevent scaling, and biocides (King, 2012a). A common fluid composition is referred to as slickwater because the presence of polymers reduces friction at high flowrates. The advantage of these fluids is that they are low cost and their performance is well understood. Their primary drawback is that they limit gas recovery from water sensitive formations because of capillary blocking and they create large volumes of difficult-to-treat wastewater (Lutz et al., 2013; Ribeiro and Sharma, 2013c).

The rapid success and expansion of these technologies has resulted in a number of environmental concerns, many associated with the sourcing and disposal of fracturing fluids. A single well completion in the Marcellus Shale, the largest natural gas play in the US, currently uses 300,000-500,000 gallons per stage for up to 30 stages per well (King, 2012a). While some shale plays, like the Eagleford in Texas, use considerably less water, escalating concerns over freshwater depletions to meet these demands are no longer restricted to arid regions (Dominguez-Faus et al., 2009; Lawson et al., 2012; Soeder et al., 2014; Vengosh et al., 2014). Fracturing fluids can contaminate groundwater supplies through wellbore leakage or seepage into overlying aquifers (Flewelling and Sharma, 2014; Myers, 2012). Flowback and produced waters are characterized by high concentrations of salts (Hayes, 2009) and trace radioactive species present significant challenges (Rowan et al., 2011). Recent efforts to treat and recycle produced water for subsequent operations can reduce, but not eliminate the impacts on water (Ferrar et al., 2013; Rassenfoss, 2011; Rozell and Reaven, 2012). During reuse, structural deficiencies in lined storage impoundments may introduce safety hazards and exposure pathways (Ziemkiewicz et al., 2014). Wastewater that cannot technically or logistically be reused must undergo energy-intensive treatment at centralized facilities or injection via deep underground disposal wells, even though injection disposal has led to widespread concerns over induced seismicity (Mauter and Palmer, 2014; Walsh and Zoback, 2015; Zoback and Gorelick, 2012). Dissolved contaminants in fracturing wastewater effluent can degrade surface water quality even when standards are met (Rahm and Riha, 2014).

The real and perceived impacts of water withdrawals and wastewater management have prompted interest in non-aqueous fracturing fluids. Alcohol, liquefied petroleum gas foams, nitrogen gas, and carbon dioxide (CO₂) have all been tested as working fluids over the past several

decades (Gupta, 2009), yet none have matched the performance characteristics and low costs that are associated with slickwater. As these have been tested primarily at pilot scale, no working alternative fluid has benefited from the significant level of refinement and tuning already devoted to water-based slickwater formulations. One notable advantage of these non-aqueous alternative working fluids is that they can reduce capillary blocking (via water imbibition) of hydrocarbons in dry formations such as the Marcellus which contain little connate brine (Bertoncello et al., 2014). Even reduced fractions of water in energized foams may be sufficient to block gas in shale pores. In addition, clay swelling can cause formation damage and further block gas flow by reducing matrix permeability (Pei et al., 2015). Other alternative fluids (e.g. liquid petroleum gas) increase risks in above-ground handling due to flammability.

CO₂ is an attractive working fluid that does not create the same capillary blocking effects downhole and is not flammable. CO₂-based fracturing has been attempted in several demonstration projects in recent years (Burke and Nevison, May 9-11, 2011; Pei et al., 2015; Reynolds et al., 2014). When used as a working fluid in hydraulic fracturing, CO₂ is first injected under pressure in the liquid phase. It then expands to fracture the surrounding formation as a supercritical fluid in the reservoir. The pressure at the wellhead is subsequently reduced and the CO₂ flows back to the surface as a gas (He et al., 2014). The low viscosity of CO₂ relative to even the most advanced slickwater formulations could enhance gas production by generating more complex and extensive fracture networks (Middleton et al., 2015a). Fluid properties also favor CO₂ in terms of improved mobility, greater penetration rates, and faster clean-up (Pei et al., 2015). Furthermore, CO₂ precludes reservoir damage and could reduce or eliminate the use of some chemical additives (e.g. biocides and surfactants). The key technical and economic driver for CO₂-based fluids will be enhanced gas (CH₄) recovery over water-based systems resulting from its miscibility with

hydrocarbons, avoided water blocking, and preferential adsorption of CO₂ over CH₄ in shales (Middleton et al., 2015a). Combined these mechanisms facilitate gas flow and could potentially unlock significant volumes of trapped and sorbed gases that cannot be readily recovered using conventional fracturing fluids. Despite these advantages, the use of low viscosity CO₂ introduces the potential for fluid leak-off into the formation and complicates proppant transport (Gupta and Bobier, 1998). More significantly, economic and logistical challenges in CO₂ sourcing currently undermine large-scale deployment (Middleton et al., 2014).

In spite of the qualitative arguments for using CO₂ as a working fluid, few studies provide quantitative comparisons of the technical performance or the systems (e.g., logistics and life cycle) implications of using CO₂ instead of water for fracturing shale formations. Several studies have documented the efficacy of liquid-free CO₂/sand stimulations in the US and Canada (Campbell et al., 2000; Lillies and King, 1982; Yost et al., 1993) but these did not provide clear comparisons between working fluids in the same formations. Heath et al. (2014) summarize GHG life cycle assessment (LCA) for water-based fracs from multiple shale gas studies. Weber and Clavin (2012) also analyzed GHG data from six LCAs and compared conventional and unconventional shale gas production. Others have performed LCA for water (Clark et al., 2013; Laurenzi and Jersey, 2013) and energy (Dale et al., 2013) impacts in shale gas water fracs. However, despite the perceived reductions in environmental impacts associated with waterless fracturing, no systems-level analysis has been reported to date. As a first attempt at bridging this gap, we conducted a comparative LCA of water- and CO₂-based fracturing fluids. Even though this analysis was performed for a gas-producing shale formation, it is expected that the underlying structure of the model would be similar for an oil-bearing shale formation. Some factors, such as the extent to which non-aqueous fracturing fluids would enhance production, would need to be adjusted but the

overall model architecture developed here could be easily modified. The environmental cost accounting of life cycle energy use, greenhouse gas (GHG) emissions, and water consumption is performed to quantify key challenges and opportunities for meeting industry and environmental protection goals. The sheer magnitude of US shale gas reserves coupled with low recovery efficiencies compel a futuristic valuation of untapped improvements in energy production from hydraulic fracturing while minimizing environmental impacts.

4.2. Methods

A complete description of the modeling structure, parameters, and assumptions used in this study is provided in the Appendix B. An overview of our approach is provided here.

4.2.1. System boundaries and functional unit

The Marcellus Shale formation was selected as the geographic boundary for this analysis because it is the largest shale gas field in the United States, with an estimated 84.5 trillion cubic feet (tcf) of proved and 119 tcf technically recoverable reserves (DOE, 2016; U.S. Energy Information Association, 2015). It is also a dry formation with little connate brine (Engelder, 2012b), which would make the production benefits of a non-aqueous fracturing fluid most clear. Energy use, GHG emissions, and water consumption are traced over four life cycle stages (transportation and storage, fracturing, flowback, and production). Site development and drilling, as well as downstream gas processing and power generation, are independent of fracturing fluid selection and consequently excluded from this analysis.

The functional unit selected for this study was 1 GJ of natural gas produced over the lifetime of a wellhead. Here, a wellhead is defined as a single site with 6 laterals in accordance with current industry practices, where multiple wells are drilled successively at a central well pad. Normalizing impacts to performance (i.e. natural gas production) accounts for anticipated production benefits

motivating the development of CO₂-based fluids. An energy-based functional unit was selected over cumulative gas volumes to contrast energy consumption and production.

4.2.2. Scenario development

The water frac fluid formulation considered here reflects state-of-the art slickwater practices in the Marcellus shale (King, 2012a). Waterless CO₂-based fracturing fluid impacts are captured via two scenarios: (1) the current status according to literature and industry experience (CO₂ base) and (2) a potential technology informed by theoretical models and industry insight (CO₂ outlook). This outlook scenario assumes research and development benefits similar to those that contributed to rapid advances in water processes over the past decade.

4.2.3. Production performance

Estimated ultimate recovery (EUR) values were applied to normalize impacts to the projected energy recovery for a single well in accordance with the functional unit. For slickwater, a weighted average EUR of 4.35 billion cubic feet (bcf) was derived using data from 2,600 horizontal Marcellus shale gas wells (Swindell, 2015). To account for performance enhancements incentivizing CO₂-based systems in the absence of data on waterless CO₂ fracs at the scale of this study, we developed stochastic projections for a term we call production increase factors (PIF) that are applied to this baseline slickwater EUR to forecast recovery under each CO₂ scenario. PIF is calculated as a factor of the water-based gas production which may also be expressed as a percentage increase in production. The baseline conditions defined here have a PIF of 1. A 100% increase in gas production over that baseline would constitute a PIF of 2. A limited number of industry and Department of Energy-sponsored pilot sites have explored the efficacy of CO₂-based fracs to date across the US and Canada, such as the Lewis Shale (NM) (Campbell et al., 2000), Devonian shale (KY) (Mazza, 2004; Yost et al., 1993), Canyon Sands (TX) (Mazza, 2004), and

scattered early vertical frac wells (Lillies and King, 1982). For the base case, results compiled from a comprehensive literature review of actual CO₂ frac jobs were applied to project CO₂ performance. These field data from early trials indicate a 50% improvement is common when CO₂ is used as a fracturing fluid. The CO₂ base scenario PIF is built around this as a conservative median value, with the lower limit chosen as equal to production from a water frac (PIF of 1, or 0% increase).

For the outlook case we develop theoretical constructs of production enhancement by considering trapping mechanisms impeding gas flow with conventional fluids. A median PIF of 3 (e.g., a 200% increase in production) can be obtained from the remaining capillary-trapped, sorbed, and inaccessible gas⁴⁵ relative to a water frac's recovery, expressed as a fraction of original gas in place (OGIP). A maximum theoretical PIF of 14.4 (1340%) is computed from reservoir geometry and gas density. At first glance this factor may appear high, but the lognormal input distribution emphasizes a lower median estimate, and ignoring the long tail of high potential PIFs could overlook important benefits of CO₂. The lower bound of the PIF distribution for the CO₂ outlook case (50%) is derived from the median PIF for the CO₂ base case to anchor the distribution to field-scale data. The PIF distributions for all three scenarios share at least one data point resulting in some overlap between scenarios. The majority of field and lab-scale investigations suggest improved gas recovery with CO₂-based fluids and thus scenarios yielding lower production than a water-based frac are not considered.

4.2.4. Fluid sourcing

A process flow diagram including system boundaries considered here is presented in Figure 4-1. The life cycle of each scenario begins with fluid acquisition. Water-based fluids are piped from a local surface source and stored in temporary on-site impoundments. Based on state-of-the

art industry practices, a uniform distribution of 300,000-500,000 gallons of fluid are applied per stage over 10 stages per lateral and 6 laterals per wellhead for the slickwater frac. The baseline CO₂ scenario utilizes 30% less fluid by volume than a water-based frac; a further 5% reduction in CO₂ volume is assumed for the outlook case. Sourced volumes for both CO₂ scenarios account for 3% losses required to control pressure in transport and storage.

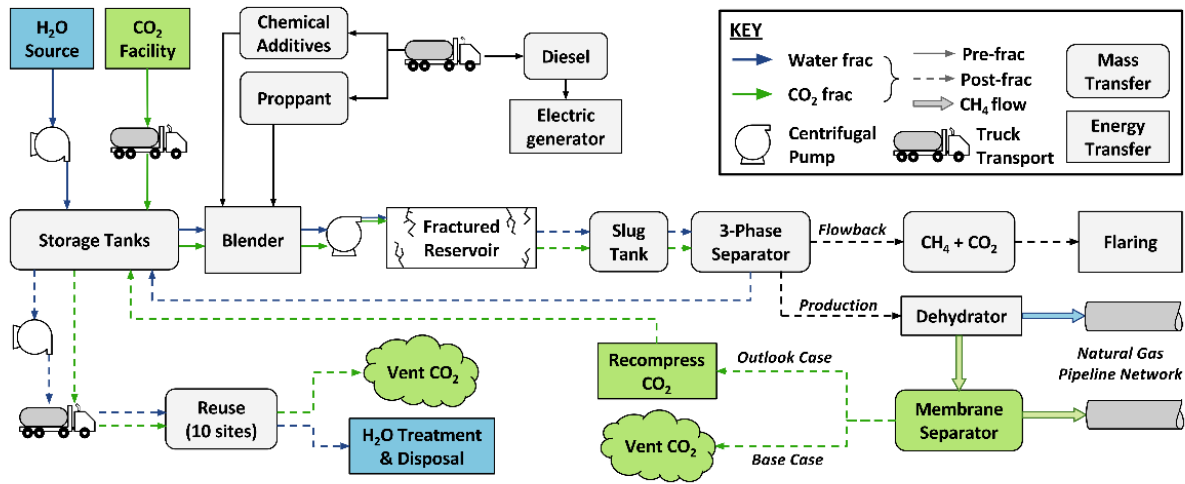


Figure 4-1: Process flow diagram and system boundaries encompassing the life cycles of water and CO₂-based fracturing fluids. Processes and flows in blue indicate a water frac and green indicates a CO₂ frac scenario.

In light of the high current costs of carbon capture from power generation, we assume that CO₂ is sourced from industrial processes that co-produce nearly-pure CO₂ streams (Middleton et al., 2015b). As such the marginal burdens of capturing and supplying this by-product CO₂ are driven by the compression energy required to pressurize CO₂ to storage and transport conditions (2 MPa) (Middleton et al., 2014). Facility-scale data provided by the EPA’s GHG Reporting Program was processed to locate ethanol, hydrogen, and natural gas processing facilities serving as likely CO₂ suppliers in the Marcellus region as detailed further in Appendix B (Middleton et al., 2014). Given that CO₂ is not yet broadly deployed and the Marcellus lacks dedicated pipeline infrastructure, we assume CO₂ is trucked to the site. We recognize that additional sources (e.g.

power plants) may be necessary to meet capacity demands with widespread application of CO₂-based fracturing.

4.2.5. Blending and fracturing

Booster pumps and a standard blending unit are applied in the slickwater frac for proppant blending prior to injection, while CO₂ requires either a pressurized batch system capable of sustaining each stage through completion (Campbell et al., 2000) or a continuous high-pressure feed stream. Here, blending is modeled as a liquid CO₂ eductor jet continuously feeding proppant into the pressurized system based on one emerging industrial process (Scharmach et al., 2015). Hydraulic fracturing fluids deliver pressures (45.2 MPa used in our analysis) (Jacot et al., 2010) required to overcome the combination of lithostatic overburden pressure and shale yield stress to generate fractures. A representative thermal gradient of 25°C/km is applied and fluid densities governing hydrostatic pressures are calculated for water and CO₂ at both the wellhead and downhole (NIST, 2016). Applying these physical conditions, pumping energy for injection via high-pressure positive displacement pumps is calculated using a modified Colebrook-White equation, where total pressurization is calculated from the formation fracture pressure, hydrostatic pressure, and frictional losses (Sonnad and Goudar, 2006). Note that CO₂ requires higher surface injection pressures than water due to its lower density, which reduces hydrostatic head. We also account for differences in fluid viscosities and reduced frictional losses with slickwater.

4.2.6. Flowback and production

Following water frac well completions, we assume gas is flared for two days with 99% efficiency before pipeline quality natural gas is achieved and the well transitions to production, per industry-best practices. For all scenarios, flared gas is considered both a GHG emission and direct energy loss. Flowback waters are reused at successive frac sites and assumed to be disposed

of at a centralized waste treatment facility after 10 injection cycles. In contrast to flowback, produced waters are not recycled due to low intermittent flow volumes and are transported directly to treatment. On-site separation at the wellhead and subsequent dehydration to prepare gas for pipeline transport continue throughout the production life of a well, but had negligible impact relative to other inputs.

The flowback phase in CO₂-based fracturing operations is modeled here using data from demonstration projects and from conversations with field engineers. Figure 4-2 illustrates the hypothetical flows of CO₂ and CH₄ in flowback, separation, and production processes applied to both CO₂ frac scenarios. Due to the dry nature of the Marcellus, produced liquids are assumed to be negligible compared to flowback gases and treatment is not considered. Immediately after completion, gas streams are flared over a three-day period as CO₂ levels decline from 100% in the first day to the 40% threshold currently required to commence separation and treatment (Campbell et al., 2000). Membrane separation was selected as the current state of the art process for removing CO₂ from CH₄ streams with low levels of liquid hydrocarbons (Reynolds et al., 2014; Zhang et al., 2013). The present model assumes three days for flaring prior to separation as recommended by industry experts. As membranes and other technologies advance, limitations due to mixed fluid quality and the associated requirement to initially vent both CH₄ and CO₂ could be reduced. Mobile service providers specializing in emerging separation technologies will be important in this regard. This separation stage continues for 12 days, at which point we assume CO₂ levels have reached the 2% pipeline quality standard for transport to downstream gas processing (Campbell et al., 2000). Dehydration is only included for this initial 12-day separation period due to the dry nature of the Marcellus and lack of injected water in a CO₂ frac. In the base case, CO₂ recovered during

separation is vented. In the outlook case, this CO₂ is recompressed and reused at subsequent frac sites over 10 injection cycles.

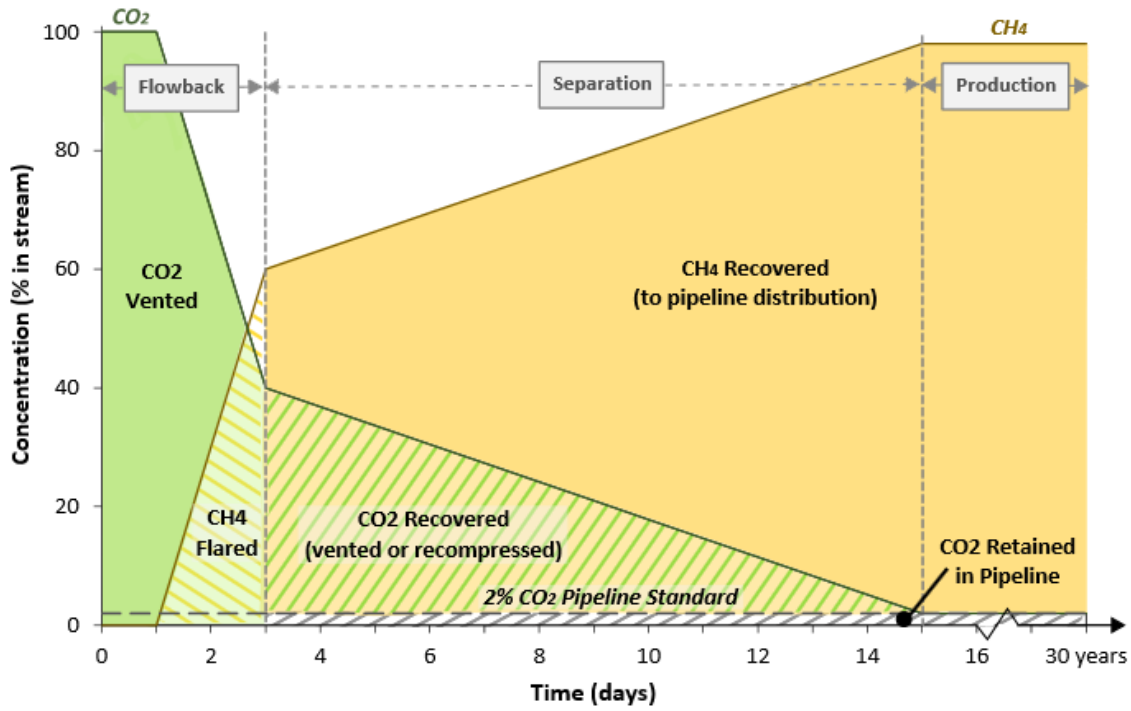


Figure 4-2: Concentration profile of CO₂ and CH₄ returned during flowback, separation, and production following well completions with liquid CO₂.

4.2.7. Allocation

The marginal approach used to estimate the impacts of CO₂ supply is consistent with studies (Middleton et al., 2014; Middleton et al., 2015a) demonstrating that mass- and economic-based allocations between primary and co-products can significantly overestimate life cycle burdens. Because CO₂ co-produced at the industrial facilities considered here would otherwise be vented to the atmosphere without an economically viable end use, we neglect CO₂ emitted during well operations as a GHG impact. We recognize this assumption may change as a result of full CO₂ utilization in the future. Thus, the 3% losses in CO₂ transport and storage and CO₂ vented or flared

in separation do not contribute to life cycle GHG emissions. By extension, any CO₂ that is permanently sequestered is credited to the CO₂ frac as a negative GHG emission.

4.2.8. Life cycle modeling and impact assessment

Process-based LCA models for each scenario were developed in Microsoft Excel with the Crystal Ball plug-in suite. Key model inputs are summarized in Table 4-1. Where applicable, input parameters were modeled stochastically as distributions in Crystal Ball to account for uncertainties and variations in data. Monte Carlo analyses were performed to generate impact distributions and evaluate model sensitivity to input uncertainties. Our full models are available for download on the ACS website along with the supporting information document.

Table 4-1: Summary of major input parameters. Stochastic inputs modeled as uniform or triangular distributions are reported as the median or likely values respectively followed by the ranges considered here.

Input	Units	Water frac	CO₂ frac, base	CO₂ frac, outlook
Estimated ultimate recovery (EUR)	GJ	4.98E+6	7.64E+6	2.67E+7
Production increase factor (PIF)	%	--	50 (0-110)	200 (50-1340)
Total fluid volume per well	m ³	9.09E+4	6.36E+4	6.04E+4
Volume of gas flared	m ³	1.03E+4	1.68E+5	1.60E+5
Flowback (% of injected fluid)	%	7 (4-47)	70 (50-90)	50 (10-90)
Produced water volume per well	m ³	1.76E+4	--	--
Truck trips per well	--	1206	3269	3036
Diesel fuel consumption	m ³	626	985	950
CO₂ compression energy (source)	MJ/tCO ₂	--	241 (72-285)	241 (72-285)

Note: Distributions and assumptions associated with stochastic inputs are detailed in the Supporting Information

Impact data for unit processes (e.g. diesel and chemical production) were obtained from the EcoInvent 2.2 database (Weidema, 2010) where applicable along with external sources for region-specific processes. Energy use is expressed as MJ of energy consumed per GJ of energy produced.

GHG emissions are converted to kgCO₂eq per the 2007 IPCC AR4 100-year global warming potential protocols (IPCC, 2007). Consumptive water use is defined as water displaced from its original source (i.e. a net loss of water availability in the watershed of origin) (Graham et al., 2015) reported in L/GJ.

4.3. Results and discussion

4.3.1. Life cycle burdens

Life cycle impacts for Energy Consumption, GHG Emissions, and Water Consumption for each of the three fracturing scenarios are summarized in Figure 4-3. Additional details including a breakdown of result by process and the full excel model are provided in the supporting information. In spite of increased energy production in the CO₂ base case, the net energy impact remains 44% greater (0.86 MJ/GJ) than for the water-based frac. This is the result of CO₂ specific processes including compression and separation at the source, energy losses for flaring, and the incremental truck trips required for transporting CO₂. In the CO₂ outlook case, CO₂ achieves a 67% reduction (-1.32 MJ/GJ) in net energy impact relative to the water-based frac largely due to a significant increase in energy production. Energy impacts for both CO₂ scenarios are dominated by fluid sourcing (nearly 45%), whereas the water-based scenario is dominated by high pressure blending and fracturing. These differences suggest reducing energy impacts will require unique approaches for each fluid. Trucking energy impacts are similar for both fluids (estimated at 10%), with CO₂ fluid sourcing and produced water transport dominating impacts for their respective fluids.

While increased energy demands and associated costs are limiting factors from the industry's perspective, CO₂ provides notable environmental benefits with respect to GHG emission reductions. In both cases, CO₂ achieved net carbon offsets driven by sequestered CO₂ that preferentially sorbs to organic surfaces within the shale.⁵⁵ The greater net credit achieved in

the base case compared to the outlook is primarily the result of a lower EUR which magnifies the credit. Note that while the outlook case considers reuse of captured CO₂ at the wellhead to reduce sourcing burdens in subsequent fracs, we do not consider end-of-life reinjection for sequestration credit. This CO₂ mass (715 tCO₂) allocated across 10 wellheads amounts to only 0.1% of the total injected CO₂ (60,808 tCO₂) or 0.2% of sequestered CO₂ (30,404 tCO₂), providing little justification for capital investment in transport and injection in dedicated wells. Low fractions of CO₂ recovered during separation relative to injection requirements along with challenges in logistical coordination for reuse will likely motivate direct venting as standard practice in the short term (as assumed in the base case), but sourcing limitations may compel reuse in close proximity wellheads.

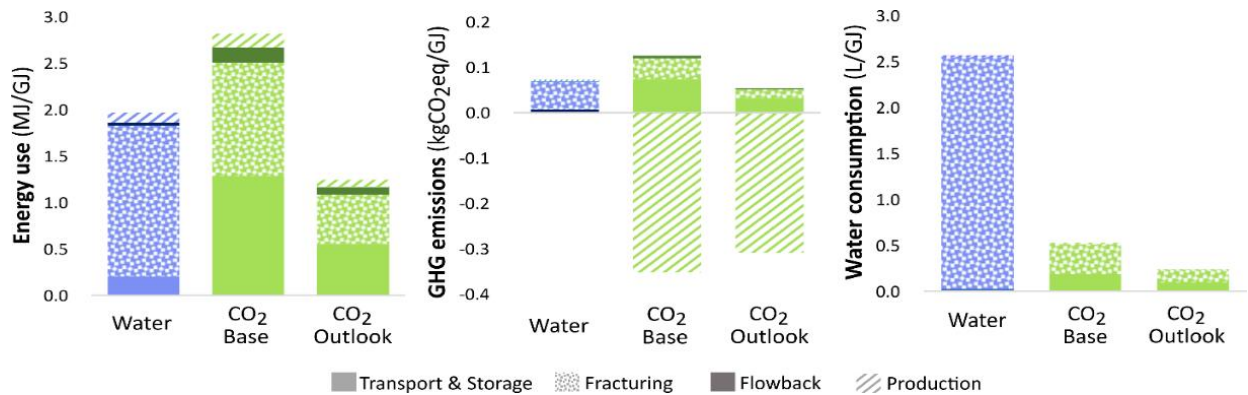


Figure 4-3: Life cycle energy use, greenhouse gas emissions, and consumptive water use associated with the production of a functional unit of energy (1 GJ) from a Marcellus shale gas well under three fracturing fluid scenarios.

Predictably, water use for a slickwater frac is dominated by direct consumption for hydraulic fracturing. This water loss is particularly pronounced in the Marcellus Shale, as capillary imbibition leads to low water recoveries in flowback and production. Consumptive water use for CO₂-based fluids is tied to energy production for initial compression and fracturing. Overall, the fracturing process itself dominates all impacts for water-based fluids, while CO₂ impacts are driven

by equal contributions from pumping and CO₂ acquisition for energy, pumping and proppant for water use, and by storage credits for GHGs. CO₂-based fluids likely have greater upside for future impact reductions (by targeting CO₂ sourcing and transport) given the maturity of water-based fracturing fluid formulation and application.

4.3.2. Key impact drivers

Tornado plots are presented in Figure 4-4 to evaluate model sensitivity by identifying critical inputs using relative sensitivity (percentage deviation, $\pm 10\%$). Absolute sensitivity (percentile of the variables, 10-90%) was also carried out and these suggest that uncertainty in input data distributions (particularly electricity and PIF) is an important consideration for the less mature CO₂ scenarios. These results are included in the SI.

Evaluation with respect to $\pm 10\%$ changes in life cycle inventory parameters reveals how impact sensitivities may change once further development in CO₂ fracturing allows more explicit definition of data input ranges. Because of the greater level of certainty in modeling a water-based frac, input variations elicit smaller changes in outputs compared to CO₂. For all three scenarios, model outputs are generally most affected by small changes in total fluid volumes required per stage, which drives pumping, sourcing, and transport impacts. Slickwater results are predictably most sensitive to sourced fluid volume. GHG emissions for CO₂-based fluids are governed by flowback fractions as expected, which dictate quantities sequestered as carbon offsets. Overall, results for CO₂-based fluids exhibit greater sensitivity than slickwater for the same percent deviation in inputs. Notably, CO₂ results in net GHG offsets under both sensitivity approaches even for “worst-case” scenarios. These coupled analyses reveal that relative model sensitivity is governed by sourced fluid and flowback volumes, while PIF estimates dominate absolute sensitivity for CO₂-based fluids due to considerable uncertainties reflected in the distributions.

Further research refining PIF projections is crucial to reduce the current risks that disincentivize operators to develop CO₂ processes beyond existing first-generation trials. Improved flowback characterization and more definitive identification of CO₂ sourcing options will further reduce uncertainties surrounding CO₂ fracs.

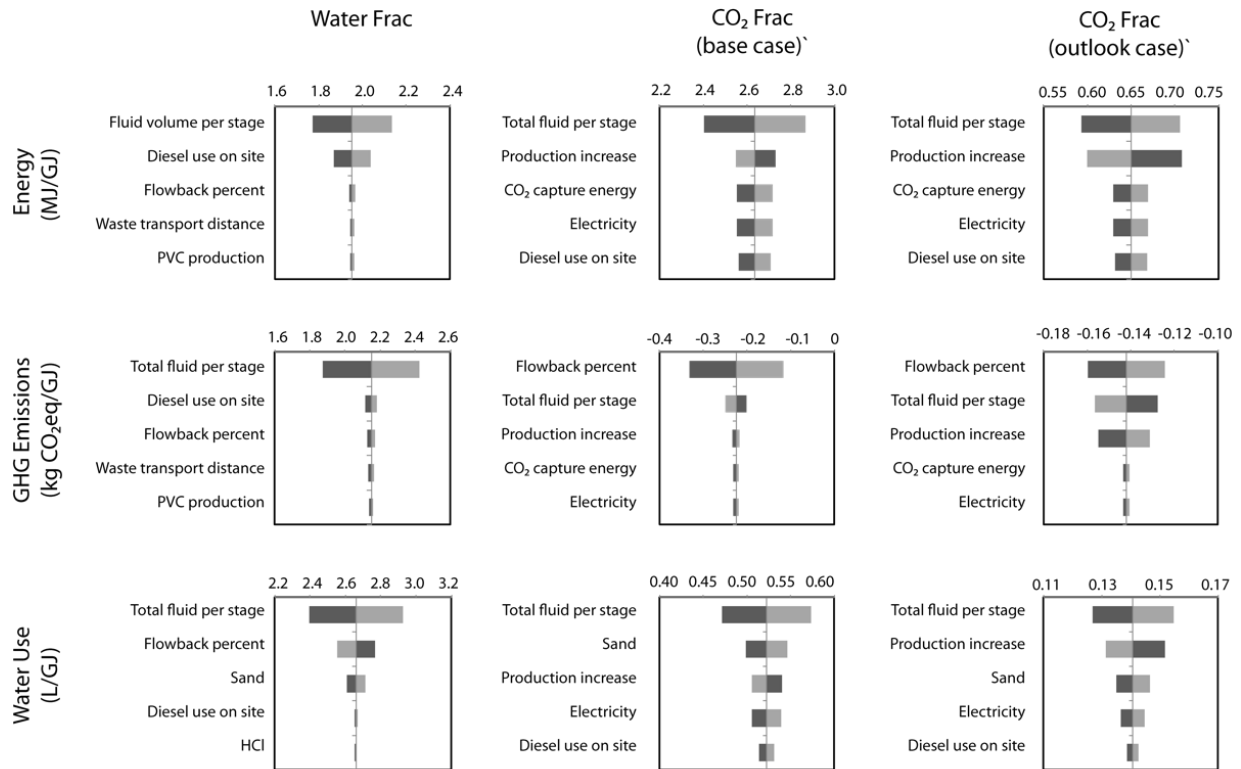


Figure 4-4: Tornado plots revealing the sensitivity of each impact to stochastic model inputs for three fracturing fluid scenarios. Centerlines represent the base case, while light and dark bars consider variations of ±10% of input distributions.

4.3.3. Environmental implications

Many of the environmental impacts associated with hydraulic fracturing are driven by the demand for water. The use of non-aqueous working fluids could reduce these impacts, particularly if the significant increases in energy production are achieved leading to fewer new wells drilled. Transitioning to a CO₂-based system avoids high-volume surface and groundwater extractions and further minimizes active fluid management over the well’s lifetime, which is conventionally

governed by produced water storage, transport and treatment at the wellhead. CO₂-based systems may mitigate the growing concern for seismic risk associated with water disposal via injection wells in water-based fracturing. Even though it was outside the scope of this study, reductions in gas stream water content could also eliminate conditioning in downstream pipelines as a result. The use of water as a fracturing fluid also enables the transport of naturally occurring radionuclides and salts to the surface. Non-polar CO₂ limits the transport of polar solutes and reduces the potential volume for flowback water. CO₂-based fluids are also likely to significantly reduce requirements for chemical additives even though continued developments may dictate the need for the addition of water and surfactants to fine-tune rheology as well as assist in the mixing and transport of other additives (e.g. HCl) for well cleanup.

Replacing water with CO₂-based fracturing fluids can significantly reduce life cycle GHG emissions of conventional fracs by creating a new sink for anthropogenic CO₂. Recent studies have demonstrated that depleted Marcellus shale wells present a viable storage repository, but their small capacities relative to large-scale point-source emissions will likely prove cost-prohibitive in the absence of a carbon market (Tao and Clarens, 2013). Reframing CO₂ as a commodity for fracturing operations could incentivize pipeline and infrastructure developments that would in turn facilitate deployment of carbon capture, utilization, and storage (CCUS) networks. Natural gas is a complex mix of methane and hydrocarbons with only a background level of CO₂ (typically 0.1-1% in the Marcellus⁵⁶). The CO₂ fraction should not be affected by the fracturing fluid choice and so we did not explicitly include any marginal CO₂ emissions tied to natural CO₂ content in our comparison.

The relative advantages of CO₂-based fracs are region-specific. In water-stressed regions where high-volume water withdrawals are technically, socially, or economically constrained, CO₂

offers clear advantages provided CO₂ sources are accessible. Even in areas where water acquisition is less constrained, such as the Marcellus, avoiding the environmental implications of wastewater management favors CO₂-based fluids in many contexts. Public health risks associated with water-based fluids may be weighted more heavily than the economic and environmental impacts of higher energy demands for CO₂.

4.3.4. Social factors

The public resistance to hydraulic fracturing has been driven by concerns over high-volume water withdrawals, drinking water contamination, fugitive methane emissions, seismic events, noise pollution, and truck traffic (Soeder et al., 2014; Vengosh et al., 2014). Although CO₂-based fluids avoid major impacts to water quality and supply, trucking for liquid CO₂ transport could become the most highly visible and socially objectionable issue to local residents. In the case studies considered here, the use of CO₂ increases total truck trips by over 100% compared to water-based fracs. Truck trips during development are not only highly visible, but pose public health risks including links to an increase in the frequency and severity of motor vehicle accidents, as well as particulate emissions from roadways and diesel trucks (Graham et al., 2015). Fine particulate matter (PM_{2.5}) emissions associated with hydraulic fracturing transport operations are outside the scope of this paper, yet represent a growing health burden. The impact of PM_{2.5} emissions will be geographically concentrated along transportation routes near wellheads such that the effect of these emissions is not evenly shared across neighboring communities (McKone et al., 2011; Strogon et al., 2012). While significant performance improvements will reduce drilling and well completions, normalized to energy production, the potential for CO₂-based fluids to reduce trucking volume for a region or a state is unlikely to resonate with a public more connected to local impacts. Mitigating local concerns of water source depletion favor CO₂, but global advantages

(e.g. carbon sequestration) provide little consolation locally in the absence of an economic connection or other means of incentivizing acceptance or offsetting burdens. The disconnect between winners and losers is a typical problem for energy infrastructure and supply as well as other large scale public works projects. This LCA provides a data-driven framework for evaluating alternatives to conventional fracturing processes, potentially addressing local concerns for the continued use of hydraulic fracturing.

4.3.5. Outlook for CO₂

While CO₂ holds promise as an alternative working fluid for shale gas development, this study reveals a suite of social, technical, and environmental trade-offs that must be addressed for effective large-scale deployment. Reducing supply constraints would prove significant for industry adoption of CO₂. Expanding source options to include power generation through targeted policies would improve reliability of and accessibility of CO₂ supplies. Fluid transport accounts for 10% of net energy consumption in a CO₂ frac. Developing regional strategies for CO₂ pipelines could dramatically improve efficiency and reduce local burdens. This important challenge highlights the need for further research to better connect sources and sinks (Middleton, 2013). The short-term demand for CO₂ in fracturing operations necessitates unique pipeline infrastructure capable of transitioning to natural gas transmission, which could help avoid stranded assets. Installation of reversing pipelines, or even co-located parallel pipelines, for CO₂ and natural gas would provide flexibility for fracturing and production as well as long term CCS (Noothout et al., 2014). Advanced pipeline strategies such as these will require coordination between CO₂ sources, field services suppliers, and producers.

Bridging the divide between the status quo and future application of CO₂-based fluids may be a challenge in the short term, as the industry must assume the capital risks of applying

unconventional techniques without a proven track record. Smaller operators in developing shale gas regions may be less capable of absorbing these risks than larger firms. Furthermore, common industry practice of compartmentalizing well development from production may fail to fully link risk and reward (Engelder, 2012b). As energy prices rise over time and the energy return on energy invested (EROI) improves for alternative energy sources, life cycle energy impacts will become more relevant. While outside the scope of this paper, the economic break-even point is a critical factor to incentivize early adopters of this technology. Sensitivity in the model developed here emphasizes a need for future work relating pore size distribution and net capillary blocking for improved understanding of trapping and recovery mechanisms to inform more robust estimates of production rates. Continued research on CO₂-based systems is further motivated by the possibility that hydraulic fracturing creates irrevocable obstructions (e.g. imbibition and formation damage) to the future recovery of stranded gas. Remaining challenges for commercial-scale application include the logistics and economics of sourcing and transporting liquid CO₂; equipment for blending proppants at high pressure; optimizing fluid properties to maintain proppant suspension; and scaling CO₂/CH₄ separation systems. Despite these challenges, the growing reliance on hydraulic fracturing to supply domestic energy needs compels consideration of alternative fluids which advance both shale gas recovery and environmental objectives.

Chapter 5: **Conclusions**

5.1. Conclusions

The growth of unconventional natural gas production in the U.S. enabled by hydraulic fracturing has changed the energy landscape significantly at the same time it has raised environmental concerns. These concerns are centered on (1) water consumption and wastewater disposal; (2) leakage of fracturing fluid and gas into drinking water formations; and (3) the low efficiencies of most fracturing operations. These concerns cannot be addressed without understanding the fate of water in hydraulic fracturing operations. To date, it had generally been assumed that capillary forces generated when fracturing fluid is injected into the porous shale matrix trap some of the gas in the formation. Fracturing fluids are generally designed to have low viscosity to minimize pressure losses downhole and to carry proppants (e.g., sand, used to keep fractured open) during fracturing operations. Little understanding in the literature or in the industry had been focused on the ways in which interfacial forces impact water fate or production. What was known was that most of the water tends to remain in the formation and that most of the gas that was estimated to exist in the shale rock was not being produced over the decades that a well would be in production.

Despite accelerating efforts to study the physicochemical processes governing water fate and transport in shale gas formations our understanding remains limited for a few reasons. First shales are highly isotropic and heterogeneous both chemically and structurally, which can make modeling flow processes challenging. Second, fluid transport through this media involves a number of coupled flow processes including Darcy flow, Fickian diffusion, and Slip Flow. Until recently, the lack of wells drilled for research purposes has confounded efforts to collect data and samples for characterization that would help study the underlying processes governing fluid fate in these formations. This dissertation used core samples and production data from the recently

drilled MSEEL wells to advance a mechanistic understanding of multiphase flow in gas shales. The work made contributions in three areas corresponding to the three core chapters presented here: (1) water fate and transport in shale formations; (2) the impact of using CO₂ as a fracturing fluid and the storage potential of depleted shale formations; and (3) life cycle implications of using no-aqueous fracturing fluids. Conclusions from these studies are as follows:

5.1.1. Water fate and transport

- Most of the water that is injected during fracturing operations remains trapped in the first few centimeters of bulk shale adjacent to the fracture face and the volume of water and the distance it imbibes into the rock is impacted strongly by the wettability of the fracturing fluid.
- At low to intermediate wettability values, the correlation is modest but at higher contact angles, which would be expected in organic-rich kerogen pores, an increase in contact angle will significantly decrease the amount of fracturing fluid that remains trapped in the bulk rock.
- Interfacial processes play an especially important role during natural imbibition (well shut in) suggesting that fracturing fluid wettability should be considered along with the traditional variables (e.g., time and pressure) that are used to design well shut in periods.
- Capillary forces change in the presence or absence of Darcy flow and with water saturation. As a result, time and spatial discretization will affect model results.
- The contact angle data and the simulations show that flow path mineralogy will impact water imbibition/production. This is especially important in organic-rich kerogen pores where the fracturing fluid may achieve non-wetting conditions (e.g., $\Theta > 90^\circ$), which create

negative P_c conditions. Understanding these dynamics requires additional knowledge of in situ flow conditions and modeling of this switch in flow dynamics.

- The movement of fracturing fluid through the shale matrix is more sensitive to residual gas saturation than it is to residual liquid saturation so additional data on the former will support future modeling efforts.
- Upscaling these results is strongly dependent on assumptions about the structure of natural fractures in the bulk shale rock.
- Natural gas production does not appear to be sensitive to fracturing fluid wettability.
- Improved pore connectivity data for shale is needed to understand the extent small pores may block larger pores by capillary forces. While high pressure processes enable Darcy flow to penetrate deeper and transport water to access small pores, this may simply increase capillary blocking of gas which resides beyond those small pores.
- The limited penetration of fracturing fluid in shale results in little risk for fluid migration outside the formation except through actual fracture

5.1.2. Use of CO₂ as a fracturing fluid and storage potential in shale formations

- Interfacial properties impact the consumption and production of fracturing fluids significantly, with little impact on actual gas production in our model using methane as a surrogate for natural gas.
- Increasing NGL concentration, and the CA change with pressure will result in a system which is actually hydrocarbon wetting at different times in the fracturing/production process.

- Our experimental work indicates reduced gas production may occur in shales with high NGL concentrations fractured using aqueous fracturing fluids.
- The dependence of CA on pressure further shows the complexity of this mechanism, as the system wettability for water or gas changes during production as pressure drops.
- This work also expands on other research showing potential fracture complexity using CO₂, and shows the potential benefit otherwise not recognized in modeling.
- We provide insights useful for understanding the conditions under which CO₂ will provide the greatest increase in gas production and potential for CO₂ sequestration.
- This work indicates fracturing with CO₂ in a typical Marcellus shale gas well potentially sequesters 9.76E5-9.98E6 kgCO₂, depending on fracture complexity.
- Combining model outputs for both gas production with spatial GIS data for the Marcellus, we will provide the first mapping to show regions most attractive for CO₂ fracturing to produce gas.
- These methods also support the development of maps for CO₂ sequestration potential using GIS data and baseline model CO₂ sequestration data.

5.1.3. Life cycle comparison of slickwater and CO₂ impacts on water, energy consumption, and GHG emissions

- Life cycle modeling results suggest that CO₂ is a viable alternative to aqueous-based fracturing fluids for reduced GHG emissions due to sequestration and water consumption.
- CO₂ has unique energy requirements for compression and separation (40% of energy impact) which requires more energy production to offset this impact.
- Slickwater is preferred over the base-case CO₂ scenario with only 50% gas production increase.

Source and logistics issues for CO₂ are a concern, and 10% of transportation energy is required for trucking. Separation and re-compression are important not only due to energy impact (6%), but also the need for technical advances in separating CH₄ and CO₂ to eliminate flaring losses and allow recycling.

5.2. Future work

5.2.1. Experimental interfacial measures for natural gas liquids (NGLs) with methane on alternate surfaces and conditions

While the current work provides missing interfacial data for the contact angle of a typical hydraulic fracturing fluid in methane and propane, the need remains for contact angle data for ethane and higher C_x NGL's including butane and pentane. NGL's have been shown to increase water contact angle in methane above a critical wettability threshold (90 degrees), and yet the combined effect of higher C_x NGL's and possibly other condensable gases is unknown. Pressure was also found to have a significant impact on contact angle measures in propane/methane, and these experiments will extend that work for NGL's over a range of well conditions. Previous work focused on shale surfaces and complete data is now needed for organic carbon surfaces matching expected pore path chemistry in shale, particularly as the higher contact angles expected for these surfaces increases potential capillary effects. To inform a full hysteresis model, advancing and receding angle experiments will be necessary for the conditions detailed above. While CO₂ is expected to be miscible in these NGL's, this will be confirmed over the pressure range expected to prepare for comparative analysis of this alternative fracturing fluid. Other than sourcing the additional gases required for this work, the present setup satisfies the experimental requirements. A second automatic syringe pump will streamline this work and provide a means to measure fluid

injection volumes more accurately. The results of the proposed work will provide a better understanding of how NGL's effect interfacial properties in natural gas, and facilitate detailed modeling for different gas compositions in the Marcellus shale.

5.2.2. Model post-fracturing CO₂ injection in a Marcellus well

The opportunity to store CO₂ in depleted gas wells has been studied by others at the pore and full reservoir scale. Performing this analysis in a flow simulation for specific well conditions will connect the fracturing and CO₂ injection processes sequentially, and provide sequestration data not found in the literature. Previous models have determined the fluid saturations of a shale gas well at the end of life with slickwater fracturing, and additional simulations exploring CO₂ fracturing provide new data for sequester from this process. This new modeling will fill in the missing pieces to fully evaluate and compare the impact of gas production processes on ultimate CO₂ sequestration. This study provides a data-driven method to support analysis of different fracturing processes while considering the additional costs and benefits of CO₂.

5.2.3. Experimental water imbibition in surface soils

Reducing nutrient loading to tributaries of the Chesapeake Bay has largely focused on managing sources and surface runoff in targeted watersheds. Fate and transport of both water soluble components and particulates has been the target for much research. However no research has explored the role of interfacial properties between specific soil types and runoff water, nor the impact of surfactants contributed by plants. This provides a unique opportunity for undergraduate research to contribute understanding from (1) experimental contact angle measures for water-based solutions on mineral and organic surfaces representative of different soil types, and (2) laboratory testing to confirm the impact of both soil type and water chemistry on runoff for typical plants and slopes of this region. These tests would be performed using grow panels constructed with defined

soil compositions and plants, and the ability to control slope and the water source/drainage. A key objective of this research will be to further evaluate the change in interfacial properties in runoff water as a function of plant type and plant residue, and determine the impact of this on soil infiltration and runoff rates.

References

Al-Bazali TM, Zhang J, Chenevert ME, Sharma MM. An Experimental Investigation on the Impact of Capillary Pressure, Diffusion Osmosis, and Chemical Osmosis on the Stability and Reservoir Hydrocarbon Capacity of Shales. 2009.

Alpern J, Marone C, Elsworth D, Belmonte A, Connelly P. Exploring the physicochemical processes that govern hydraulic fracture through laboratory experiments 2012.

Apaydin OG, Ozkan E, Raghavan R. Effect of discontinuous microfractures on ultratight matrix permeability of a dual-porosity medium. SPE Reservoir Evaluation & Engineering 2012;15:473-85.

Balashov VN, Engelder T, Gu X, Fantle MS, Brantley SL. A model describing flowback chemistry changes with time after Marcellus Shale hydraulic fracturing Marcellus Shale Hydraulic Fracturing. AAPG Bull 2015;99:143-54.

Bažant ZP, Salviato M, Chau VT, Viswanathan H, Zubelewicz A. Why fracking works. Journal of Applied Mechanics 2014;81:101010.

Berg JC. An introduction to interfaces & colloids: the bridge to nanoscience: World Scientific; 2010.

Bertoncello A, Wallace J, Blyton C, Honarpour M, Kabir C. Imbibition and water blockage in unconventional reservoirs: well management implications during flowback and early production 2014.

Bertrand E, Bonn D, Broseta D, Dobbs H, Indekeu J, Meunier J et al. Wetting of alkanes on water. Journal of Petroleum Science and Engineering 2002;33:217-22.

Bethel F, Calhoun JC. Capillary desaturation in unconsolidated beads. J Pet Technol 1953;5:197-202.

Birdsell DT, Rajaram H, Dempsey D, Viswanathan HS. Hydraulic fracturing fluid migration in the subsurface: a review and expanded modeling results. Water Resour Res 2015a;51:7159-88.

Birdsell DT, Rajaram H, Lackey G. Imbibition of hydraulic fracturing fluids into partially saturated shale. Water Resour Res 2015b;51:6787-96.

Blake T, De Coninck J. The influence of pore wettability on the dynamics of imbibition and drainage. Colloids Surf Physicochem Eng Aspects 2004;250:395-402.

Blunt MJ. Pore level modeling of the effects of wettability. SPE Journal 1997;2:494-510.

- Bocquet L, Charlaix E. Nanofluidics, from bulk to interfaces. *Chem Soc Rev* 2010;39:1073-95.
- Bonn D, Eggers J, Indekeu J, Meunier J, Rolley E. Wetting and spreading. *Reviews of modern physics* 2009;81:739.
- Boyce ML, Carr TR. Lithostratigraphy and petrophysics of the Devonian Marcellus interval in West Virginia and southwestern Pennsylvania. *T.Carr* 2009:254-81.
- Burke LH, Nevison GW. Improved Hydraulic Fracture Performance with Energized Fluids: A Montney Example. Proceedings of the CSPG/CSEWG/CWLS GeoConvention, Calgary, Alberta, Canada May 9-11, 2011.
- Byrnes AP. Role of induced and natural imbibition in frac fluid transport and fate in gas shales. for the Hydraulic Fracturing Study: Fate and Transport 2011:70.
- Byrnes AP. Issues With Gas And Water Relative Permeability In Low-Permeability Sandstones 2005a.
- Byrnes AP. Permeability, capillary pressure, and relative permeability properties in low-permeability reservoirs and the influence of thin, high-permeability beds on production 2005b.
- Calderón AJ, Guerra OJ, Papageorgiou LG, Sirola JJ, Reklaitis GV. Preliminary evaluation of shale gas reservoirs: Appraisal of different well-pad designs via performance metrics. *Ind Eng Chem Res* 2015;54:10334-49.
- Campbell S, Fairchild Jr N, Arnold D. Liquid CO₂ and sand stimulations in the lewis shale, San Juan Basin, New Mexico: A case study 2000.
- Chakraborty N, Karpyn Z, Liu S, Yoon H. Permeability evolution of shale during spontaneous imbibition. *Journal of Natural Gas Science and Engineering* 2017;38:590-6.
- Cheng Y. Impact of water dynamics in fractures on the performance of hydraulically fractured wells in gas-shale reservoirs. *J Can Pet Technol* 2012;51:143-51.
- Clark CE, Horner RM, Harto CB. Life cycle water consumption for shale gas and conventional natural gas. *Environ Sci Technol* 2013;47:11829-36.
- Clarkson C, Haghshenas B, Ghanizadeh A, Qanbari F, Williams-Kovacs J, Riazi N et al. Nanopores to megafactures: Current challenges and methods for shale gas reservoir and hydraulic fracture characterization. *Journal of Natural Gas Science and Engineering* 2016;31:612-57.
- Clarkson C, Jensen J, Chipperfield S. Unconventional gas reservoir evaluation: What do we have to consider?. *Journal of Natural Gas Science and Engineering* 2012;8:9-33.

Cole DR, Ok S, Striolo A, Phan A. Hydrocarbon behavior at nanoscale interfaces. *Reviews in Mineralogy and Geochemistry* 2013;75:495-545.

Dale AT, Khanna V, Vidic RD, Bilec MM. Process based life-cycle assessment of natural gas from the Marcellus Shale. *Environ Sci Technol* 2013;47:5459-66.

De Gennes P. Wetting: statics and dynamics. *Reviews of modern physics* 1985;57:827.

Dehghanpour H, Lan Q, Saeed Y, Fei H, Qi Z. Spontaneous imbibition of brine and oil in gas shales: effect of water adsorption and resulting microfractures. *Energy Fuels* 2013;27:3039-49.

Dehghanpour H, Zubair H, Chhabra A, Ullah A. Liquid intake of organic shales. *Energy Fuels* 2012;26:5750-8.

Dobson P, Houseworth J. *Inventory of Shale Formations in the US, Including Geologic, Geochemical, Hydrological, Mechanical, and Thermal Characteristics* 2014.

DOE. *Modern shale gas development in the United States: A primer*. Office of Fossil Energy and National Energy Technology Laboratory, United States Department of Energy 2009.

DOE USEIA. *Drilling Productivity Report*. DOE, US Energy Information Administration 2016.

Dominguez-Faus R, Powers SE, Burken JG, Alvarez PJ. The water footprint of biofuels: A drink or drive issue?. *Environ Sci Technol* 2009;43:3005-10.

Edwards RW, Doster F, Celia MA, Bandilla KW. Numerical Modeling of Gas and Water Flow in Shale Gas Formations with a Focus on the Fate of Hydraulic Fracturing Fluid. *Environ Sci Technol* 2017a;51:13779-87.

Edwards RW, Doster F, Celia MA, Bandilla KW. Numerical Modeling of Gas and Water Flow in Shale Gas Formations with a Focus on the Fate of Hydraulic Fracturing Fluid. *Environ Sci Technol* 2017b;51:13779-87.

Engelder T, Cathles LM, Bryndzia LT. The fate of residual treatment water in gas shale. *Journal of Unconventional Oil and Gas Resources* 2014;7:33-48.

Engelder T. Capillary tension and imbibition sequester frack fluid in Marcellus gas shale. *Proc Natl Acad Sci U S A* 2012a;109:E3625; author reply E3626.

Engelder T. Capillary tension and imbibition sequester frack fluid in Marcellus gas shale. *Proc Natl Acad Sci U S A* 2012b;109:E3625; author reply E3626.

Ferrar KJ, Michanowicz DR, Christen CL, Mulcahy N, Malone SL, Sharma RK. Assessment of effluent contaminants from three facilities discharging Marcellus Shale wastewater to surface waters in Pennsylvania. *Environ Sci Technol* 2013;47:3472-81.

Flewelling SA, Sharma M. Constraints on upward migration of hydraulic fracturing fluid and brine. *Groundwater* 2014;52:9-19.

Gale JF, Holder J. Natural fractures in some US shales and their importance for gas production 2010;7:1131-40.

Gale JF, Laubach SE, Olson JE, Eichhubl P, Fall A. Natural fractures in shale: A review and new observations. *Natural Fractures in Shale: A Review and New Observations. AAPG Bull* 2014;98:2165-216.

Gan Q, Elsworth D, Alpern J, Marone C, Connolly P. Breakdown pressures due to infiltration and exclusion in finite length boreholes. *Journal of Petroleum Science and Engineering* 2015;127:329-37.

Gao Z, Hu Q. Initial water saturation and imbibition fluid affect spontaneous imbibition into Barnett shale samples. *Journal of Natural Gas Science and Engineering* 2016;34:541-51.

Gaurav A, Dao E, Mohanty K. Evaluation of ultra-light-weight proppants for shale fracturing. *Journal of Petroleum Science and Engineering* 2012;92:82-8.

Gensterblum Y, Ghanizadeh A, Cuss RJ, Amann-Hildenbrand A, Krooss BM, Clarkson CR et al. Gas transport and storage capacity in shale gas reservoirs—A review. Part A: Transport processes. *Journal of Unconventional Oil and Gas Resources* 2015;12:87-122.

Ghanbari E, Dehghanpour H. The fate of fracturing water: A field and simulation study. *Fuel* 2016;163:282-94.

Graham J, Irving J, Tanga X, Sellers S, Crisp J, Horwitz D et al. D. 2015. Increased traffic accident rates associated with shale gas drilling in Pennsylvania. *Accident Analysis and Prevention* 2015;74:203-9.

Gupta D. *Unconventional Fracturing Fluids for Tight Gas Reservoirs* 2009.

Gupta D, Bobier D. The history and success of liquid CO₂ and CO₂/N₂ fracturing system. *SPE* 1998;40016:15-8.

Hamdi Z, Awang M. CO₂ Minimum Miscibility Pressure Determination of Pure Hydrocarbons in Different Temperatures Using Slimtube Simulations. *Research Journal of Applied Sciences, Engineering and Technology* 2014;7:3159-63.

Handy L. Determination of effective capillary pressures for porous media from imbibition data 1960.

Hayes T. Sampling and analysis of water streams associated with the development of Marcellus shale gas. *Marcellus Shale Initiative Publications Database* 2009;10.

- He L, Feng W, ZHANG J, Siwei M, Yongwei D. Fracturing with carbon dioxide: Application status and development trend. *Petroleum Exploration and Development* 2014;41:513-9.
- Heath GA, O'Donoghue P, Arent DJ, Bazilian M. Harmonization of initial estimates of shale gas life cycle greenhouse gas emissions for electric power generation. *Proc Natl Acad Sci U S A* 2014;111:E3167-76.
- Hudson JD, Civan F, Michel G, Devegowda D, Sigal RF. Modeling multiple-porosity transport in gas-bearing shale formations 2012.
- Hyman JD, Jimenez-Martinez J, Viswanathan HS, Carey JW, Porter ML, Rougier E et al. Understanding hydraulic fracturing: a multi-scale problem. *Philos Trans A Math Phys Eng Sci* 2016;374:10.1098/rsta.2015.0426.
- IPCC. Climate Change 2007: Synthesis Report. Contribution of Working Groups I, II and III to the Fourth Assessment Report of the Intergovernmental Panel on Climate Change [Core Writing Team, Pachauri, R.K and Reisinger, A. (eds.)]. IPCC, Geneva, Switzerland 2007.
- Ishida T, Aoyagi K, Niwa T, Chen Y, Murata S, Chen Q et al. Acoustic emission monitoring of hydraulic fracturing laboratory experiment with supercritical and liquid CO₂. *Geophys Res Lett* 2012;39.
- Jacot RH, Bazan LW, Meyer BR. Technology Integration: A Methodology to Enhance Production and Maximize Economics in Horizontal Marcellus Shale Wells 2010.
- Jessop PG, Leitner W. Chemical synthesis using supercritical fluids: John Wiley & Sons; 2008.
- Jia Y, Lu Y, Elsworth D, Fang Y, Tang J. Surface characteristics and permeability enhancement of shale fractures due to water and supercritical carbon dioxide fracturing. *Journal of Petroleum Science and Engineering* 2018;165:284-97.
- Kanfar M, Alkough AB, Wattenbarger RA. Modeling Guidelines for Analyzing and Forecasting Shale Well Performance 2013.
- Kang SM, Fathi E, Ambrose RJ, Akkutlu IY, Sigal RF. Carbon dioxide storage capacity of organic-rich shales. *Spe Journal* 2011;16:842-55.
- Keating K, Sun Y, Dai Z, Zheng L, Bacon D. Code Verification and Confidence-building. U S Department of Energy, Groundwater Working Group 2013.
- King G. Hydraulic fracturing 101: what every representative, environmentalist, regulator, reporter, investor, university researcher, neighbor and engineer should know about estimating frac risk and improving frac performance in unconventional gas and oil wells 2012a.

King GE. Hydraulic fracturing 101: what every representative, environmentalist, regulator, reporter, investor, university researcher, neighbor and engineer should know about estimating frac risk and improving frac performance in unconventional gas and oil wells 2012b.

Kumar H, Elsworth D, Mathews J, Marone C. Permeability evolution in sorbing media: analogies between organic-rich shale and coal. *Geofluids* 2016;16:43-55.

Laurenzi IJ, Jersey GR. Life cycle greenhouse gas emissions and freshwater consumption of Marcellus shale gas. *Environ Sci Technol* 2013;47:4896-903.

Lawrence Berkeley National Laboratory. TOUGH2 EOS7C.

Lawson R, Lyons B, Lyman J, Carstei M. Fueling America and the Energy Water Nexus. The Atlantic Council 2012.

Leverett M. Capillary behavior in porous solids. *Transactions of the AIME* 1941;142:152-69.

Li J, Sultan AS. Klinkenberg slippage effect in the permeability computations of shale gas by the pore-scale simulations. *Journal of Natural Gas Science and Engineering* 2017;48:197-202.

Li X, Feng Z, Han G, Elsworth D, Marone C, Saffer D et al. Breakdown pressure and fracture surface morphology of hydraulic fracturing in shale with H₂O, CO₂ and N₂. *Geomechanics and Geophysics for Geo-Energy and Geo-Resources* 2016;2:63-76.

Lillies AT, King SR. Sand fracturing with liquid carbon dioxide 1982.

Liu L, Zhu W, Wei C, Elsworth D, Wang J. Microcrack-based geomechanical modeling of rock-gas interaction during supercritical CO₂ fracturing. *Journal of Petroleum Science and Engineering* 2018;164:91-102.

Lucas R. Rate of capillary ascension of liquids. *Kolloid Z* 1918;23:15-22.

Lutz BD, Lewis AN, Doyle MW. Generation, transport, and disposal of wastewater associated with Marcellus Shale gas development. *Water Resour Res* 2013;49:647-56.

Makhanov K, Habibi A, Dehghanpour H, Kuru E. Liquid uptake of gas shales: A workflow to estimate water loss during shut-in periods after fracturing operations. *Journal of Unconventional Oil and Gas Resources* 2014;7:22-32.

Makhanov K, Dehghanpour H, Kuru E. An experimental study of spontaneous imbibition in Horn River shales 2012.

March R, Doster F, Geiger S. Accurate early-time and late-time modeling of countercurrent spontaneous imbibition. *Water Resour Res* 2016;52:6263-76.

Marder M, Chen C, Patzek T. Simple models of the hydrofracture process. *Physical Review E* 2015;92:062408.

Mauter MS, Palmer VR. Expert elicitation of trends in marcellus oil and gas wastewater management. *J Environ Eng* 2014;140:B4014004.

Mazza RL. Field testing & optimization of CO₂/sand fracturing technology. 2004.

McKone T, Nazaroff W, Berck P, Auffhammer M, Lipman T, Torn M et al. Grand challenges for life-cycle assessment of biofuels. *Environ Sci Technol* 2011;45:1751-6.

MCOR PSU. Marcellus shale gas maps;2018.

McWhorter DB, Sunada DK. Exact integral solutions for two-phase flow. *Water Resour Res* 1990;26:399-413.

Middleton RS. A new optimization approach to energy network modeling: anthropogenic CO₂ capture coupled with enhanced oil recovery. *Int J Energy Res* 2013;37:1794-810.

Middleton RS, Carey JW, Currier RP, Hyman JD, Kang Q, Karra S et al. Shale gas and non-aqueous fracturing fluids: Opportunities and challenges for supercritical CO₂. *Appl Energy* 2015a;147:500-9.

Middleton RS, Clarens AF, Liu X, Bielicki JM, Levine JS. CO₂ deserts: Implications of existing CO₂ supply limitations for carbon management. *Environ Sci Technol* 2014;48:11713-20.

Middleton RS, Gupta R, Hyman JD, Viswanathan HS. The shale gas revolution: Barriers, sustainability, and emerging opportunities. *Appl Energy* 2017;199:88-95.

Middleton RS, Levine JS, Bielicki JM, Viswanathan HS, Carey JW, Stauffer PH. Jumpstarting commercial-scale CO₂ capture and storage with ethylene production and enhanced oil recovery in the US Gulf. *Greenhouse Gases: Science and Technology* 2015b;5:241-53.

Mirchi V, Saraji S, Goual L, Piri M. Dynamic interfacial tension and wettability of shale in the presence of surfactants at reservoir conditions. *Fuel* 2015;148:127-38.

Mohammadmoradi P, Kantzas A. Wettability and Capillary Imbibition in Shales; Analytical and Data-Driven Analysis 2018.

Myers T. Potential Contaminant Pathways from Hydraulically Fractured Shale to Aquifers. *Ground Water* 2012;50:872-82.

Naar J, Wygal R, Henderson J. Imbibition relative permeability in unconsolidated porous media. *Society of Petroleum Engineers Journal* 1962;2:13-7.

Naik S, You Z, Bedrikovetsky P. Rate enhancement in unconventional gas reservoirs by wettability alteration. *Journal of Natural Gas Science and Engineering* 2015;26:1573-84.

Nature Editors. Code Check. *Nature* 2018;555 (March 18, 2018).

NIST. Thermophysical properties of fluid systems. US Department of Commerce, National Institute of Standards and Technology. 2016;2016.

Noothout P, Wiersma F, Hurtado O, Macdonald D, Kemper J, van Alphen K. CO₂ Pipeline Infrastructure—Lessons Learnt. *Energy Procedia* 2014;63:2481-92.

Oldenburg C, Law D, Le Gallo Y, White S. -Mixing of CO₂ and CH₄ in Gas Reservoirs: Code Comparison Studies 2003:443-8.

Oldenburg C, Law D, Le Gallo Y, White S. Mixing of CO₂ and CH₄ in gas reservoirs: code comparison studies. Lawrence Berkeley National Laboratory 2002.

O'Malley D, Karra S, Currier R, Makedonska N, Hyman J, Viswanathan H. Where does water go during hydraulic fracturing?. *Groundwater* 2016;54:488-97.

Pagels M, Hinkel JJ, Willberg DM. Measuring capillary pressure tells more than pretty pictures 2012.

Patzek TW, Male F, Marder M. Gas production in the Barnett Shale obeys a simple scaling theory. *Proc Natl Acad Sci U S A* 2013;110:19731-6.

Pei P, Ling K, He J, Liu Z. Shale gas reservoir treatment by a CO₂-based technology. *Journal of Natural Gas Science and Engineering* 2015;26:1595-606.

Pruess K. The TOUGH codes—a family of simulation tools for multiphase flow and transport processes in permeable media. *Vadose Zone Journal* 2004;3:738-46.

Pruess K. TOUGH2-A general-purpose numerical simulator for multiphase fluid and heat flow 1991.

Pruess K, García J, Kavscek T, Oldenburg C, Rutqvist J, Steefel C et al. Code intercomparison builds confidence in numerical simulation models for geologic disposal of CO₂. *Energy* 2004;29:1431-44.

Rahm BG, Riha SJ. Evolving shale gas management: water resource risks, impacts, and lessons learned. *Environmental Science: Processes & Impacts* 2014;16:1400-12.

Rassenfoss S. From flowback to fracturing: water recycling grows in the Marcellus Shale. *J Pet Technol* 2011;63:48-51.

- Ren W, Li G, Tian S, Sheng M, Yang R, Wang T. Comparison of capillary pressure-saturation models for gas-water systems in shale gas reservoirs 2016.
- Reynolds M, Bachman R, Peters W. A Comparison of the Effectiveness of Various Fracture Fluid Systems Used in Multistage Fractured Horizontal Wells: Montney Formation, Unconventional Gas 2014.
- Ribeiro L, Sharma M. Fluid selection for energized fracture treatments 2013a.
- Ribeiro L, Sharma M. Fluid selection for energized fracture treatments 2013b.
- Ribeiro L, Sharma M. Fluid selection for energized fracture treatments 2013c.
- Rodriguez RS, Soeder DJ. Evolving water management practices in shale oil & gas development. *Journal of Unconventional Oil and Gas Resources* 2015;10:18-24.
- Roshan H, Andersen M, Rutledge H, Marjo C, Acworth R. Investigation of the kinetics of water uptake into partially saturated shales. *Water Resour Res* 2016;52:2420-38.
- Rowan E, Engle M, Kirby C, Kraemer T. Radium content of oil-and gas-field produced waters in the northern Appalachian Basin (USA)—Summary and discussion of data. *US Geological Survey Scientific Investigations Report* 2011;5135:2011.
- Roy S, Raju R, Chuang HF, Cruden BA, Meyyappan M. Modeling gas flow through microchannels and nanopores. *J Appl Phys* 2003;93:4870-9.
- Roychaudhuri B, Tsotsis TT, Jessen K. An experimental investigation of spontaneous imbibition in gas shales. *Journal of Petroleum Science and Engineering* 2013;111:87-97.
- Rozell DJ, Reaven SJ. Water Pollution Risk Associated with Natural Gas Extraction from the Marcellus Shale. *Risk Analysis* 2012;32:1382-93.
- Scharmach W, Dalton D, Panuccio GJ. Control system and apparatus for delivery of a non-aqueous fracturing fluid 2015.
- Sharma M, Agrawal S. Impact of liquid loading in hydraulic fractures on well productivity 2013.
- Singh H. A critical review of water uptake by shales. *Journal of Natural Gas Science and Engineering* 2016;34:751-66.
- Soeder DJ, Sharma S, Pekney N, Hopkinson L, Dilmore R, Kutchko B et al. An approach for assessing engineering risk from shale gas wells in the United States. *International Journal of Coal Geology* 2014;126:4-19.
- Sonnad JR, Goudar CT. Turbulent flow friction factor calculation using a mathematically exact alternative to the Colebrook–White equation. *J Hydraul Eng* 2006;132:863-7.

Stalder A, Kulik G, Sage D, Barbieri L, Hoffmann P. A snake-based approach to accurate determination of both contact points and contact angles. *Colloids Surf Physicochem Eng Aspects* 2006;286:92-103.

Stalder AF, Melchior T, Müller M, Sage D, Blu T, Unser M. Low-bond axisymmetric drop shape analysis for surface tension and contact angle measurements of sessile drops. *Colloids Surf Physicochem Eng Aspects* 2010;364:72-81.

Strogen B, Horvath A, McKone TE. Fuel miles and the blend wall: Costs and emissions from ethanol distribution in the united states. *Environ Sci Technol* 2012;46:5285-93.

Swindell GS. Marcellus Shale in Pennsylvania: A 2,600 Well Study of Estimated Ultimate Recovery (EUR)–2015 Update. month 2015;1351:1339.

Tanino Y, Blunt M. Laboratory investigation of capillary trapping under mixed-wet conditions. *Water Resour Res* 2013;49:4311-9.

Tao Z, Clarens A. Estimating the carbon sequestration capacity of shale formations using methane production rates. *Environ Sci Technol* 2013;47:11318-25.

U.S. Energy Information Association. *Annual Energy Outlook 2015* 2015.

Van Genuchten MT. A closed-form equation for predicting the hydraulic conductivity of unsaturated soils. *Soil Sci Soc Am J* 1980;44:892-8.

Vengosh A, Jackson RB, Warner N, Darrah TH, Kondash A. A critical review of the risks to water resources from unconventional shale gas development and hydraulic fracturing in the United States. *Environ Sci Technol* 2014.

Vincent O, Szenicer A, Stroock AD. Capillarity-driven flows at the continuum limit. *Soft Matter* 2016;12:6656-61.

Walsh FR, Zoback MD. Oklahoma's recent earthquakes and saltwater disposal. *Science advances* 2015;1:e1500195.

Washburn EW. The dynamics of capillary flow. *Physical review* 1921;17:273.

Weber CL, Clavin C. Life cycle carbon footprint of shale gas: Review of evidence and implications. *Environ Sci Technol* 2012;46:5688-95.

Weidema BP. Ecoinvent data v2.2 2010.

Wilkins R, Menefee AH, Clarens AF. Environmental life cycle analysis of water and CO₂-based fracturing fluids used in unconventional gas production. *Environ Sci Technol* 2016;50:13134-41.

Yethiraj A, Striolo A. Fracking: What Can Physical Chemistry Offer?. *J Phys Chem Lett* 2013;4:687-90.

Yost A, Mazza R, Gehr J. CO₂/Sand fracturing in devonian shales 1993.

Yu W, Sepehrnoori K. Simulation of gas desorption and geomechanics effects for unconventional gas reservoirs. *Fuel* 2014;116:455-64.

Yu W, Wu K, Sepehrnoori K, Xu W. A Comprehensive Model for Simulation of Gas Transport in Shale Formation With Complex Hydraulic-Fracture Geometry. *SPE Reservoir Evaluation & Engineering* 2016.

Zeppieri S, Rodríguez J, López de Ramos A. Interfacial tension of alkane water systems. *Journal of Chemical & Engineering Data* 2001;46:1086-8.

Zhang K, Liu Q, Wang M, Kong B, Lv J, Wu K et al. Investigation of CO₂ Enhanced Gas Recovery in Shale Plays 2016.

Zhang X, Lu Y, Tang J, Zhou Z, Liao Y. Experimental study on fracture initiation and propagation in shale using supercritical carbon dioxide fracturing. *Fuel* 2017;190:370-8.

Zhang Y, Sunarso J, Liu S, Wang R. Current status and development of membranes for CO₂/CH₄ separation: a review. *International Journal of Greenhouse Gas Control* 2013;12:84-107.

Zhou Z, Abass H, Li X, Teklu T. Experimental investigation of the effect of imbibition on shale permeability during hydraulic fracturing. *Journal of Natural Gas Science and Engineering* 2016;29:413-30.

Zhou Z, Hoffman BT, Bearinger D, Li X. Experimental and numerical study on spontaneous imbibition of fracturing fluids in shale gas formation 2014.

Ziemkiewicz P, Quaranta J, Darnell A, Wise R. Exposure pathways related to shale gas development and procedures for reducing environmental and public risk. *Journal of Natural Gas Science and Engineering* 2014;16:77-84.

Zoback MD, Gorelick SM. Earthquake triggering and large-scale geologic storage of carbon dioxide. *Proc Natl Acad Sci U S A* 2012;109:10164-8.

Appendix A

Post-Processing TOUGH2 Output

TOUGH2 simulation outputs are first post-processed using the EXT text script to select and format the desired data columns. Subsequently an R-script reads the EXT file, plotting water saturation and pressure as discretized spatially in TOUGH2. Integrating flows at the interface between element 1 (source/sink block) and adjacent element 2 provides the total flow volumes for liquid and gas phases, again using the R-script. Reported values in TOUGH2 output are for the actual interface between grid blocks and thus represent the average flow between the nodes (centers) of two gridblocks. EXT reports values for the nodes, resulting in an average flow value between the no flow boundary (i.e., 0) and the 2-1 grid block interface. As these values are essentially half of the interfacial flow desired at the 2-1 grid block interface, we multiply all EXT flows given for the source/sink grid block node by two to arrive at the 2-1 interface value. Note this applies to phase flow data, not component fractions which are reported in both TOUGH2 and EXT by node.

Component fractions used in component mass flowrate calculations use the upstream grid block values. Thus, the source grid block (element 1) assigned saturations drive the imbibition calculations. In contrast, when flow is reversed during production element 1 becomes a sink grid block, and element 2 supplies the correct upstream component fractions. With CO₂ assigned to the Xncg (non-condensable gas) field in the TOUGH2 output, the mass equations used to integrate the total flow in R are:

$$CH4(liq) = (XCH4liq)x(FLO liq)$$

$$CO2(liq) = (XNCGliq)x(FLO liq)$$

$$H2O(liq) = (1 - XCH4liq - XNCGliq)x(FLO liq)$$

$$CH4(gas) = (XCH4gas)x(FLO gas)$$

$$CO2(gas) = (XNCGgas)x(FLO gas)$$

$$H2O(gas) = (1 - XCH4gas - XCO2gas)x(FLO gas)$$

Well Production Model : 10M Induced Fracture Spacing

$$=(\text{Model Element Lifetime Flow}) * (\text{Frac Area}) * (2 \text{ Faces/Frac}) * (\# \text{ Intervals}) * (1/\text{gas density at wellhead, 60F 1 atm}) / (\text{ft}^3/\text{m}^3) * 10^9$$

TOUGH Input Variable	Units	TOUGH Inputs		
		Low	Reference	High
IFT	mN/m		59	
Contact Angle			83.1/13.3	
TOC	%		3.2	
VG-M, Pore Size Dist, λ		.3 data fit Imbib	6.15E-01	.5 data fit Drainage
VG-M, 1/Po			4.12E-08	
VG-M, Slr			1.00E-01	
VG-M, Sls			1.01E+00	
VG-M, Sgr			4.75E-01	
Sorption Parameters			in ECBM	
Permeability			4.40E-21	
Porosity			0.10	
Rock Density	kg/m ³		2.74E+03	
Diff Coef, H2O	m ² /s		1E-6 Gas, 1E-10 Liq	
Diff Coef, CH4	m ² /s		1E-6 Gas, 1E-10 Liq	
Klinkenburg, b	1/Pa			
Viscosity				
Fluid Density				
Flowing BHP	Mpa		4	
Interval Spacing		10	20	40
TOUGH Output, CH₄	kg/m ² (30 yr)		26.47	
Physical Scaling Parameters		Scaling Inputs		
		Low	Med	High
Shale Thickness	m	20	50	80
Horizontal Length	m	831	1215	1847
Stages			14	
Interval Spacing	m	10	20	40
# Intervals			61	
Single Fracture Geometry Area	m ²	3.14E+02	9.46E+03	3.06E+04
Total Well Surface Area (no microfractures)	m ²	0.00E+00	1.15E+06	0.00E+00
Microfracture Depth in Fracture Face	cm		1	
Microfracture Width	m		5.0E-06	
Total Well Surface Area (with microfractures)	m ²		7.97E+07	
Marcellus EUR	BCF	0.43	4.34	8.93
Scaling Model CH4 Output	BCF (CH ₄)		1.59	

Conversion Factors				
CH4 Density 60F, 1 atm	kg/m ³		6.79E-01	
CH4 Density 70C, 4 Mpa	kg/m ³		2.37E+01	
BCF/m3 conversion			3.53E-08	
H2O Density 60F, 1 atm	m3/kg		1.000981E-03	
m3/gal conversion			3.78541E-03	

Water Imbibition/Production Model

TOUGH Scenario				
TOUGH Output, Forced Imbil	kg/m2 (30 yr)		0.369	
TOUGH Output, Natural Imbil	kg/m2 (30 yr)		0.709	
TOUGH Output, Produced Wate	kg/m2 (30 yr)		0.05917861	
Lit Hyd Frac Water (Vol/Stage)	gal	300,000	400,000	500,000
Lit Hyd Frac Water (Vol/Tot # Stages)	m3	0.00E+00	2.12E+04	0.00E+00
Well Tubular Calculated Vol	m3	3.26E+01	3.70E+01	4.42E+01
Well Fracture Calculated Vol (total well)	m3	0.00E+00	1.44E+02	0.00E+00
Well Microfracture Vol/frac m ² /cm depth ¹	m ³ /m ²		1.70E-04	
Well Microfracture Calculated Vol/cm depth	m3		1.96E+02	
TOUGH Total H2O: Forced Imbil	m3	0.00E+00	4.26E+02	0.00E+00
TOUGH Total H2O: Natural Imbil	m3	0.00E+00	8.19E+02	0.00E+00

TOUGH Total H2O: Produced Wate	m3	0.00E+00	6.84E+01	0.00E+00
TOTAL Produced Water (TOUGH+Frac+Tube			2.50E+02	
Imbided Fraction of Calc Frac Vol-no microfrac Vol		0.00E+00	8.25E-01	0.00E+00
Imbided Fraction of Calc Frac Vol-w/microfrac vol all produced			7.25E-01	
Imbided Fraction of Calc Frac Vol-w/microfrac vol all imbided			8.46E-01	
Imbided Fraction of Literature Frac Vol		#DIV/0!	5.55E-02	#DIV/0!
Produced Fraction of Calc Frac Injected V_i		0.00E+00	1.75E-01	0.00E+00
Produced Fraction of Lit Frac Injected V_i		#DIV/0!	3.23E-03	#DIV/0!

Carbon % Measures on Shimadzu SSM5000A

	TC1	TC2	TC3	TC Average	IC1	IC2	IC3	IC Average	TOC
Shale	3.133	3.246	3.250	3.210	0.008	0.022	0.111	0.047	3.163
Coal	72.43	75.92	75.57	74.640	0.0174	0		0.009	74.631
Shale	3.125	3.224	3.139		Std Dev	0.043963			
Coal	72.413	75.920	75.570		Std Dev	1.577393			

Carlo Erba Flash 2000 CHN analyzer

	TOC Average			
Shale	3.0757	3.078	3.07685	Std Dev 0.00115
Coal	68.4465	69.4547	68.9506	Std Dev 0.5041

Saturation Point Calculations from Contact Angle

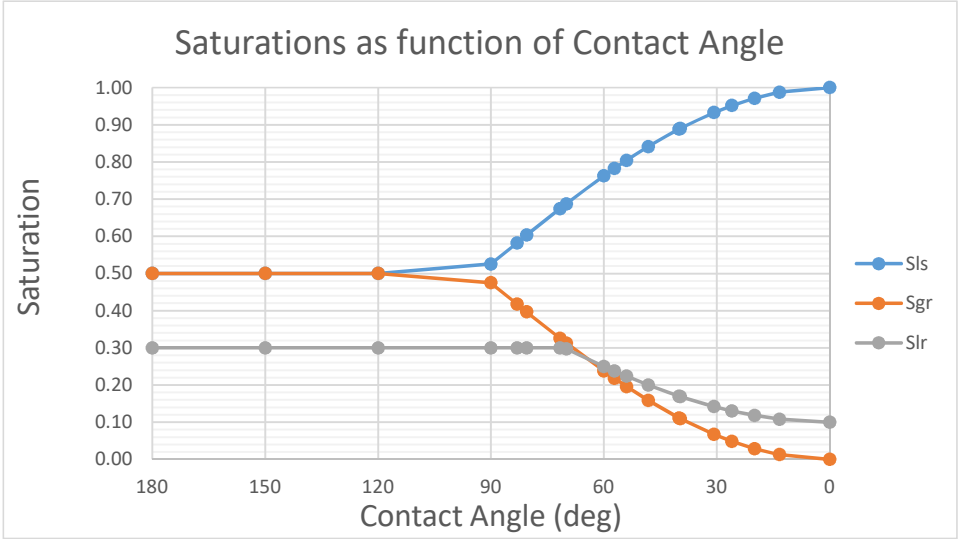
	Adv/Rec				MIP Manual Intrusion/Extrusion		
	θ	Sls	Sgr	Slr	λ	Po (Mpa)	1/Po (Pa ⁻¹)
Shale							
Forced (MIP Extrusion)	83.1	0.58	0.42	0.30	0.30	0.07	1.45E-05
Natural	48.2	0.84	0.16	0.20	0.43	7.28	1.40E-07
Production (MIP Intrusion)	13.3	0.99	0.01	0.11	0.55	14.50	6.90E-08
Coal							
Forced	90	0.53	0.48	0.30	0.30	0.00	E99
Natural	80.5	0.60	0.40	0.30	0.43	6.40	1.56E-07
Production	30.8	0.93	0.07	0.14	0.55	12.80	7.81E-08
Quartz							
Forced	54	0.80	0.20	0.22	0.30	0.34	2.96E-06
Natural	40	0.89	0.11	0.17	0.43	6.86	1.46E-07
Production	26	0.95	0.05	0.13	0.55	13.39	7.47E-08

Assume:
 $S_{gr(max)} = .5 S_{gi} = .475$
 (Naar & Henderson 1961)
 $S_{lr(max)} = .3$ (Byrnes)
 $S_{wi} = .1$

$S_{ls} = 1 - (1 - \cos\theta) S_{gr(max)}$
 $S_{gr} = 1 - S_{ls}$
 $S_{gr} = .5 S_{gi} (1 - \cos\theta)$

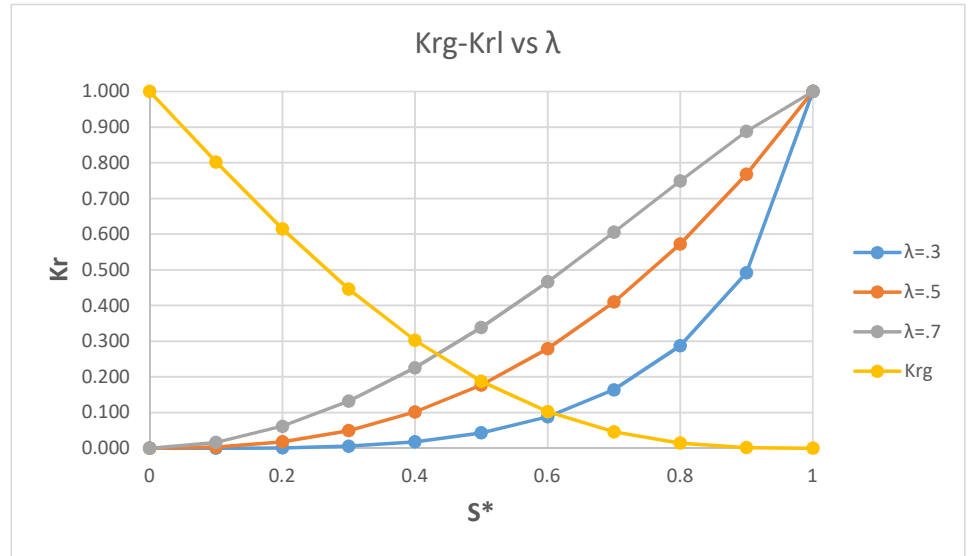
$S_{lr} = S_{lr(max)} (1 - \cos\theta) + S_{wi}$
 (Bethel & Calhoun 1953)

180	0.50	0.50	0.30
150	0.50	0.50	0.30
120	0.50	0.50	0.30
90	0.53	0.48	0.30
83.1	0.58	0.42	0.30
80.5	0.60	0.40	0.30
71.7	0.67	0.33	0.30
70	0.69	0.31	0.30
60	0.76	0.24	0.25
57.2	0.78	0.22	0.24
54	0.80	0.20	0.22
48.2	0.84	0.16	0.20
40	0.89	0.11	0.17
39.7	0.89	0.11	0.17
30.8	0.93	0.07	0.14
26	0.95	0.05	0.13
20	0.97	0.03	0.12
13.3	0.99	0.01	0.11
0	1.00	0.00	0.10



VG-Mualem Kr from TOUGH Manual

S*	Krl			Krg
	$\lambda=3$	$\lambda=5$	$\lambda=7$	
0	0.000	0.000	0.000	1
0.1	0.000	0.003	0.016	0.8019
0.2	0.001	0.018	0.062	0.6144
0.3	0.006	0.049	0.132	0.4459
0.4	0.018	0.101	0.225	0.3024
0.5	0.043	0.177	0.338	0.1875
0.6	0.088	0.279	0.466	0.1024
0.7	0.164	0.410	0.605	0.0459
0.8	0.287	0.572	0.749	0.0144
0.9	0.492	0.768	0.888	0.0019
1	1.000	1.000	1.000	0



Appendix B

Environmental life cycle analysis of water and CO₂-based fracturing fluids used in unconventional oil and gas production

List of Figures

Figure S1 - Process schematic and system boundaries for water-based fracturing fluid.	4
Figure S2 - Process schematic and system boundaries for CO ₂ -based fracturing fluid.	4
Figure S3 - Simulation results from ArcGIS network CO ₂ source analysis.	15
Figure S4 - CO ₂ flowback and production timeline.	23
Figure S5 - Schematic of the CO ₂ and CH ₄ membrane separation process	26
Figure S6 - Effective reservoir volume modeled for OGIP calculations.	32
Figure S7 - Output distributions from Crystal Ball for each forecast and scenario.	35
Figure S8 - Sensitivity analysis: Tornado plots	36

List of Tables

Table S1 - Modeling assumptions for CO ₂ -based fracturing fluids	5
Table S2 - Assumptions and parameters relevant to both water and CO ₂	6
Table S3 - Assumptions and parameters unique to water-based fluids	7
Table S4 - Assumptions and parameters unique to CO ₂ -based fluids	8
Table S5 - Fluid properties (obtained from NIST database.	9
Table S6 - Pumping parameters.	9
Table S7 - Ecoinvent impact factors.	9
Table S8 - Ecoinvent unit processes used to model the inputs listed in Table S7.	10
Table S9 - Independently derived impact factors	10
Table S10 - Summary of input parameters and energy requirements for compression	14
Table S11 - Comparison of additives used in water- and CO ₂ -based fracturing fluids	18
Table S12 - Literature review of production increases observed with CO ₂ -based frac fluids	30
1. Model overview	2
1.1. Functional unit.....	2
1.2. Model outputs, boundaries, and scope.....	2
1.3. Scenarios.....	4
1.4. Input parameters.....	5
1.5. Allocation.....	10
2. Equipment operation	11
2.1. Pumping energy.....	11
2.2. Diesel and operation.....	12
3. Transportation and storage	12
3.1. Pipeline transport and on-site water storage.....	12
3.2. CO ₂ compression and transport.....	13
3.3. Truck transport.....	16
4. Fracturing	17
4.1. Fluid volumes.....	17

4.2. Additives: Chemicals and proppant.....	18
4.3. Blending.....	19
4.4. High-pressure injection.....	20
5. Flowback.....	20
5.1. Water-based fluids.....	20
5.1.1. Flaring.....	20
5.1.2. Reuse and treatment.....	21
5.2. CO ₂ -based fluids.....	22
6. Production.....	25
6.1. Water-based fluids.....	25
6.2. CO ₂ -based fluids.....	26
7. Estimated ultimate recovery.....	30
7.1. Water-based fluids.....	30
7.2. CO ₂ -based fluids.....	30
7.2.1. Base case.....	30
7.2.2. Outlook case.....	32
8. Results.....	33
9. Sensitivity analysis.....	36

1. Model overview

The life cycle analysis models for water- and CO₂-based fracturing fluids were developed in Microsoft Excel with the Crystal Ball plug-in suite.^[1] Crystal Ball enabled us to account for the uncertainty in input parameters by conducting Monte Carlo simulations, which randomly vary inputs based on user-defined distributions (“assumptions”) to generate distributions for designated outputs (“forecasts”). Each Monte Carlo simulation was run for 100,000 replicates; resulting distributions and statistics for all forecasts are provided in sheet 2. In addition to quantifying uncertainty in the model outputs, this approach allows users to assess the sensitivity of the model to each input parameter and establish which variables most strongly influence the impacts of interest. All inputs and calculations are retained in the Excel file available along with this document. Results from the sensitivity analyses are also included in sheet 3 of this workbook and are included in Section 9 of this document.

1.1 Functional unit

Here, the function of a fracturing fluid is defined as facilitating energy production from unconventional gas wells. To this end, the functional unit (FU) selected for this study was 1 GJ of natural gas produced over the lifetime of a wellhead. An average unconventional well in Pennsylvania produced using hydraulic fracturing methods produces on average 5×10^6 GJ of natural gas over its lifetime.^[2] 1 GJ was selected to be large enough to avoid rounding areas (roughly equivalent to the amount of energy that an average American uses in a day) and small enough to be meaningful in the marginal sense of production for one well. Normalizing impacts to production performance accounts for the production increase associated with CO₂-based fluids, which is detailed in Section 7.2. An energy-based unit was selected as opposed to cumulative gas volumes to provide an intuitive sense for the net energy involved in gas production under each

scenario. Furthermore, inputs and impacts are based on one wellhead to best capture the burdens associated with a current fracking operation, where multiple wells are drilled successively at a central wellpad. We define a wellhead as a single site (pad) with 6 wells, or laterals. The computational implications of this approach are discussed throughout this document where applicable, but note that all material flows and associated burdens are quantified for 1 wellhead as opposed to a single well. Thus, total injected fluid volumes and EUR values represent the required fracking fluid and anticipated production, respectively, for developing 6 laterals.

1.2. Model outputs, boundaries, and scope

The LCA model developed here traces energy consumption, greenhouse gas (GHG) emissions, and consumptive water use over the life cycle of two working fluids for shale gas development: water (slickwater) and CO₂. Energy use is reported in units of MJ/GJ (MJ of energy consumed per GJ of energy produced). GHG emissions are normalized to kgCO₂eq/GJ based on 100-year global warming potential (GWP) values specified by the IPCC.^[3] Consumptive water use is defined as water displaced from its original source (i.e. a net loss of water availability in the watershed of origin)^[4] and is reported as L/GJ. This impact includes evaporative losses and water embedded in products, but excludes cooling water withdrawn for power generation or processing. Potential degradative ecological effects of returning heated, reduced-quality water to the waterway from which it was extracted after use are beyond the scope of this study.

The life cycle is divided into four major stages: (1) transportation and storage, (2) fracturing, (3) flowback, and (4) production. The first stage includes transporting diesel, work fluids (e.g., water or CO₂), and additives to the site along with transfer to and from storage facilities. Note that upstream impacts associated with on-site storage tank production are not considered since the life cycle of these structures extends far beyond well completion and production; for slickwater, water impoundment construction is included because the pits are temporary and fully attributed to shale gas development. Fracturing accounts for blending base fluids and additives at a manifold and then injecting the combined fluid via a high-pressure pump. Flowback involves the separation of gas and liquid phases and disposal of waste streams, including gas flaring and wastewater transport to other frac sites or treatment facilities. Production continues for the lifetime of the well and also considers phase separation and waste management. Detailed schematics of specific flows and processes involved at each stage are provided in Figures S1 and S2 below. The two scenarios developed for CO₂-based fluids noted in Figure S2 are discussed in Section 1.3.

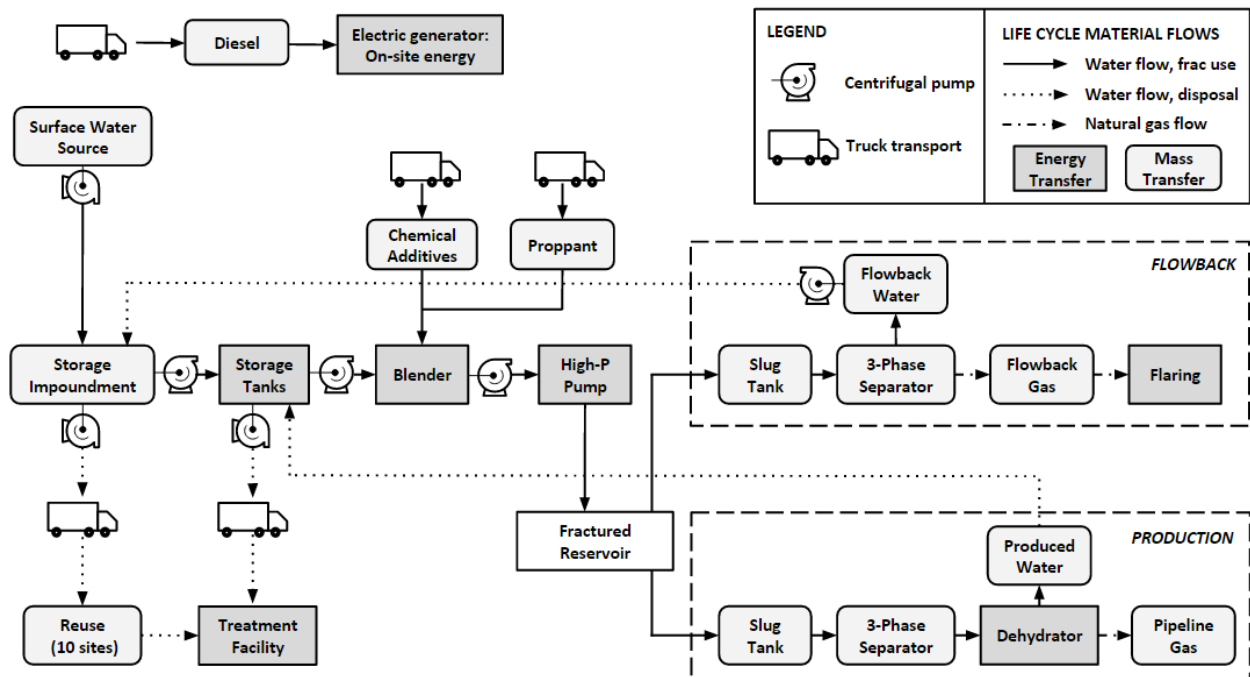


Figure S1. Process schematic and system boundaries for water-based fracturing fluid.

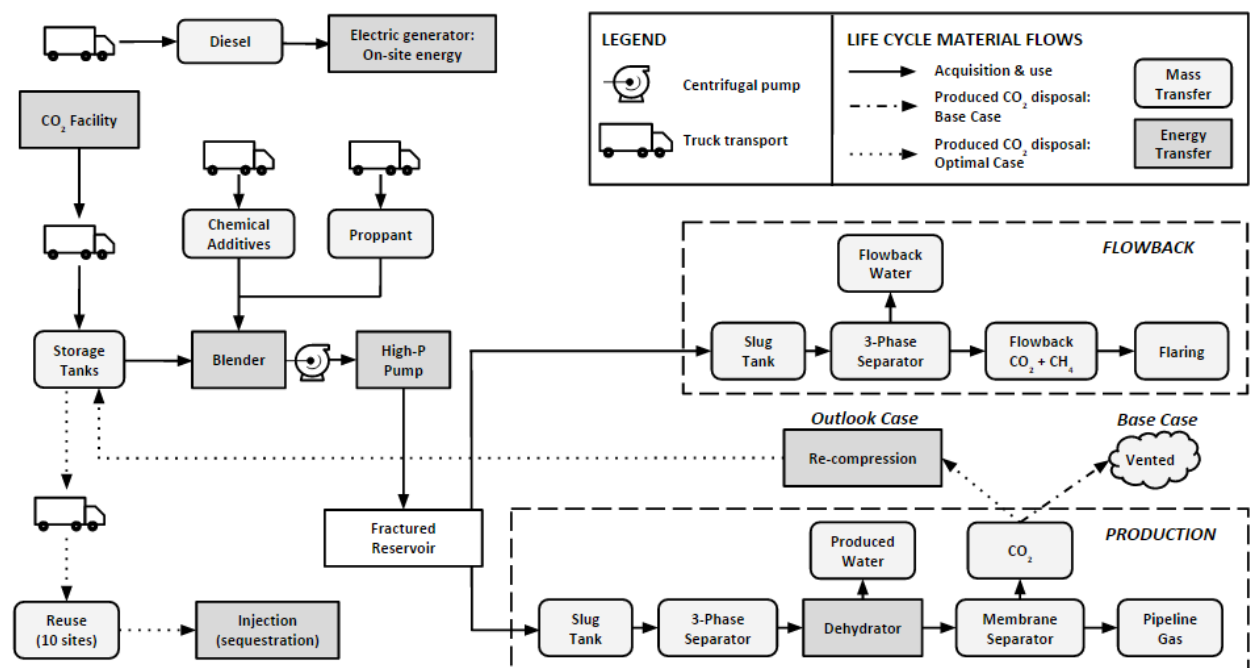


Figure S2. Process schematic and system boundaries for CO₂-based fracturing fluid.

1.3. Scenarios

To evaluate and compare the impacts of interests for water- and CO₂-based fracturing fluids, we developed three scenarios:

1. **Water-based fluids:** This scenario reflects nominal hydraulic fracturing practices in the Marcellus shale.

2. **CO₂-based fluids, base case:** This scenario models the flows and results projected for a “current” large-scale CO₂ frac based on extensions of available data and industry input.
3. **CO₂-based fluids, outlook case:** This scenario represents a best-case CO₂ frac scenario. In light of the fact that water-based fluids have been developed extensively for years, we established a series of theoretical models to conjecture advances in CO₂ performance following the same level of investment.

Note that while the CO₂ scenarios seemingly differentiate between a “current” and “future” case, we propose that the “outlook case” could be realized in a present-day CO₂ frac, but is unproven as operators have yet to demonstrate the viability of completing and optimizing a large-scale CO₂ frac comparable to those modeled here. The differences between the two CO₂ scenarios are highlighted in Table S1 below and detailed through specific stages in sections 2-7.

Table S1. Modeling assumptions used to differentiate between the base and outlook case for CO₂-based fracturing fluids.

Input	Base Case	Outlook Case
Injected fluid volume	70% of volume injected for water-based frac	65% of volume injected for water-based frac
Recovered CO ₂ (flowback + production)	60-90% of injected fluid (median 75%)	10-90% of injected fluid (median 50%)
Separated CO ₂ disposal (in membrane separation)	Vented/flared	Recompressed and reused at 10 subsequent frac sites
Production increase factor (over water-based fluids)	0-110% (median 50%), see section 7.2.1	50-1340% (median 200%), see section 7.2.2
Well lifetime	30 years	40 years

Numerical inputs for each of the three scenarios are presented in Section 1.4.

1.4. Input parameters

All three scenarios trace the life of the fracturing fluid through transport and storage, including upstream material acquisition, the fracturing process, flowback, and production. The major assumptions and relevant inputs for Monte Carlo simulations are summarized in Tables S2-S8. Applications of these inputs are explained in sections 2-7.

Table S2. Assumptions and parameters relevant to both water and CO₂.

Input	Units	Min	Likely (Median)	Max	Distribution	Source¹
<i>Transportation and storage</i>						
Transport distance, diesel to well pad	km	45	(82.5)	120	Uniform	[5]

Diesel tank truck capacity	m ³	--	30	--	--	
Fuel economy, heavy-duty highway truck	km/m ³	--	2515	--	--	[6]
Acid tanker truck capacity	m ³	--	19	--	--	[7]
HDPE chemical tote capacity	m ³	--	1.325	--	--	[8]
Chemical totes per truck	--	--	20	--	--	[8]
Chemical trucking distance	km	804.5	(925.18)	1045.85	Uniform	[5]
Proppant truck capacity	t		30		--	
Proppant trucking distance	km	80.45	(88.5)	96.54	Uniform	[5]
Fracturing						
Stages per lateral	--	--	10	--	--	
Laterals per well	--	--	6	--	--	
Proppant	kg/m ³	--	120	--	--	
Acid (HCl)	m ³ /m ³ fluid	--	0.0067	--	--	[9]
Corrosion inhibitor	m ³ /m ³ fluid	--	1E-5	--	--	[9]
Scale inhibitor	m ³ /m ³ fluid	--	2.15E-5 ²	--	--	[9]
Injection flow rate	m ³ /s	--	0.212	--	--	
Production wellbore diameter	m	--	0.121 ³	--	--	
Vertical wellbore depth	m	--	2000	--	--	
Horizontal lateral length	m	--	1067	--	--	[10]
Pipeline length between well pad equipment	m	--	10	--	--	
Fracture pressure	MPa	--	45.22	--	--	
Flowback						
Flowback time, flaring	d	--	2	--	--	
Flaring combustion efficiency	%	--	99	--	--	
Production						
EUR, water frac (for a single lateral)	bcf	--	4.35	--	--	[10]
	GJ	--	4,979,690	--	--	Calc.
Dehydration energy	MJ/kgCH ₄	--	4.162E-5	--	--	Calc. [11]

1. Unreferenced inputs for all tables are derived from industry input and best engineering judgement.

2. Scale inhibitor is added in the same mass concentration as biocide.

3. Production wellbore is a 4.788" ID tubular.

Table S3. Assumptions and parameters unique to water-based fluids

Input	Units	Min	Likely	Max	Distribution	Source
<i>Transportation and Storage</i>						
Pipeline length, source to impoundment	km	0.5	(2.66)	4.83	Uniform	
Pipeline length, impoundment to well pad	m	304.8	(914.4)	1524	Uniform	
Pipeline weight, source to well pad (8" PVC)	kg/m	--	13.62	--	--	[12]
Flow rate, source to storage	m ³ /s	--	0.126	--	--	
Impoundment capacity	m ³	--	18927	--	--	
Liner thickness	m	--	0.002	--	--	[13]
<i>Fracturing</i>						
Base fluid volume per stage	m ³	1136	1514	1893	Triangular	
Fluid fraction from reused water	%	6	10	18	Triangular	[14]
Friction reducer	m ³ /m ₃	--	1.65E-4	--	--	[9]
Biocide	m ³ /m ₃	--	1.30E-4	--	--	[9]
<i>Flowback</i>						
Initial gas flowback rate, 0-2 days	m ³ /d	--	5178	--	--	Calc.
Flowback water (% of injected fluid)	%	4	7	47	Triangular	[14]
Flowback to recycling (% of total flowback)	%	--	98 ¹	--	--	
Flowback to CWT (% of total flowback)	%	--	8 ²	--	--	
Water truck capacity	m ³	--	30	--	--	
Flow rate, flowback to storage tanks	m ³ /s	--	3.15E-3	--	--	
Pipeline diameter, well pad storage to impoundment	m	--	0.051	--	--	
Pipeline diameter, storage to trucks	m	--	0.102	--	--	
Transport distance to other sites for recycling	km	8.05	(11.3)	14.5	Uniform	[15, 16]
Transport distance to CWT facility	km	155	(166)	177	Uniform	[17, 18]
<i>Production</i>						
Well lifetime	yrs	--	30	--	--	

1. Percent of total flowback water, assuming 2% evaporative losses

2. Percent of total flowback water, assuming 2% evaporative losses per site; 10% of the treatment burdens are allocated to this model well, assuming reuse at 10 sites

Table S4. Assumptions and parameters unique to CO₂-based fluids

Input	Units	Min	Likely	Max	Distribution	Source
<i>Transportation and Storage</i>						
CO ₂ tanker truck capacity	m ³	--	20	--	--	[19]
CO ₂ transport distance	km	14.8	92.7	243.6	Triangular	Calc. ¹
<i>Fracturing</i>						
Fluid volume per stage						
Base Case	m ³	795	1060	1325	Triangular	Calc. ³
Outlook Case		738	984	1230	Triangular	Calc. ³
<i>Flowback</i>						
Initial gas flow rate (days 0-3)	m ³ /d	--	283,168	--	--	
Flowback time, CO ₂ venting	d	--	1	--	--	
Total flowback and produced CO ₂ , % of injected fluid						
Base Case	%	50	70	90	Triangular	See section 5.2
Outlook Case		10	50	90	Triangular	See section 5.2
<i>Production</i>						
Separation time	d	--	12	--	--	
Average gas flow rate, separation	m ³ /d	--	169,901	--	--	
Production increase factor						
Base Case	%	0	50	110	Triangular	See section 7.2.1
Outlook Case		50	200	1340	Triangular	See section 7.2.2
CO ₂ recompression energy (Outlook Case)	MJ/tCO ₂	--	231	--	--	Calc. [11, 20]
Well lifetime						
Base Case	years	--	30	--	--	
Outlook Case		--	40	--	--	

1. CO₂ capture impact calculations are described in Section 3.1

2. CO₂ transport distance determined with GIS network analysis (Section 3.2)

3. The base case uses 70% of the fluid volume injected for an equivalent water-based frac, while the outlook case uses 65% (see Section 4.1).

Fluid properties used in calculations for water- and CO₂-based fluids are listed in Table S5,^[21] while mechanical pumping parameters are summarized in Table S6.

Table S5. Fluid properties (obtained from NIST database^[21])

Input	Units	Water	CO₂
Fluid density, injection conditions ¹	kg/m ³	997.1	1031.8
Fluid density, bottomhole ²	kg/m ³	983.3	435.4
Dynamic viscosity, injection conditions	Pa·s	8.9E-4	1.395E-4
Dynamic viscosity, bottomhole	Pa·s	3.828E-4	3.285E-5

CO ₂ density in flowback, surface conditions (25°C, 1 atm)	kg/m ³	NA	1.808
CH ₄ density, standard measuring conditions (60°F, 1 atm)	kg/m ³	0.6785	0.6785

1. Injection conditions correspond to the surface conditions (25°C, atmospheric pressure) for water and storage/transport conditions (-20°C, 2 MPa) for CO₂.
2. Bottomhole temperature is 75°C (assuming 25°C surface temperature and a 20°C/km temperature gradient). Bottomhole pressure is hydrostatic pressure at 2 km: 19.6 MPa for water-based fluids and 14.4 MPa for CO₂.

Table S6. Pumping parameters

Input	Units	Value
Absolute roughness, PVC pipe	m	1.52E-6
Absolute roughness, iron pipe	m	4.57E-5
Efficiency, centrifugal pump	--	0.7
Efficiency, positive displacement pump	--	0.9
Efficiency, electric motor	--	0.9
Efficiency, diesel to electric generator	--	0.405
Energy content, diesel	MJ/kg	45
Fracture pressure, Marcellus	MPa/km	22.61

Impact factors for upstream and downstream processes were obtained from the Ecoinvent v2.2 database.^[22] For water use, only consumptive (i.e. non-cooling or turbine use) water inputs were included. The factors are normally distributed according to the parameters listed in Table S7; Ecoinvent unit processes selected to model each input process are listed in Table S8.

Table S7. Ecoinvent impact factors

Process	FU	Energy (MJ/FU)		GHG (kgCO ₂ eq/FU)		Water use (m ³ /FU)	
		Mean	St. Dev.	Mean	St. Dev.	Mean	St. Dev.
Acid	1 kg	17.2	3.28	0.833	0.149	1.30E-2	0.00183
Polyacrylamide	1 kg	88.2	9.30	3.01	0.329	1.27E-2	8.77E-4
Glutaraldehyde	1 kg	52.8	6.19	1.37	0.135	1.35E-1	2.93E-2
Methanol	1 kg	38.5	6.15	0.726	0.0625	2.26E-3	2.69E-4
Phosphoric acid	1 kg	20.4	2.62	1.38	0.149	1.29E-1	2.33E-2
Sand	1 kg	0.058	6.2E-3	2.4E-3	2.31E-4	1.42E-3	9.35E-5
PVC pipe:							
(a) production	1 kg	62.8	5.16	2.02	0.163	1.06E-2	5.38E-4
(b) extrusion	1 kg	8.09	1.2	0.373	0.0534	2.81E-3	4.65E-4
Diesel	1 kg	54.4	2.1	0.506	0.0466	5.91E-3	1.13E-3
Excavation	1 m ³	8.11	0.724	0.53	0.051	1.15E-3	1.17E-4
Liner	1 kg	93.4	6.77	2.66	0.206	1.41E-2	1.3E-3
Wastewater treatment*	1 m ³	--	--	--	--	7.58E-3	1.48E-3

Electricity	1 MJ	3.39	2.69	0.21	0.01	5.94E-4	1.30E-4
-------------	------	------	------	------	------	---------	---------

*Energy and GHG impacts for wastewater treatment were derived separately from NETL data on Marcellus-specific treatment processes (see section 5.1.2) and are listed in Table S9. Note that water use impacts are converted from m³ to L for final reporting.

Table S8. Ecoinvent unit processes used to model the inputs listed in Table S7

Process	Ecoinvent unit process
Acid	HCl, 30% in H ₂ O, at plant/RER U
Polyacrylamide	Acrylonitrile from Sohio process, at plant/RER U
Glutaraldehyde	Acetaldehyde, at plant/RER U
Methanol	Methanol, at plant/GLO U
Phosphoric acid	Phosphoric acid, industrial grade, 85% in H ₂ O, at plant/RER U
Sand	Sand, at mine/CH U
PVC pipe: (a) production (b) extrusion	Polyvinyl chloride, at regional storage/RER U Extrusion, plastic pipes/RER U
Diesel	Diesel, at regional storage/RER U
Excavation	Excavation, hydraulic digger/ RER U
Liner	Synthetic rubber, at plant/RER U
Wastewater treatment	Treatment, sewage, to wastewater treatment, class 3/ CH U
Electricity	Electricity, production mix, US/US U

Note: European unit process values (RER) are not expected to deviate significantly from U.S values in production processes.

Impact factors were derived separately for some processes where Ecoinvent factors were either insufficient or not applicable. These factors are summarized in Table S9 below; calculations are included where applicable in sections 2-7 of this document.

Table S9. Independently derived impact factors

Process	FU	Energy (MJ/FU)	GHG (kgCO ₂ eq/FU)	Water use (m ³ /FU)
CO ₂ capture at source	1 tCO ₂	675	42	0.118
Trucking diesel consumption	m ³ diesel	80856	3391	3.71
Trucking emissions (in transit)	vehicle-km	--	9.69E-4	--
Diesel emissions, combustion in industrial engine	MJ	--	0.0705	--
Wastewater treatment	m ³	5.51	1.09	--

1.5. Allocation

For both CO₂ scenarios, the CO₂ is assumed to have been produced as a byproduct of another industrial process, such as ammonia, hydrogen, or ethanol production or acid gas removal. In the Marcellus, the most likely sources are the nearby ethanol, hydrogen, and acid gas removal facilities (see section 2.2). Because these industries generate nearly-pure CO₂ streams as byproducts, they can currently capture and sell CO₂ at commercial scale; conversely, large-scale carbon capture in power plants is not yet economically feasible and thus is not considered in this study. However,

utilizing byproduct CO₂ presents allocation challenges, both in ascribing upstream production burdens and CO₂ emissions throughout the life cycle. Here, we apply the same marginal approach as Middleton et al. (2014), where only processes associated with CO₂ capture and transport are considered as marginal impacts.^[11] These burdens are exclusive of upstream impacts from the core process itself, which occurs regardless of the fate of the CO₂ byproduct. By extension, any captured CO₂ emitted throughout the fluid's life cycle is not counted as a GHG emission since this CO₂ byproduct is vented in the absence of an economically viable end use or storage option. Determining whether the CO₂ source or sink receives sequestration credits has been debated, but the focus here is on evaluating system-scale implications of a CO₂-based fluid. To this end, we do not attempt to allocate between supply- and demand-side credits, but rather recognize that a CO₂-based frac creates a market and storage repository for CO₂ that does not exist with slickwater fracturing. Thus, any CO₂ that is permanently sequestered in the formation (e.g., the volume that does not return in flowback or production) is credited to the CO₂ frac as a negative GHG emission.

2. Equipment operation

2.1. Pumping energy

Energy required to pump the fracturing fluid over its entire life cycle spanning acquisition through production was estimated using a bottom-up approach. As discussed in Section 1.1, all material flows are computed for a wellhead containing 6 laterals. To obtain systems-level estimates for the energy associated with developing all of these wells, we calculate the energy burdens for moving the entire fluid volume for the wellhead through each individual system. For each pump, the Reynold's number was first calculated for flow through the discharge pipeline based on fluid velocity V , density ρ , dynamic viscosity μ , and pipe diameter D :

$$R_e = \frac{VD\rho}{\mu} \quad \text{Eq.S1}$$

Reynold's numbers were in the turbulent regime (>4000) throughout, requiring a turbulent flow friction factor calculation accounting for pipeline roughness (ϵ). A Darcy-Weisbach friction factor f was calculated using the empirical approach presented by Gouder-Sonnad (2006), an explicit approximation of Colebrook-White with improved accuracy in mid-ranges of $(\epsilon/D)^{[23]}$:

$$\frac{1}{\sqrt{f}} = 0.868 \ln \left(\frac{0.4587 R_e}{s^{s/(s+1)}} \right) \quad \text{Eq. S2}$$

$$s = 0.124 \left(\frac{\epsilon}{D} \right) R_e \quad \text{Eq. S3}$$

Frictional losses through the pipeline were then computed as:

$$\Delta p_f = f \frac{LV^2\rho}{2D} \quad \text{Eq. S4}$$

Accounting for efficiencies of the pump (η_P), motor (η_M), and diesel-electric generator (η_{DE}), the required hydraulic power for on-site equipment is then calculated from the total pressure differential and flow rate:

$$P = \frac{Q\Delta p}{\eta_P\eta_M\eta_{DE}} \quad \text{Eq. S5}$$

Here, Δp depends on tubular friction losses derived above; minor friction losses from fittings and perforations (Δp_m), taken as a fraction of Δp_f ; any differential applied to boost fluid pressure; and, in the case of injection, the hydrostatic pressure in the wellbore and formation fracture pressure. Finally, energy consumed in driving the pump is calculated from the operating time, which is derived from the flow rate and total volume of fluid flowing through the pump:

$$E = Pt = P \frac{V_{fluid}}{Q} \quad \text{Eq. S6}$$

Specific calculations for each pumping scenario are detailed in corresponding sections below.

2.2. Diesel and operation

Diesel indirectly fuels all on-site equipment, including pumps, blenders, and separation units, via diesel-electric generators powered by electric motor drives. Life cycle impacts account for a) diesel production and transport to the site, and b) diesel combustion in the engines. Direct energy use for on-site operation was calculated as detailed in Section 2.1 above, which accounts for pump and electric motor efficiencies. Because these units are assumed to be powered by an electric generator, an additional diesel-electric efficiency factor (0.405) was also applied.

Upstream impacts for diesel production were attained by multiplying the total energy used in MJ by Ecoinvent impact factors for diesel produced at regional storage facilities after unit conversions from a per kg to per MJ diesel basis using an energy content of 45 MJ/kg (see Table S7). To account for diesel transport to the frac site, the energy input required for each system was first converted to an equivalent volume of diesel using an energy density of 45 MJ/kg, or 37,440 MJ/m³ (applying a diesel density of 832 kg/m³). Impacts for trucking diesel to the site were then computed based on total vehicle-km traveled as detailed in Section 3.3, using the truck capacity and average transport distance specified in Table S2.

The total energy footprint of on-site equipment operation is the sum of the direct energy use in operation and upstream impacts from production and transportation. GHG emissions from diesel combustion were calculated using the EPA's emission factor of 164lb CO₂/MMBtu (0.0705 kgCO₂eq/MJ) of power input for a stationary diesel industrial engine.^[25] The total emissions associated with an equipment unit are the sum of this value from direct combustion and the upstream impact derived from the Ecoinvent factor in kgCO₂eq per MJ energy consumed. No water consumption is considered in diesel combustion, so total water use is the sum of the upstream production and transportation impacts.

3. Transportation and Storage

3.1. Pipeline transport and on-site water storage

For water-based frac fluids, water is piped from a local surface source and stored in a temporary impoundment on site before being incrementally pumped into storage tanks at the well pad in accordance with common industry practice in the Marcellus shale. Overland pipes (8" or 20 cm PVC) run 0.5 km - 4.8 km from the surface source to the impoundment and 305 - 1524 m (1000-5000 ft) from the impoundment to the well pad. Upstream emissions for pipeline production were calculated using Ecoinvent factors for both PVC production and pipeline extrusion per kg of pipeline, based on a standard 8" DR-18 pipeline weight of 9.15 lb/ft (13.62 kg/m).^[12]

The storage impoundment holds 5 million gallons of water, or 18,927 m³, with a square footprint of 150x150 ft, or 45.72x45.72m, and corresponding 9m depth.^[26] To approximate construction costs, it was assumed that two-thirds of this volume will be excavated, while the remaining third will be used as fill around the perimeter to build in the remaining volume. Impacts from impoundment construction were taken as the excavation impacts per m³ of cut from Ecoinvent factors. Since flowback water will also be routed to this impoundment post-fracturing, a low-permeability liner must be installed with primary and secondary layers, each having a minimum thickness of 40 mil for a total thickness of 80 mil (0.2 cm).^[13] Upstream production impacts for the liner were calculated by applying Ecoinvent impact factors for synthetic rubber to the volume of liner required, calculated by approximating the impoundment as a box to estimate the internal surface area:

$$\text{Liner volume} = (\text{Thickness} * \text{Length}^2) + 4(\text{Depth} * \text{Thickness} * \text{Length}) \quad \text{Eq. S7}$$

The energy required to pump water from a surface source to the on-site impoundment and then from the impoundment to storage units at the well pad was calculated according to the approach outlined in Section 2. Properties of water at the surface were applied in Reynold's number calculations, assuming a flow rate of 1000 gpm (0.063 m³/s). Both segments applied centrifugal pumps with a Δp equal to the sum of pipeline and fitting frictional losses. From source to impoundment, fitting losses were taken as 10% of tubular losses; from impoundment to storage, minor losses are assumed to be more significant such that $\Delta p_m = \Delta p_f$. As noted in section 1.2, the upstream production and transport of storage tanks was neglected for both water and CO₂, as the lifetime of these units extends well beyond the duration of a fracturing job.

3.2. CO₂ compression and transport

As discussed in section 1.5, we assumed that a CO₂-based frac will repurpose byproduct CO₂ from an industrial process that already generates a nearly-pure stream. Here, CO₂ is sourced from the nearest ethanol, hydrogen, or acid gas removal facility. These are the primary sources of industrial-grade CO₂ in proximity to the Marcellus Shale. The energy associated with preparing CO₂ for truck transport was modeled based on the simplified approach used by Middleton et al. (2014) to determine the marginal burdens for capturing and supplying CO₂ from these facilities.^[11] Impacts are driven by the compression energy required to pressurize CO₂ from the effluent process streams to storage and transport conditions. The required energy per tonne CO₂ was calculated for each

compression stage using modified equations presented by McCollum and Ogden (2006), assuming a compressor efficiency of 0.75:^[20]

$$\frac{W_{Stage}}{m_{CO_2}} = \left(\frac{Z_s R T_{in}}{0.75 M} \right) \left(\frac{k_s}{k_s - 1} \right) \left[(CR)^{\frac{k_s}{k_s - 1}} - 1 \right] \quad \text{Eq. S8}$$

The compression ratio (CR) is calculated based on a cut-off pressure of 2 MPa, the level assumed for transport and storage conditions, and the initial pressures for effluent CO₂ streams in each facility reported in Table S10. Four compression stages are required for CO₂ from hydrogen and ethanol production, while only two are necessary for CO₂ from acid gas removal due to the greater initial pressure in the gas stream. The work requirements at each stage are summed to yield the total compression energy requirements for each facility listed in Table S10. To account for uncertainty and variability in CO₂ sources, capture energy is modeled as a triangular distribution in Crystal Ball, with ethanol plants corresponding to the “likely” value and acid gas and hydrogen production facilities taken as the min and max, respectively.

Table S10. Summary of input parameters and calculated energy requirements for compression.

CO ₂ Source	P _{in} (MPa)	Compression Ratio	T _{in} (K)	Compression energy (MJ/tCO ₂)
Hydrogen	0.1	2.11	355.15	284.8
Ethanol	0.1	2.11	300.15	240.7
Acid gas	0.8	1.26	308.15	71.9

Energy at each facility is supplied as electricity from the grid, so the ultimate burdens associated with capturing and supplying CO₂ account for upstream impacts of electricity production. These life cycle impacts per tCO₂ were calculated by multiplying the compression energy distribution (MJ/tCO₂) by the Ecoinvent energy use, GHG emission, and consumptive water impact factors per MJ of electricity from the US grid (see Table S7).

The CO₂ is assumed to be trucked from these facilities to the wellhead, as there is currently no pipeline infrastructure that operators in the Marcellus region could tie into and developing a full-scale network would be logistically and economically challenging given the short time frame of well completions. Average transport distances from sources to frac sites were computed using ArcGIS 10.2.^[26] Middleton et al. (2014) included processed data for CO₂ capture facilities from the EPA’s GHG Reporting Program in their supporting information; 29 of these facilities in the Marcellus region were considered here as potential CO₂ sources.^[11] Frac sites were modeled as 49 shale well clusters throughout Pennsylvania, West Virginia, and Ohio, each consisting of tens to hundreds of individual wells.^[28] Using the coordinates for the sources and sites along with a comprehensive U.S. street network dataset, the ArcGIS Network Analyst extension was applied to run a “closest facility” analysis for each well cluster to determine the travel distance from the nearest CO₂ capture plant. Resulting routes from this analysis are shown in Figure S3 below.

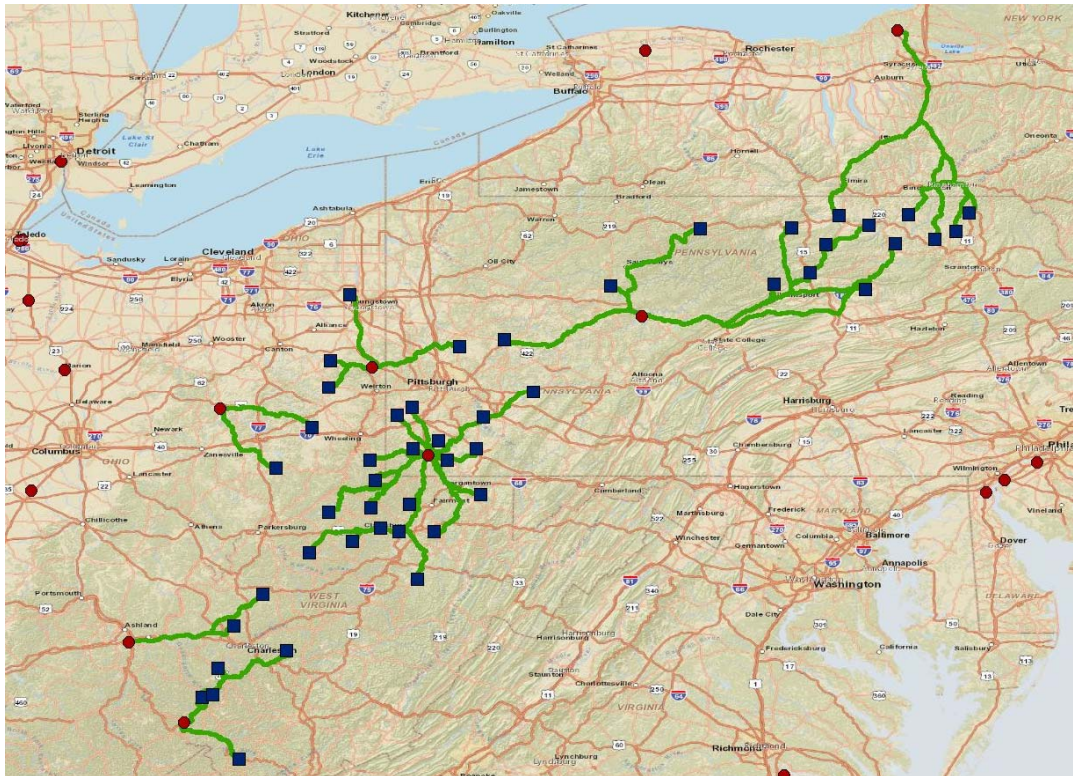


Figure S3. Simulation results from ArcGIS network analysis linking Marcellus frac sites to CO₂ sources. Red dots correspond to sources, while blue squares represent shale well clusters.

Three ethanol, two hydrogen, and two acid gas removal facilities were deployed to serve Marcellus wells. Travel distance was modeled as a triangular distribution using the minimum, mean, and maximum distances returned in ArcGIS. Although CO₂ supply was not considered for facilities serving multiple wells, this study does not assume that all new wells in the region would be stimulated with CO₂, and it is likely that a wellhead would need to obtain CO₂ from multiple sources. Supply will ultimately be driven by market demand and capture costs, which are beyond the scope of this study. Thus, this simplified model serves as a rough but adequate gauge of potential trucking distances associated with CO₂ acquisition for hydraulic fracturing in the Marcellus shale.

Based on insight from industry, no specific refrigeration units are required for CO₂ transport or storage; cooling and pressure control is provided by venting the gas. We take these losses as 3% of the total amount of CO₂ delivered and used throughout well completion to account for all transport, storage, and use-related processes. Per the allocation method, these losses are not counted as a direct GHG emission, but are added to the total fluid volume required for the well completion to determine the total fluid volume acquired from the source. Due to its high pressure in transport and on-site storage, no additional pumping energy is required to load the CO₂ into trucks or storage tanks.

3.3. Truck transport

For water-based fracture fluids, trucks transport all flowback and produced water from the site to subsequent sites for reuse and ultimately to centralized waste treatment (CWT) facilities. For CO₂-based fluids, sourced CO₂ is trucked to the site as described in Section 3.2, and CO₂ recovered in separation is trucked to other frac sites for reuse in the outlook case. In all scenarios, trucks are used to transport chemicals, proppant, and diesel for the on-site generator.

Impacts from trucking fluids, additives, and diesel to and from sites included well-to-pump production of diesel fuel and greenhouse gases emitted during transit. All trucks were assumed to be heavy-duty highway diesel vehicles with an average fuel economy of 5.92 mi/gal or 2515.6 km/m³.^[5] Truck capacities for specific uses are listed in Tables S2-S4. Fracturing fluids and additives are transported by tanker trucks, with the number of required trucks calculated as the total fluid volume divided by the fluid volume per truck, rounded up to the nearest truck. Chemicals are assumed to be transported in 350-gallon (1.325 m³) storage totes contained in flatbed trailers that can each handle 20 totes.^[8] Individual chemicals are not mixed between totes, but different chemical totes can travel on the same truck. Thus, the number of trucks for chemical transport is calculated as:

$$N_T = \text{m}^3 \text{ of chemical} * \frac{\text{Tote}}{1.325 \text{ m}^3} * \frac{\text{Truck}}{20 \text{ Totes}} \quad \text{Eq. S9}$$

Proppant (sand) is delivered in 30-tonne dump trucks. The number of trucks required for proppant transport is calculated as:

$$N_T = \text{kg of proppant} * \frac{\text{Truck}}{30,000\text{kg}} \quad \text{Eq. S10}$$

The number of diesel-carrying tanker trucks required to fuel the generators throughout the entire fracturing job is determined in the same way as fluid-carrying trucks, based on the density of diesel fuel (832 kg/m³) and the truck capacity noted in Table S2.

Energy use for truck transport was derived from diesel consumption per vehicle-km traveled and well-to-use impacts for diesel production. Diesel consumed during transit was calculated as:

$$\text{Vol. Diesel} = N_T * \text{Distance (km)} * \frac{\text{m}^3}{2515.6 \text{ km}} \quad \text{Eq. S11}$$

With an equivalent energy consumption of:

$$\text{Diesel energy, transit} = \text{m}^3 \text{ diesel} * \frac{832 \text{ kg diesel}}{\text{m}^3} * \frac{45 \text{ MJ}}{\text{kg diesel}} = \frac{37,740 \text{ MJ}}{\text{m}^3 \text{ diesel}} \quad \text{Eq. S12}$$

Upstream impacts were calculated based on the GREET factor for well-to-pump (WTP) energy consumption for conventional US diesel fuel:^[29]

$$\text{Diesel energy, WTP} = \text{m}^3 \text{ diesel} * \frac{43,416 \text{ MJ}}{\text{m}^3 \text{ diesel}} \quad \text{Eq. S13}$$

Summing these factors yields 80,856 MJ of energy consumed per m³ of diesel used in transport. Thus for each transport stage, the volumes of diesel consumed were computed based on total vehicle-km traveled and multiplied by this aggregated factor to obtain the total associated embodied and use-phase energy consumption. While GREET also provides well-to-wheels impact factors, these are only available for a set of specific vehicle models and none are representative of the typical heavy-duty diesel truck employed in this setting. Thus, GREET was only used for well-to-pump impacts, and pump-to-wheels impacts were calculated separately.

GHG emissions associated with use-phase trucking were calculated using EPA emission factors for carbon dioxide (CO₂), methane (CH₄), and nitrous oxide (N₂O) produced in fuel combustion for heavy-duty diesel trucks.^[6] Direct CO₂ emissions are based on volume of diesel consumed:

$$\text{Diesel GHG, CO}_2 = \frac{10.15 \text{ kg CO}_2}{\text{gal diesel}} * \frac{264.172 \text{ gal}}{\text{m}^3 \text{ diesel}} * \text{m}^3 \text{ diesel} = 2,681.35 \frac{\text{kgCO}_2\text{eq}}{\text{m}^3 \text{ diesel}} \quad \text{Eq. S14}$$

Emissions of CH₄ and N₂O were calculated based on vehicle-km traveled:

$$\text{Diesel GHG, CH}_4 = \frac{5.1 \cdot 10^{-6} \text{ kg CH}_4}{\text{vehicle-mi}} * \frac{\text{mi}}{1.609 \text{ km}} * \frac{\text{km}}{\text{truck}} * N_T * \frac{25 \text{ kg CO}_2\text{eq}}{\text{kg CH}_4} = 7.9 \cdot 10^{-5} \frac{\text{kgCO}_2\text{eq}}{\text{vehicle-km}} \quad \text{Eq. S15}$$

$$\text{Diesel GHG, N}_2\text{O} = \frac{4.8 \cdot 10^{-6} \text{ kg CH}_4}{\text{vehicle-mi}} * \frac{\text{mi}}{1.609 \text{ km}} * \frac{\text{km}}{\text{truck}} * N_T * \frac{298 \text{ kgCO}_2\text{eq}}{\text{kg N}_2\text{O}} = 8.9 \cdot 10^{-4} \frac{\text{kgCO}_2\text{eq}}{\text{vehicle-km}} \quad \text{Eq. S16}$$

All three factors were applied to determine vehicle emissions during transit. WTP GHG emissions were calculated using an aggregated emission factor based on GREET data of 2.685 kg CO₂ eq/gal, or 709.3 kg CO₂eq/m³ of diesel consumed.^[17]

Consumptive water uses reported in GREET for the same process are summed to obtain an upstream transportation water consumption impact of 3.71 m³ H₂O/m³ diesel. Water consumed directly in transit is considered negligible.

4. Fracturing

4.1. Fluid volumes

To capture variability in the amount of fluid required for hydraulic fracturing of a single well, total fluid volumes are computed stochastically in Crystal Ball. Based on state-of-the-art input from industry, fluid volume per stage will range from 300,000-500,000 gal (1136-1893 m³) for a water-based frac, with an average of 10 stages per lateral and 6 laterals per well (see Tables S1-S2). The total required fluid volume for one wellhead (base fluid of water or CO₂ + additives) is thus calculated by multiplying fluid volume per stage by 10 stages and 6 laterals. Conversations with industry representatives indicated 30% less fluid is used in a CO₂ frac compared to slickwater on a volume basis. This factor is also consistent with relative changes in fluid densities; whereas the density of water varies minimally from the surface to the injection point, CO₂ density drops roughly 30%. The resulting additional expansion would allow CO₂ to generate comparable fracture networks with less fluid volume. Thus, for the CO₂ base case, the distribution for fluid volume per stage was taken as 70% of the min, max, and likely values for slickwater. For the outlook case, we assume a further 5% reduction in fluid volume is possible with improvements in proppant transport

(i.e. total fluid volume is 65% of that needed for a water-based frac). The equivalent mass of CO₂ injected in each case is computed using the density at injection conditions (2 MPa, -20°C) for use in calculations.

The volumes of chemical additives in each formulation (see Section 4.2) were subtracted from the total fluid volume in each scenario to obtain the base fluid volume (i.e. water or CO₂). These volumes were used to determine the amount of fluid needed from the source. Based on data for the Marcellus region, we assume that 6-18% (with an expected value of 10%) of the water-based fluid consists of recycled fluid from other well sites; the remainder must be withdrawn from a surface source as described in Section 3.1.^[14] For CO₂, the total volume obtained from a capture facility included an additional 3% of the base fluid to account for refrigerative losses in transport and storage. In the outlook case, we also account for obtaining recycled CO₂ from another frac site by subtracting the volume of CO₂ recompressed in separation (see Section 6.2) from the total required volume.

4.2. Additives: Fluid compositions and upstream impacts

Conventional fracturing fluids consist primarily of water and proppant, along with a small percentage of chemical additives that vary widely by site and operator. A simplified composition was applied for the purposes of this study, modeled after King 2012^[9] and input from industry. Acid, corrosion inhibitor, and scale inhibitor are used in equal proportions in both cases, while biocide and friction reducer only apply to slickwater. Representative chemicals for each additive function and their concentrations in the total fracturing fluid volume are summarized in Table S11 below; note that the same fluid composition is used for both CO₂ frac scenarios, though total volumes differ as discussed in Section 4.1. Due to significant uncertainty in the amount of proppant required for a CO₂ frac job relative to a water-based system, equal proportions of sand are added to each.

Table S11. Comparison of additives used in water- and CO₂-based fracturing fluids

Additive	Units	Water	CO₂
Proppant (sand)	kg/m ³ fluid	120	120
Acid (30% HCl)	m ³ /m ³ fluid	0.0067	0.0067
Friction reducer (polyacrylamide)	kg/m ³ fluid	0.046	--
Biocide (glutaraldehyde)	kg/m ³ fluid	0.035	--
Corrosion inhibitor (methanol)	m ³ /m ³ fluid	0.00001	0.00001
Scale inhibitor (phosphonate)	kg/m ³ fluid	0.035	0.035

Specific quantities of these additives used in the model are also listed in Tables S2-S4 by volumetric concentration. These values were multiplied by the distributions for the total amount of injected fluid in Crystal Ball to estimate total chemical and proppant demands for storage and transport sizing. The figure listed in Table S11 for HCl is based on a 30% concentration in H₂O. For the other additives, chemical transport volumes were adjusted to account for the following concentrations in solution: 100% methanol, 85% phosphoric acid, and 25% polyacrylamide and glutaraldehyde. These concentrations were applied along with chemical densities to convert chemical volumes to an equivalent mass:

$$\text{Chemical mass} = \text{Volume} * \rho * \% \text{ in solution} \quad \text{Eq. S16}$$

Life cycle energy use, emissions, and water use for upstream chemical and proppant production were then calculated based on the Ecoinvent impact factors cited in Table S7. Proxies were used for chemicals not explicitly listed in Ecoinvent to estimate impacts based on a similar process. Polyacrylamide was modeled as acrylonitrile, which is hydrolyzed to form acrylamide units, and glutaraldehyde was represented by acetaldehyde due to similarities in chemical structure and manufacturing techniques.^[4]

4.3. Blending

4.3.1 Water-based fluids

Water must be pumped from storage tanks at the well pad to the blender. We assume all well pad equipment is connected by 10m long, 6" PVC pipes. Energy for this process was calculated in the same way as impoundment-to-storage transmission described in Section 3.1, using a centrifugal pump where Δp consists of frictional losses and equivalent minor losses. Typical slickwater formulations will reduce friction by 65%; thus, 35% of the calculated Δp_f was assumed to be the friction pressure drop for this pump. The flow rate is also ramped up to the injection rate of 80 bbl/min or 0.212 m³/s.^[9] CO₂ is stored at sufficient pressure to omit this pumping stage.

According to an industry expert, a 100 bbl/min blending unit for the slickwater system consumes approximately 60 gal of diesel per hour, or 6.3E-5 m³/s. We took 80% of this value (48 gal/hr or 5.1E-5 m³/s) to account for the reduced flow rate of 80 bbl/min for the system considered here. This power rating was multiplied by the time required to pump all fluids through the blender and converted to MJ of diesel using the density (832 kg/m³) and heating value (45 MJ/kg). Impacts from diesel consumption and combustion were calculated according to Section 2.2.

4.3.2 CO₂-based fluids

The CO₂ is stored at sufficiently high pressure that no pump is required to transfer the fluid from storage to the blending units. We assumed blending follows a model process whereby CO₂ flow through a venturi stage educts proppant directly into the fluid stream entering the high-pressure pumps. Because this system is driven by fluid pressure and flow, no external energy inputs are required, and any GHG losses from cycling fluid through the system are incorporated in the 3% refrigerative losses taken from the total sourced CO₂ volume. Although this process is still in the early stages of commercialization, it is expected to be state-of-the-art for blending in a large-scale CO₂ frac according to industry experts. While other blending options similar to those used in water-based fractures were considered, this model process addresses issues with proppant blending at pressure in large frac operations and the technology could be applied at the scale of this study.

4.4. High-pressure injection

In both cases, fluid is pumped from the blender to the high-pressure pump used for fracturing. The energy consumed in this step is calculated in the same way outlined in section 4.3 for pumping water from storage to blending, but here a pressure differential is added to the Δp to attain sufficient inlet pressure for the injection pump. Water pressure is raised from atmospheric pressure to 75 psi,

or 0.52 MPa, while CO₂ is pressurized from 200 to 300 psi (1.4 to 2.1 MPa). While CO₂ is initially transported and stored at 2 MPa, we account for pressure losses accrued over time in storage units and through pipeline transmission by assuming pressure has dropped to roughly 1.4 MPa by the time the fluid exits the blender.

Fluids are then injected via a high-pressure positive displacement pump into a 2-km vertical well with a 1067m lateral. The required pressure at the outlet is determined from the inlet pressures coming off the blenders, formation fracture pressure, frictional losses and equivalent fitting frictional losses, and hydrostatic pressure applied by fluid in the wellbore:

$$\Delta p = (p_{fracture} - p_{inlet}) + 2\Delta p_f - p_h \quad \text{Eq. S17}$$

Pumping energy is thus calculated as detailed in Section 2, using the average of surface and bottomhole fluid properties for Reynold's number calculations. Note that the 65% friction reduction for slickwater discussed in Section 4.1 applies to pumping the water-based fluids both into and out of the high-pressure injection pump. Hydrostatic pressure is the product of the fluid density, gravitational constant, and well depth (2 km), which equates to 19.56 MPa for slickwater and 14.41 MPa for CO₂. Formation fracture pressure is assumed to be 45.22 MPa based on a fracture pressure gradient of 22.61 MPa/km.

5. Flowback

5.1. Water-based fluids

5.1.1. Flaring

Although regulations and economics incentivize operators to capture and sell 100% of the gas produced, an initial flowback period is required before gas can be treated. We assume this period lasts 2 days based on industry experience. Flowback is primarily water entrained with intermittent streams of gas. Using initial water and gas production rate data from industry, we estimated a nominal average natural gas flow rate of 0.18 MMcf/d (5178 m³/d) during this time. The gas composition is simplified as 100% methane, the primary constituent, which is oxidized to form CO₂ during flaring via the following reaction:



Based on molecular weights, 2.75 kg of CO₂ is produced per kg of methane burned. The gas flowback rate noted above is assumed constant over the brief flowback period and multiplied by the flare time to determine total gas flared. Assuming a 99% combustion efficiency, GHG emissions from flaring are calculated as:

$$\text{kgCO}_2\text{eq} = \left(\frac{\text{m}^3\text{gas}}{\text{d}}\right) (t, \text{d}) \left[0.01 \left(\frac{0.717\text{kgCH}_4}{\text{m}^3\text{gas}}\right) \left(\frac{25\text{kgCO}_2\text{eq}}{\text{m}^3\text{gas}}\right) + 0.99 \left(\frac{0.717\text{kgCH}_4}{\text{m}^3\text{gas}}\right) \left(\frac{2.75\text{kgCO}_2}{\text{kgCH}_4}\right) \right] \quad \text{Eq. S19}$$

Because energy production is modeled as gross EUR per well, we count flared gas as lost energy. Using an average HHV of 1193 Btu/scf for Marcellus shale gas,^[5] this direct energy consumption is calculated as:

$$\text{Flaring energy} = \left(\frac{\text{m}^3\text{gas}}{\text{d}}\right) (t, \text{d}) \left(\frac{35.31\text{ft}^3}{\text{m}^3}\right) \left(\frac{1193 \text{ Btu}}{\text{scf}}\right) \left(\frac{1 \text{ MJ}}{947.8 \text{ Btu}}\right) \quad \text{Eq. S20}$$

No consumptive water use occurs in flaring.

5.1.2. Reuse and Treatment

Wastewater generated during well completion must be removed from the site for reuse or disposal. A distribution for total water flowback fraction was obtained from US EPA data^[14] (Table S3) and multiplied by the total volume of injected fluid in Crystal Ball to estimate a bulk volume of flowback fluid. This water is routed through a 2" PVC pipeline back to the initial on-site impoundment; thus, no new storage burdens are incurred. Pumping energy is calculated according to Section 2, applying a lower flow rate of 50 gpm (0.00315 m³/s) and assuming that fitting friction losses now equal 10% of tubular losses. Note the friction reduction used for slickwater injection does not apply to flowback water. All water not returned as flowback is taken as a direct consumptive water use (i.e., the difference between the injected and flowback fluid volumes).

It is common practice for operators to reuse flowback water at another well site. Industry indicated this cycle would continue indefinitely, but we end recycling after 10 well sites to account for salt and chemical accumulation. We further assume that this equivalent amount of wastewater would be sent to a centralized waste treatment (CWT) facility after 10 reuses and thus allocate 10% of the treatment burdens to our site. To roughly account for evaporative losses, we assume 98% of flowback is transported for reuse; assuming 2% evaporative losses at each subsequent site, 80% is ultimately treated after 10 uses. The energy required to pump 98% of the flowback onto trucks for reuse was calculated as described in Section 2.1, using a 4" PVC pipeline and flow rate of 500 gpm (0.0315 m³/s).

Truck transport was the only burden associated with reuse, while treatment involved both transport to the facility and downstream wastewater treatment impacts. NETL compiled a life cycle inventory for treating wastewater from Marcellus shale wells, reporting an energy use of 4.49E-4 kWh/kg water, or 1.62 MJ/m³.^[30] Since the facility draws energy from the grid, this factor was multiplied by the Ecoinvent factor for electricity (average US mix) to obtain a net energy impact of 5.51 MJ/m³. NETL also computed life cycle CO₂, CH₄, and N₂O emissions of 339.1, 3.7, and 1.38 g/m³ wastewater, respectively.^[30] The CO₂ emissions directly equate to 0.3391 kgCO₂eq/m³; methane and nitrous oxide emissions were converted to 0.0925 and 0.4104 kgCO₂eq/m³, respectively, based on the IPCC 100-year GWP factors. Summing these emissions yields a GHG impact of 0.842 kgCO₂eq/m³ at the treatment facility; upstream electricity impacts were again added based on the Ecoinvent factor, yielding a total GHG impact of 1.086 kgCO₂eq/m³. These factors are listed in Table S9. Because water use was not included in this report, the impact factor was approximated from Ecoinvent as the consumptive water use for a class 3 (medium-sized)

wastewater treatment plant (see Table S7). All three factors were multiplied by the wastewater volume sent to treatment in flowback to calculate corresponding life cycle impacts.

5.2. CO₂-based fluids

In the absence of empirical data on the quantities and rates of CO₂ flowback in a large-scale fracturing job, we modeled CO₂ and CH₄ flows during flowback and production based primarily on industry input along with available academic research. For the base case, the total quantity of flowback and produced CO₂ (i.e. total amount of CO₂ recovered over the wellhead's lifetime) is assumed to be between 60 and 90% of the injected fluid based on input from industry experts, with a median of 75% (see Table S1). For the outlook case, we estimate a median of 50% of the injected CO₂ will be recovered in flowback and production by extending data and theory from available literature. According to Cipolla (2010), 46.5% of natural gas is adsorbed in the Marcellus shale.^[31] Assuming most of the CO₂ molecules preferentially absorb to organic surfaces, this indicates the upper limit for CO₂ sequestration may be 46.5% of the CH₄ volume, and the remaining CO₂ would flow back. Kang (2011) reports that CO₂ can access 1.38 to 4 times more pore space than CH₄, which would reduce flowback because more pore space is available.^[32] Applying the theoretical CO₂ storage capacities defined by these authors, we derived an estimate for minimum CO₂ flowback from the maximum CO₂ storage capacity.

The CH₄ reservoir volume contributing to a single lateral is first computed from the EUR (based on the produced gas for a slickwater frac, as this volume is best understood) and ratio of produced CO₂ to the original gas in place (OGIP). To back out the original in-situ gas volume, a density ratio between CH₄ in the reservoir and at the wellhead is first computed, assuming nominal reservoir conditions of 75°C and 20 MPa and wellhead conditions of 25°C and 5 MPa:

$$\text{CH}_4 \text{ density ratio} = \frac{\text{Reservoir density}}{\text{Wellhead density}} = \frac{120.40 \text{ kg/m}^3}{35.27 \text{ kg/m}^3} = 3.4 \quad \text{Eq. S21}$$

For a reservoir with a typical production factor of 0.25 for a slickwater frac (i.e. 25% of the OGIP is produced), the initial CH₄ reservoir volume is back-calculated using this density ratio and the EUR volume for the single wellhead defined in this study (i.e. a system of 6 laterals):

$$\text{Reservoir CH}_4 \text{ vol.} = \frac{\text{EUR}}{(\text{Production factor})(\text{CH}_4 \text{ density ratio})} = \frac{7.39 \times 10^8 \text{ m}^3}{(0.25)(3.26)} = 9.07 \times 10^8 \text{ m}^3 \quad \text{Eq. S22}$$

In contrast, the total volume of CO₂ injected in the base case is on average 63,595 m³ for one wellhead (again, 6 laterals), or 0.007% of the original CH₄ in place. Extending this first-order calculation demonstrating that the injected CO₂ volume is a mere fraction of the in-situ gas along with Kang's data indicating shales can store up to four times more CO₂ than methane under reservoir conditions, we posit that the majority of CO₂ could be sequestered as kinetics will favor CO₂ sorption and corresponding CH₄ displacement over long-term production. While the concepts discussed here seemingly build a case for nearly 100% CO₂ storage, early flowback will be primarily CO₂, and the desorption mechanisms dominating both CO₂ and CH₄ recovery rates during long-term production do not effect flow dynamics during injection and flowback. Based on

these inputs, we conservatively assume the lowest theoretical amount of CO₂ recovered (and greatest amount sequestered) would be 10% of the injected fluid. The total recovered CO₂ in the outlook case is modeled stochastically with a range of 10-90% and median of 50% to account for uncertainty in our application of this theoretical data and again entertain the possibility of nearly complete flowback. These estimates of CO₂ recovery rates will vary widely with the formation structure, porosity, and pore space distribution between organic and inorganic substrates, but serve as a realistic first-level approximation of the total amount of CO₂ that must be managed during flowback and production operations.

In both cases, flowback gases will follow a series of processing stages similar to the treatment train associated with water-based fluids. Gas will first pass through a slug tank and three-phase liquid separator at the wellhead. However, because the Marcellus is a dry formation and in the CO₂ scenarios no water is injected during fracturing, we assume the volume of any liquids collected at the wellhead is negligible during flowback and production and thus do not consider wastewater disposal. The gas stream (CO₂ + CH₄) is flared during flowback until the CO₂ concentration reaches the 40% threshold required by current membrane separation technology. The gas then passes through a series of membrane separators that remove CO₂ until the untreated gas stream reaches an acceptable pipeline quality. At this point, membranes are no longer needed and production begins. These processes are described in detail in Section 6.2, but a schematic overview of the flowback and production timeline with corresponding CO₂ and CH₄ concentrations is presented in Figure S4.

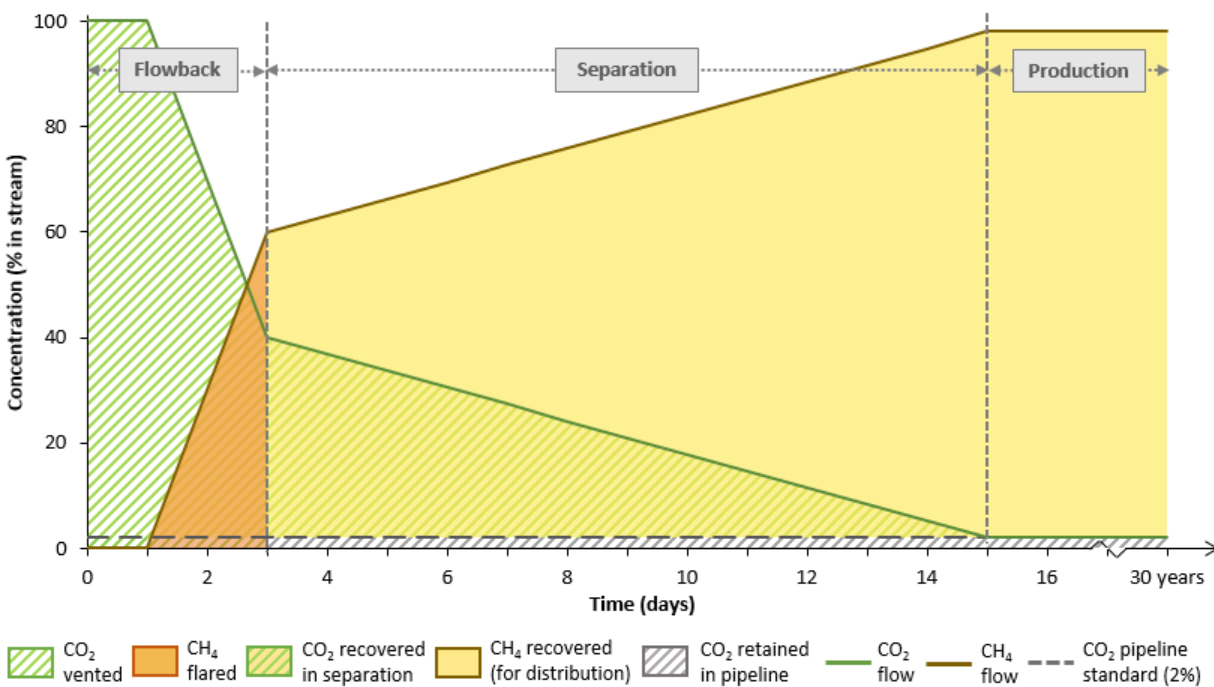


Figure S4. CO₂ flowback and production timeline. The gas stream is assumed to be 100% CO₂ for the first day, but CO₂ levels rapidly drop to 40% from days 1-3. Once this threshold is reached,

separation begins; a high flow rate is maintained to quickly bring the CO₂ content down to pipeline quality (~2%) for long-term production.

The total gas volumes recovered in flowback are estimated equivalently for both scenarios using a fixed flow rate and time frame characteristic of actual wellhead operations. We assume a constant flow rate of 10 MMcf/d (283,168 m³/d) during flowback, where the CO₂ concentration drops from 100 to 40%. Due to the high volumes of CO₂ injected, we also assume gas breakthrough will not occur for at least one day. To this end, the CO₂ content of the gas stream is 100% for the first day before decreasing linearly to 40% between days 1 and 3. These rates and concentrations stem from industry input indicating a 2-day window to reach the 40% CO₂ threshold necessary to commence separation. In both scenarios, we assume CO₂ and CH₄ released during flowback will be flared. While our outlook case considers CO₂ capture and reuse as opposed to release during separation, the gas flow rate will still be too high initially and the quality too inconsistent to feasibly capture and treat CO₂ during this initial flowback period.

Because the initial gas flow is 100% CO₂, the volume recovered in the first day simply equates to the total gas flow during this time (10 MMcf or 283,168 m³/d). From days 1-3, recovered CO₂ can be taken as the integral of the CO₂ flow rate over time. Because the total gas flow rate is fixed and the CO₂ concentration declines linearly, it was possible to calculate this volume as the product of the average CO₂ concentration, total gas flow rate, and time. This quantity is added to the CO₂ recovered in day 1 to approximate the total CO₂ released in flowback:

$$\text{Vol. CO}_2 \text{ flowback} = 283,168 \frac{\text{m}^3}{\text{d}} (1\text{d}) + \frac{(1+0.4)}{2} \left(283,168 \frac{\text{m}^3}{\text{d}} \right) (2\text{d}) = 679,604 \text{ m}^3 \text{ CO}_2 \quad \text{Eq.S23}$$

As discussed in Section 1.5, this CO₂ is neglected as a direct GHG emission, as it was originally sourced from facilities where it would otherwise be vented and thus does not induce a net emission. The volume of natural gas flared during flowback is calculated in the same way by integrating the CH₄ flow curve from days 0-3, based on the average CH₄ concentration during this time:

$$\text{Vol. CH}_4 \text{ flared} = \left(0 \frac{\text{m}^3}{\text{d}} \right) (1 \text{ d}) + \frac{(0+0.6)}{2} \left(283,168 \frac{\text{m}^3}{\text{d}} \right) (2\text{d}) = 169,901 \text{ m}^3 \text{ CH}_4 \quad \text{Eq. S24}$$

As in the case of water-based fluids, we count flared gas as a direct energy loss since gross EUR values were used. Thus, the volume of gas flared computed above is converted to its energy equivalent in MJ using the energy content of Marcellus shale gas (see section 5.1.1). The emissions associated with flaring flowback methane are converted to CO₂ equivalents using the calculation outlined in Section 5.1.1:

$$(169,901 \text{ m}^3 \text{ CH}_4) \left[0.01 \left(\frac{0.717 \text{ kg CH}_4}{\text{m}^3 \text{ CH}_4} \right) \left(\frac{25 \text{ kg CO}_2 \text{ eq}}{\text{m}^3 \text{ CH}_4} \right) + 0.99 \left(\frac{0.717 \text{ kg CH}_4}{\text{m}^3 \text{ CH}_4} \right) \left(\frac{2.75 \text{ kg CO}_2}{\text{kg CH}_4} \right) \right] = 30,456 \text{ kg CO}_2 \text{ eq} \quad \text{Eq. S25}$$

Following flowback, gas will be treated according to the separation and long-term production stages defined in Figure S4; these processes are detailed in Section 6.2.

6. Production

6.1. Water-based fluids

In addition to flowback, water is produced incrementally throughout the production life of the well. According to the US EPA, the total volume of wastewater generated over the life cycle of a well is approximately 50% flowback and 50% produced water.^[14] For the purposes of this study, we assume total produced water volume equals the initial flowback volume. Since this water is produced intermittently and in varying quantities, it is transported directly to a centralized waste treatment facility. The burdens associated with pumping, trucking, and treating this water are calculated in the same way as flowback water (Section 5.1.2).

After the 2-day flowback period described in Section 5.1.1, gas breakthrough occurs and the well transitions to production. The stream of gas and liquids must be treated through a series of separation and purification processes to reach pipeline quality. A slug tank is placed at the well outlet to capture and mechanically separate large volumes of gases and liquids. The stream then flows through a 3-phase gas-liquid separator to further remove flowback water. Since both separation systems are driven by gravity and fluid differences, no energy and water inputs or emissions are considered.

Finally, the stream passes through a dehydrator to remove water vapor prior to pipeline transport. According to Middleton et al (2014), the energy required to dehydrate 10⁵ m³ of natural gas at 10 MPa and 30°C is 90 kW.^[11] Applying the density of methane under these conditions, energy use in dehydration is approximated as:

$$\text{Dehydration energy} = \frac{90\text{kW}}{\frac{10^5\text{m}^3}{\text{hr}} * 77.84 \frac{\text{kg}}{\text{m}^3}} = 4.162 * 10^{-5} \text{MJ/kg CH}_4 \quad \text{Eq. S26}$$

The dehydration units will also be fueled by the on-site generator and operate for the 30-year production phase. Thus, energy consumed by the dehydrator over the life of the well was calculated from the well's EUR and the density of methane under the standard conditions assumed in gas measurement (60°F or 15.6°C, atmospheric pressure):

$$\text{Dehydrator, LC energy} = \frac{4.162 * 10^{-5} \text{MJ}}{\text{kg CH}_4} * \frac{\text{EUR (m}^3\text{)}}{\rho_{\text{CH}_4 (60\text{F}, 1\text{atm})}} \quad \text{Eq. S27}$$

The Ecoinvent factors in Table S7 were applied to determine the life cycle energy, GHG, and consumptive water impacts of diesel use for dehydration. Once gas is treated to pipeline specifications, it is piped downstream for further processing and distribution. These stages are beyond the scope of the fracturing fluid's life cycle and thus are not considered in this study.

6.2. CO₂-based fluids

Following the 3-day flowback period described in Section 5.2, gas is suitable for treatment and a separation period begins to bring CO₂ concentrations to or near the pipeline standard of 2%. Industry data from smaller CO₂ frac jobs indicated CO₂ levels would fall below 2% after 12 days of separation, where the mixed gas stream is routed through a series of membranes to separate

CO₂. As in the case of water-based fluids, a slug tank will first catch the large, erratic volumes of gases and fluids (primarily heavier mass fraction hydrocarbons) exiting the wellhead and provide preliminary gas-liquid separation. Because the Marcellus is a dry formation, and no water is used in CO₂ fracturing, few liquids are expected in the gas streams. Thus, dehydration impacts are only calculated for gas produced during the 12-day separation period with the same approach described in Section 6.1, assuming a reduced average flow rate of 6 MMcf/d (169,901 m³/d):

$$\text{Dehydrator, LC energy} = \frac{4.162 \times 10^{-5} \text{ MJ}}{\text{kg CH}_4} * \frac{\text{Gas flow (m}^3/\text{d)}}{\rho_{\text{CH}_4, 60\text{F}, 1 \text{ atm}} (\text{kg/m}^3)} * t(\text{d}) \quad \text{Eq. S28}$$

Once liquids are removed, the gas is suitable for membrane treatment. This 12-day separation period is modeled similarly to flowback, assuming the CO₂ concentration declines linearly from 40 to 2% under the constant flow rate of 6 MMcf/d. In reality, the CO₂ content will drop rapidly at the start of separation before the rate of decline levels out, but a linear approach is sufficient to approximate the bulk quantities of gases needed for this model. The volumes of CO₂ removed and CH₄ recovered in separation are calculated by effectively integrating the individual CO₂ and CH₄ flow curves using the approach defined in Section 5.2:

$$\text{Total volume of CO}_2 \text{ separated} = \frac{(0.4+0.02)}{2} \left(169,901 \frac{\text{m}^3}{\text{d}}\right) (12\text{d}) = 428,150 \text{ m}^3 \text{ CO}_2 \quad \text{Eq.S29}$$

$$\text{Total volume of CH}_4 \text{ separated} = \frac{(0.6+0.98)}{2} \left(169,901 \frac{\text{m}^3}{\text{d}}\right) (12\text{d}) = 1,610,660 \text{ m}^3 \text{ CH}_4 \quad \text{Eq.S30}$$

These volumes represent the CO₂ and CH₄ fractions of the 2,038,810 m³ of gas produced during the 12-day separation period, but further breakdown is needed to estimate the quantities of each gas that need to be compressed at the onset of each compression stage. Figure S5 illustrates the bulk quantities of gases that will ultimately pass through each stage along with the fate of the separated CO₂ and CH₄ streams. Note that in reality, the total volume of gas recovered in separation will not pass through the membranes all at once, as the incremental gas flowing back each day will move sequentially through the four stages. However, since we are concerned with estimating the bulk quantities of gas requiring compression during this process, it suffices to estimate the total volumes of gas that will ultimately be sent to pipelines or compressed at each membrane stage.

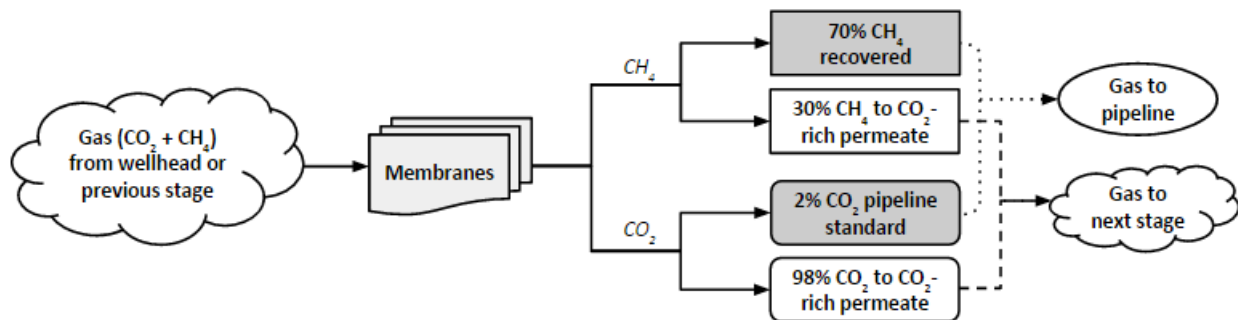


Figure S5. Schematic of the membrane separation process tracing the fate of the CO₂ and CH₄ fractions of the produced gas stream. 70% of the influent methane to each stage along with 2% of

the influent CO₂ are sent to pipelines, while the remaining gases comprise the CO₂-rich permeate stream and must be re-compressed before entering the next stage. After four stages, the process is no longer efficient; remaining gases (i.e. not sent to pipelines) are either vented (base case) or recompressed for reuse (outlook case).

According to industry experts, 70% of the influent methane at each stage will be recovered as pipeline-quality gas. We assume the total gas routed to the pipeline following each stage will be 1.02 times this volume, as CO₂ will comprise 2% of the stream per pipeline standards. To illustrate how the numbers in Figure S5 were derived, the flows for the first stage can be traced as follows: 70% of 1,610,660 m³ CH₄ or 1,127,462 m³ CH₄ will be recovered as sellable gas with a total volume of 1.02(1,127,462 m³ CH₄) or 1,150,011 m³ CH₄ directed to a pipeline. Two percent of this gas volume (23,000 m³) will be CO₂. Thus, the remaining mixture of CH₄ and CO₂ that will be sent to the second stage is taken as the differences between the inflow volumes and pipeline volumes of each gas:

$$1,160,660 \text{ m}^3\text{CH}_4 \text{ in} - 1,127,462 \text{ m}^3\text{CH}_4 \text{ to pipeline} = 483,198 \text{ m}^3\text{CH}_4 \text{ to Stage 2} \quad \text{Eq.S31}$$

$$428,150 \text{ m}^3\text{CO}_2 \text{ in} - 23,000 \text{ m}^3\text{CH}_4 \text{ to pipeline} = 405,150 \text{ m}^3\text{CO}_2 \text{ to Stage 2} \quad \text{Eq. S32}$$

This process is repeated for the subsequent stages. The energy required to compress the mixed gas stream back to the required inlet pressure of 800 psi between stages is again calculated using McCollum and Ogden's approach outlined in Section 3.2 for CO₂ capture at the source.^[19] However, to account for the difference in molecular weight between the two gases in the mixed stream, we separately calculate the recompression energy for CO₂ and CH₄ and approximate the total energy requirement for the mixture, which is the sum of the energy requirement to compress each stream separately. Both gases will be compressed from ambient surface conditions (25°C and 1 atm or 0.1 MPa) at the outlet from the membranes to 800 psi (5.5 MPa) going into the subsequent stage. Note that gas will not be compressed entering the first stage, as industry indicates the pressure of gas exiting the wellhead will be sufficient to drive it through the first round of membrane separation. Thus, compression impacts are only considered for the gas volumes entering Stages 2, 3, and 4. Five compression stages are needed to reach a cutoff pressure of 5.5 MPa; summing the energy inputs for each stage yields a CO₂ compression energy factor of 318 MJ/tCO₂. The energy required to compress the methane portion of the stream is calculated in the same way, substituting the molecular weight of methane for that of CO₂ to obtain a factor of 872 MJ/tCH₄. As opposed to CO₂ capture, which occurs at an industrial facility and draws power from the electric grid, the on-site compressors are powered by the diesel-electric generator. Thus, we factor in the efficiencies of the electric motor (0.90) and diesel-to-electricity conversion (0.405) and determine the life cycle energy burdens in the same way as all on-site equipment, accounting for both energy consumed directly in the process and upstream impacts from diesel production:

$$\text{Compression, separation} = \frac{\left(318 \frac{\text{MJ}}{\text{tCO}_2}\right)(\text{Mass CO}_2) + \left(872 \frac{\text{MJ}}{\text{tCH}_4}\right)(\text{Mass CH}_4)}{(0.405)(0.9)} \left(1 + 1.21 \frac{\text{MJ upstream}}{\text{MJ diesel}}\right) \quad \text{Eq. S33}$$

At the end of Stage 4, separation is no longer economically or energetically favorable. At this point, the total volume of CO₂ for disposal (i.e. CO₂ not entrained in pipeline gas that will be vented or recompressed depending on the scenario) is obtained by subtracting the CO₂ that will be entrained in the recovered pipeline-quality gas at each stage (i.e. 2% of the total gas flow) from the bulk volume of CO₂ separated. Similarly, the total volume of methane that is not recovered is determined by subtracting the volumes sent to pipelines at each stage from the total volume of methane that passes through the membranes in separation. This methane is either flared or recompressed along with the residual CO₂ in accordance with the scenario.

In the base case, the recovered permeate stream of mixed gases will be flared; the GHG impact is calculated by converting the volume of CH₄ flared to kgCO₂eq, as described in Section 5.1.1. As before, this flared gas is also counted as a direct energy impact. Per the allocation method described in section 1.5, the CO₂ vented during separation is not counted as a GHG emission, since this gas would have otherwise been vented at the source. No water consumption is involved in flaring or venting.

For the outlook case, gases recovered in separation are recompressed for reuse at another frac site. While this gas is not pure CO₂, the roughly 3% methane content should not prohibit reinjection in another well, particularly when mixed with other CO₂ streams. Again, we separately compute the energy required to compress the CO₂ and CH₄ portions of the stream and assume the total energy demand can be approximated as the sum of these inputs. The effluent pressure and temperature off of the membranes are assumed to be at ambient surface conditions of 0.1 MPa and 15°C, respectively; a 4-stage system is needed to recompress the stream to storage and transport conditions of 2 MPa and -20°C. The compression ratio is again calculated from the final cut-off pressure (2 MPa) and the inlet pressure (e.g. the effluent pressure from the membrane separators), which results in a CR of 2.11. Applying this CR, inlet temperature, and inlet pressure to McCollum and Ogden's approach^[20] over 4 stages for each of the two gases yields an energy consumption factor of 239 MJ/tCO₂ and 656 MJ/tCH₄. Here, the compressors are driven by an on-site diesel-electric generator, so this value is divided by the efficiency factors for diesel-to-electricity conversion (0.405) and the electric motor (0.9) to determine the total amount of energy needed to achieve recompression. The total energy impact is thus calculated in the same way as the compression energy involved in membrane separation:

$$\text{Recompression energy} = \frac{\left(\frac{239 \text{ MJ}}{\text{tCO}_2}\right)(\text{Mass CO}_2) + \left(\frac{656 \text{ MJ}}{\text{tCH}_4}\right)(\text{Mass CH}_4)}{(0.405)(0.9)} \left(1 + 1.21 \frac{\text{MJ upstream}}{\text{MJ diesel}}\right)$$

Eq. S34

The emissions associated with recompression are calculated by summing upstream emissions in diesel production and direct on-site combustion in the compressor. The Ecoinvent factor for diesel use and the EPA factor for on-site combustion are applied to the total energy consumption to obtain the total GHG impact, as documented in Section 2.2. We also account for trucking this CO₂ (and residual CH₄) to a subsequent frac site for reuse per the method outlined in Section 3.3, where burdens are calculated based on the fuel consumption associated with transporting the separated

volume of CO₂. Because the CO₂ and residual CH₄ were compressed to transport conditions of -20°C and 2 MPa, the total masses recovered in separation was converted to equivalent compressed volumes using the densities under storage and transport conditions (1031.8 kg/m³ for CO₂ and 16.24 kg/m³ for CH₄) to obtain the required number of tanker trucks. We assume the transport distance to the next frac site is the same as the distance for recycling flowback water to a subsequent site in the first scenario (see Table S3). For consistency, the fluid volume is again reused at 10 frac sites before ultimate disposal. As opposed to the case of water-based fluids where flowback is sent to treatment after 10 reuses, we assume any CO₂ not sequestered in formations during reuse would simply be vented, as the volume would be too small to justify reinjection. In accordance with our allocation method, no net emissions result from releasing the remaining CO₂ at end of life.

The recovered CH₄ is piped downstream for further processing. As discussed in section 1.5, all CO₂ that remains in the formation (i.e. not returned in flowback, separation, or production) is considered an emission credit. For each scenario, this quantity is computed based on the total amounts of recovered CO₂ expected in flowback and production (see section 5.2):

$$\text{CO}_2\text{Credit} = (\text{Total recovered CO}_2, \% \text{ of injected fluid})(\text{Total mass injected CO}_2, \text{kg}) \quad \text{Eq.S35}$$

The mass of sequestered CO₂ divided by the EUR is taken as a negative GHG impact. Note that although the total amount of CO₂ stored is greater for the outlook case owing to a lower assumed recovery fraction, the GHG credit is actually greater in the base case because the lower EUR increases the credit achieved per GJ of energy.

7. Estimated ultimate recovery

7.1. Water-based fluids

To normalize impacts to the FU, we calculated lifetime energy production from estimated ultimate recovery (EUR) volumes. For wells stimulated with water-based fluids, an average EUR of 4.35 bcf was taken from a 2015 assessment of over 2,600 horizontal Marcellus shale gas wells.^[10] This value reflects the expected energy output with current practices and is thus consistent with our model inputs that capture the state of the art in the fracking industry. The gas volume was converted to GJ of energy based on the HHV of pipeline quality Marcellus shale gas:^[5]

$$\text{EUR, GJ} = 4.35 \text{ bcf gas} * \frac{10^9 \text{ scf}}{\text{bcf}} * \frac{1085 \text{ btu}}{\text{scf}} * \frac{1 \text{ MJ}}{947.8 \text{ Btu}} * \frac{\text{GJ}}{1000 \text{ MJ}} = 4.98 * 10^6 \text{ GJ} \quad \text{Eq. S36}$$

As noted in each section, all impacts associated with water-based fluids were divided by this EUR to normalize outputs to the functional unit.

7.2. CO₂-based fluids

Production data for shale gas wells fractured with CO₂ is lacking, and available estimates are typically based on data from vertical wells developed in Western Canada in the 1990's or isolated non-shale formations. Furthermore, because modern horizontal frac jobs employ much greater fluid volumes, advances in fracturing technology will strain any desire for CO₂ fracking in light

of limited CO₂ supply and more challenging transport and storage. However, the mechanics of shale gas production favor CO₂ as a frac fluid over water; the resulting production increase coupled with recent technological advances and a breakthrough in logistics create a compelling case for the potential of CO₂-based fracturing fluids. The potential success of a CO₂-based frac system driving this work is largely predicated on the potential increase in EUR. While quantifying this increase is hindered by a lack of data, we derived estimates for the base case from literature and developed a high-level theoretical model for the outlook case, as detailed in the following sections.

7.2.1. Base case

For both CO₂ scenarios, a production increase factor (here abbreviated as PIF) was applied to this EUR to account for the increased performance in natural gas recovery that serves as the impetus for a CO₂ frac. For the base case, an assumption for this increase factor was developed based on a comprehensive analysis of available literature on field-tested and simulated CO₂ frac jobs. The most relevant data are summarized in Table S12.

Table S12. Literature review of production increases observed with CO₂-based frac fluids

Frac Fluid	Control	Production Increase	Formation	Source
<i>Field tests</i>				
CO ₂ foam	Slickwater	51.4%, 18-mo. cumulative production, 12 wells	Montney, Canada, Heritage field	[33]
CO ₂ foam	Slickwater	110% average increase for 7 CO ₂ foam and 5 nitrified slickwater fracs	Upper Montney, Canada	[34]
CO ₂ /sand	N ₂ gas	133% average for 7 wells, 5-yr cumulative production	Devonian shale, Pike Co, KY	[35]
CO ₂ /sand	N ₂ foam	510% in Pike Co, 6 wells; 77.6% in Perry Co, 3 wells; 5-year cum. production	Devonian shale, Pike and Perry Co, KY	[35]
CO ₂ /sand	Conventional treatments	50% average estimated productivity increase	Various (across FracMaster jobs in the United States)	[36]
<i>Simulations</i>				
Supercritical CO ₂	Slickwater	50% increase in productivity index	Low-permeability sand formation	[37]
CO ₂ energized	Non-energized	169% production benefit	Tight gas wells, Canyon Sands, TX	[38]
CO ₂ energized	Slickwater	25% improvement ratio	Eagle Ford, TX	[39]

Characterizing a production benefit is inherently subjective, as no two wells have the same EUR regardless of fracturing technique. In the absence of a clear performance benefit, a distribution of factors for CO₂ was inferred from the aggregated data set presented in Table S12. Of the CO₂-fractured formations, the dry, low-permeability Montney formation is most similar to the Marcellus shale; results from these studies are thus weighted more heavily for our scenario. We consider the potential for no production benefit (0%) as the minimum, and apply a conservative

maximum of 110% observed in the Montney. An expected value of 50% was selected for the CO₂ base case, as this was the most frequent reported percentage based on the number of wells fracked, and was also observed in the Montney. Although several studies have reported failed CO₂ stimulations,^[40,41] many cited geologic differences and external errors such as casing failures as primary explanations. Furthermore, recovery hinges on formation characteristics and initial gas volumes that are independent of fracturing fluid, so no definitive conclusions can be drawn based on a limited number of attempts with no effective control. Because improved gas recovery with CO₂ is the impetus for this study and has been corroborated by the majority of field- and lab-scale testing and research, we do not consider a scenario with reduced production compared to a water-based frac.

7.2.2. Outlook case

While the science and art of forecasting well production is beyond the scope of this study, industry projections of EUR and estimations of OGIP (Original Gas in Place) provide a basis for defining the maximum gas recovery that can be achieved using CO₂ as a fracturing fluid. Prior to actual production, a well's prospective yield is estimated from the calculated OGIP in the reservoir along with an experientially defined recovery factor for the particular resource. Once a well is online, EUR can then be separately determined from early production data based on experience in a given formation or similar formations and decline curve analysis.^[42] Both of these methods estimate resource recovery on the basis of unique historical data factors and are applied here to define a plausible ceiling for gas production that could be achieved using CO₂ as opposed to water as a base fracturing fluid. The upper limit for the production increase distribution is derived as follows:

(1) Volumetric approach. A maximum production increase factor can be derived by comparing estimates of the OGIP for a typical Marcellus well with the expected EUR for a water-based frac. The theoretical reservoir potential per well is computed based on the Marcellus gas density and the effective production zone volume (i.e. volume of shale contributing to production for a given well). This volume is calculated from the geometry of a typical Marcellus horizontal wellbore defined in this LCA. According to industry experts, a typical fracture half-length ranges from 600-1000ft in length in the Marcellus; here, we conservatively assume a fracture extends 600ft (183m) horizontally from the lateral. While the formation thickness extends to 600ft in northeast portions of the state, we apply a nominal value of 100ft (30.5m) as a conservative area average, particularly considering that operators are now moving into thinner areas as remaining "sweet spots" are drilled.^[42] This information was applied to create the model reservoir in Figure S6 associated with gas production for a given well.

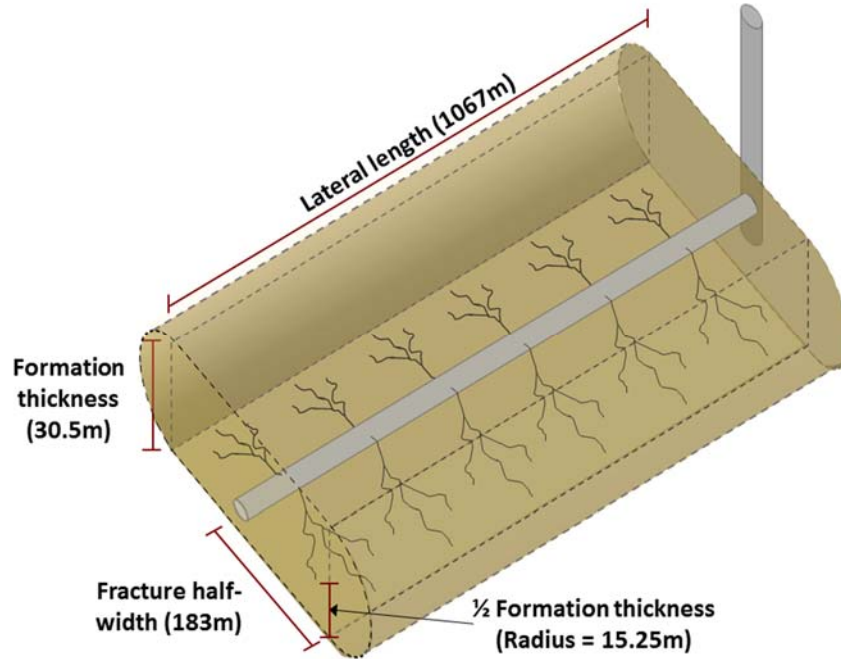


Figure S6. Effective reservoir volume modeled for OGIP calculations.

Based on the data and geometry in Figure S6, the effective reservoir volume contributing to shale gas production can be calculated as:

$$\begin{aligned} \text{Effective reservoir volume} &= \frac{6 \text{ laterals}}{\text{well}} [1067\text{m lateral}] \left[2(183\text{m})(30.5\text{m}) + \pi \left(\frac{30.5\text{m}}{2} \right)^2 \right] \\ &\text{Eq. S37} \\ &= \mathbf{7.6 * 10^7 \text{ m}^3/\text{well}} \end{aligned}$$

Because heterogeneity introduces inherent uncertainty in gas density estimates, which are often based on limited samples, we calculate a production increase factor based on two cited values. Cipolla et al (2010) include data on total free and sorbed gas in the Marcellus; at reservoir pressure, the gas content would be approximately 275 scf/ton shale. For an average shale density of 2.6 ton/m³, this equates to 715 scf/m³ shale. The OGIP volume based on this density estimate can be calculated as:

$$\text{OGIP}_1 = \left(\frac{715 \text{ scf}}{\text{m}^3 \text{ shale}} \right) (7.6 \times 10^7) \text{m}^3 = \mathbf{5.4 \times 10^{10} \text{ scf}} \quad \text{Eq. S38}$$

Using the same logic as the first approach, we assume the OGIP represents the maximum achievable EUR with a CO₂-based frac. The corresponding production increase factor is calculated by applying the median EUR of 4.35 bcf defined in section 7.1:

$$\text{CO}_2 \text{ frac PIF (OGIP}_1) = \frac{\text{Theoretical reservoir potential}}{\text{Water frac median EUR}} = \frac{5.4 \times 10^{10}}{4.35 \times 10^9} = \mathbf{12.4} \quad \text{Eq. S39}$$

Alternatively, Soeder (1988) analyzed a Marcellus shale core sample and correlated measured porosity with in-situ gas content, calculating a density of 26.5 scf gas/ft³ shale (936 scf/m³).^[44] Using the same approach outlined above, OGIP can be determined:

$$\text{OGIP}_2 = \left(\frac{936 \text{ scf}}{\text{m}^3 \text{ shale}} \right) (7.6 \times 10^7) \text{m}^3 = 7.1 * 10^{10} \text{ scf} \quad \text{Eq. S40}$$

The maximum production increase factor if all OGIP is recovered with CO₂ is:

$$\text{CO}_2 \text{ frac PIF (OGIP}_2) = \frac{\text{Theoretical reservoir potential}}{\text{Water frac median EUR}} = \frac{7.1 \times 10^{10}}{4.35 \times 10^9} = 16.3 \quad \text{Eq. S41}$$

Since both density estimates offer equally reasonable projections of CO₂ performance based on OGIP, the average of these two factors (14.4) is taken as the maximum theoretical CO₂ performance benefit. Applying capillary availability to EUR defines a more conservative and likely median for this distribution through the following theoretical constructs:

(2) Available capillary reduction factor. Capillarity is essentially an additional pressure drop in the production system, increasing the formation pressure required to economically (or physically) produce the gas. From Young-Laplace the capillary pressure may be calculated and plotted as a function of pore size to illustrate the significant potential for increased gas production with CO₂ as a frac fluid.^[32] Note that pore size distribution in a given formation is a spatial variable that is difficult to define, but additional research and field data are improving our ability to predict formation capacity based on these distributions.

As in the first approach (EUR), we assume a water frac production factor of 25%, with the remaining 75% of gas trapped by a combination of three mechanisms: (a) in capillary pores blocked by water, (b) sorbed on surfaces (40-50% of total gas in place),^[31] or (c) contained in inaccessible pores. Assuming these inaccessible pores account for 10% of OGIP in shale coupled with the slickwater recovery factor of 25% OGIP,^[31] 65% of OGIP remains sorbed or trapped in water-blocked pores. CO₂ potentially alters these mechanisms, effecting greater CH₄ gas transfer for production. As the Marcellus is significantly undersaturated with respect to water, we assume a water-based fracturing fluid itself supplies the primary water source for capillary blocking.^[45] Recognizing that CO₂ is not guaranteed to recover all of the gas blocked by a water frac system, particularly in areas with higher resident brine saturations, a CO₂-based fluid is conservatively assumed to overcome 75% of the water blocking induced by a water frac. Similarly, we assume CO₂ preferentially sorbed to organic surfaces releases 75% of the adsorbed gas that remains after a water frac. Linking these paradigms, a new CO₂ recovery factor can be calculated by considering that of the 65% of OGIP remaining after a slickwater frac, 75% of the accessible gas in both capillaries and sorbed surfaces can recovered with CO₂:

$$\text{CO}_2 \text{ frac recovery factor} = (\% \text{H}_2\text{O recovery factor}) + (\% \text{Released by CO}_2 \text{ sorption}) \\ (\% \text{sorbed remaining}) + (\% \text{Released by CO}_2 \text{ pores}) (\% \text{water blocked remaining}) \quad \text{Eq.S42}$$

Where %Released by CO₂, sorption = %Released by CO₂, pores = 75%, and total %OGIP remaining due to sorption and water blocking = 65%, reducing the above equation to:

$$\text{CO}_2 \text{ frac recovery factor} = 0.25 + (0.75)(0.65) = \mathbf{0.74} \quad \text{Eq. S43}$$

Comparing this fraction of OGIP recovered to that of a slickwater system, the corresponding production increase factor is:

$$\text{CO}_2 \text{ frac PIF (capillary reduction)} = \frac{\text{CO}_2 \text{ frac recovery factor}}{\text{Water frac recovery factor}} = \frac{0.74}{0.25} = \mathbf{3.0} \quad \text{Eq. S44}$$

This factor (a 200% EUR improvement over a water-based frac) is taken as the “likely” value of the production increase distribution for the outlook case. Finally, we take the median production increase value from the base case (50%) as the lower limit of the distribution. This conservative estimate serves to tie the distribution to available data in light of the theoretical nature of the constructs developed here and serves as a defensible floor for future CO₂ performance benefits.

8. Results

The output distributions from Crystal Ball for each forecast (i.e. energy use, GHG emissions, and consumptive water use for all three scenarios) are provided in Figure S7.

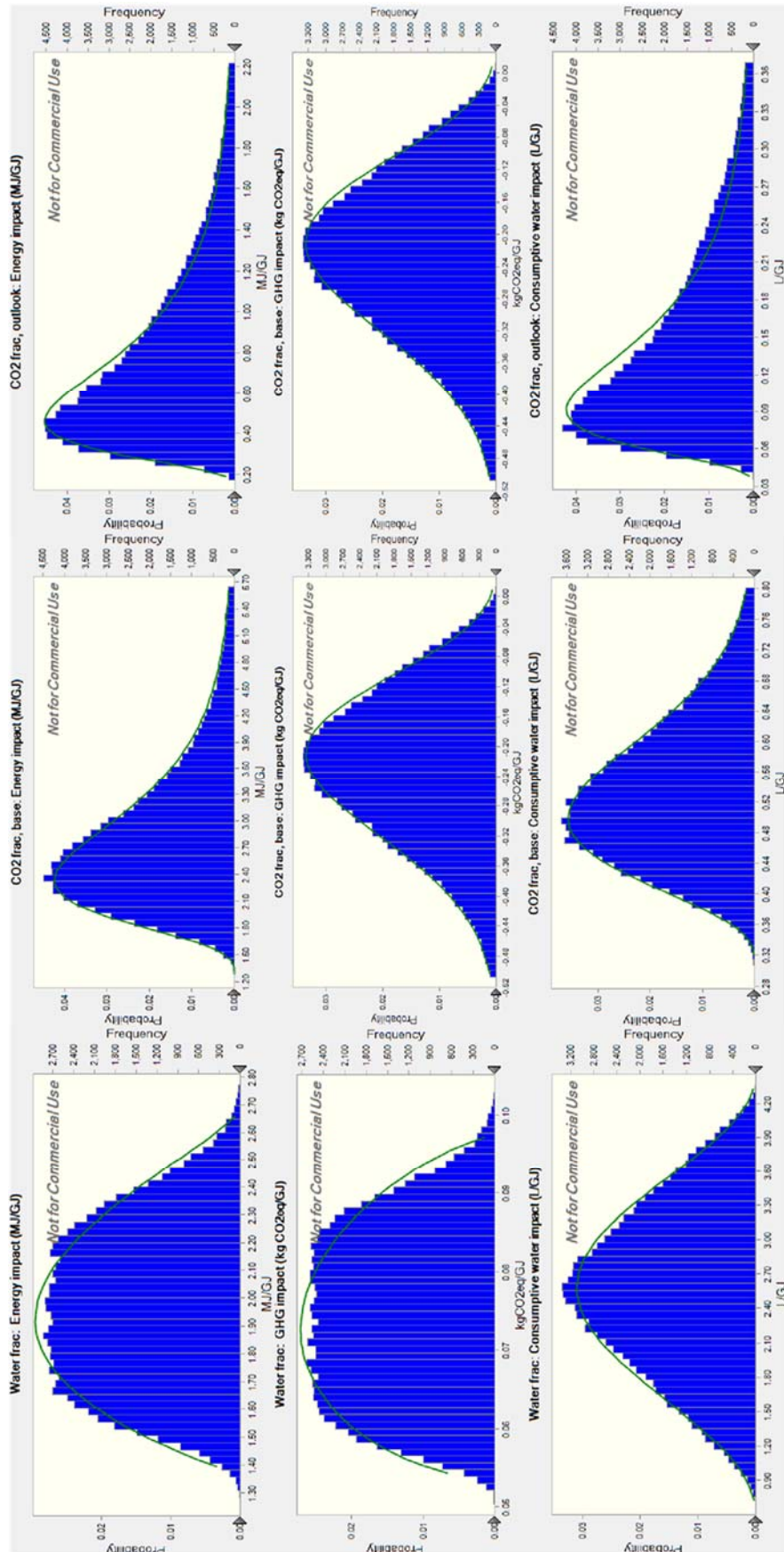


Figure S7. Output distributions from Crystal Ball for each forecast and scenario.

9. Sensitivity Analysis

Tornado plots showing the absolute sensitivity of output parameters to input parameters ranging between the 10th and 90th percentiles of the input distributions are included below in Figure S8. The water frac scenario results are similar to those obtained in the +/-10% relative sensitivity analysis used in the paper. But the high degree of uncertainty in many CO₂ frac inputs, particularly those with a high ratio of standard deviation to the mean, shifts the sensitivity from fluid volumes to electricity and PIF for all impacts. Whereas fluid volume requirements will be driven by reservoir conditions somewhat irrespective of fluid choice, this analysis indicates a need to refine PIF and recognize the impact of energy consumption by CO₂ capture and compression processes.

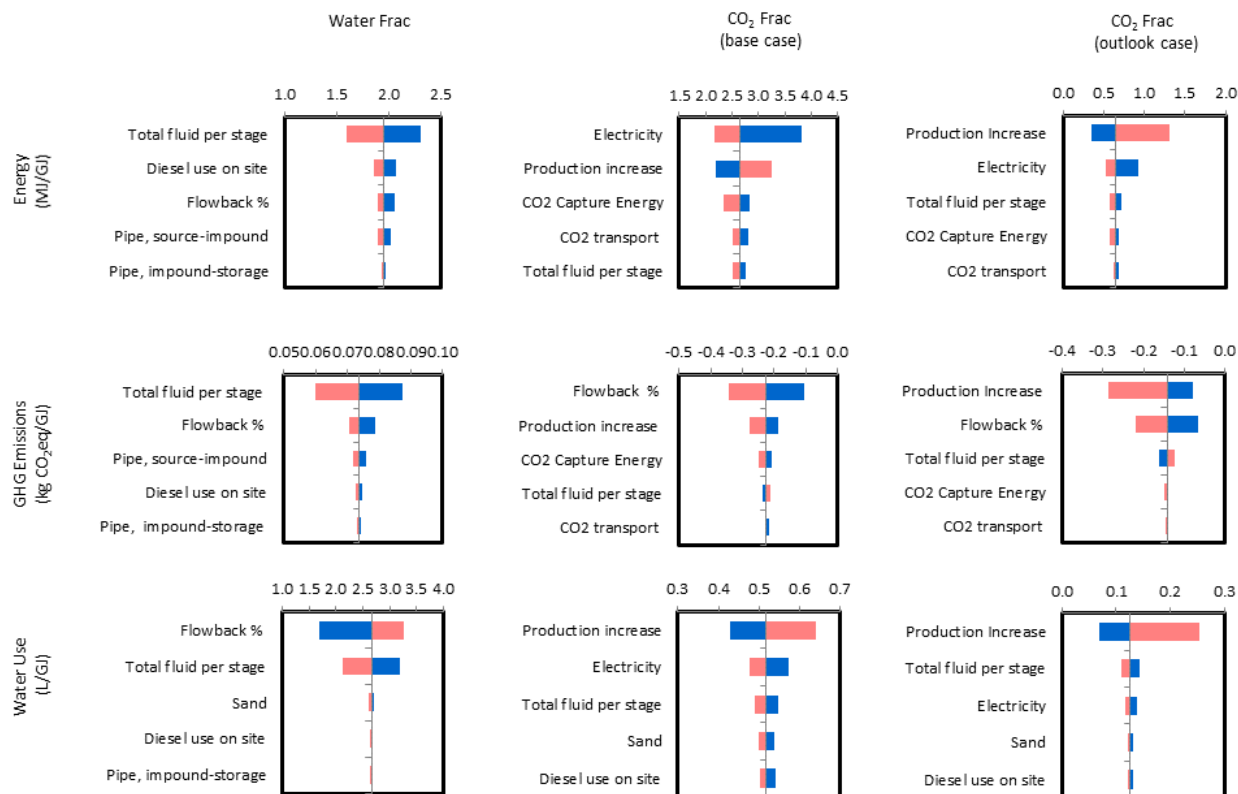


Figure S8. Sensitivity Analysis Tornado Plots

References

1. Oracle. Oracle Crystal Ball. Redwood Shores, CA, 2008.
2. U.S. DOE. *Annual Energy Outlook*; Energy Information Administration, 2015.
3. IPCC. *Global warming potentials*; Intergovernmental Panel on Climate Change, 2007.
4. Jiang, M.; Hendrickson, C.T.; VanBriesen, J.M. Life cycle water consumption and wastewater generation impacts of a Marcellus shale gas well. *Environ. Sci. Technol.* **2014**, *48*(3), 1911-1920.
5. Laurenzi, I.J.; Jersey, G.R. Life cycle greenhouse gas emissions and freshwater consumption of Marcellus shale gas. *Environ. Sci. Technol.* **2013**, *47*, 4896-4903.
6. U.S. EPA. *Direct emissions from mobile combustion sources*; U.S. Environmental Protection Agency: Washington, DC, 2008.
7. Arthur, J.D.; Bohm, B.; Coughlin, B.J.; Layne, M. Evaluating the environmental implications of hydraulic fracturing in shale gas reservoirs. Proceedings of the SPE Americas E&P Environmental and Safety Conference, San Antonio, TX, USA, Mar 23-25 2009.
8. N.Y. DEC. *Final supplemental generic environmental impact statement on the oil, gas and solution mining regulatory program*; New York Department of Environmental Conservation: Albany, NY, 2015.
9. King, G. Hydraulic fracturing 101: What every representative, environmentalist, regulator, reporter, investor, university researcher, neighbor, and engineer should know about estimating frac risk and improving frac performance in unconventional gas and oil wells. Proceedings of the SPE Hydraulic Fracturing Technology Conference, The Woodlands, Texas, USA., Feb 6-8 2012.
10. Swindell, G. Marcellus shale in Pennsylvania: A 2,600 well study of estimated ultimate recovery (EUR) - 2015 update. Gary S. Swindell Petroleum Engineering, 2015.
11. Middleton, R.S.; Clarens, A.F.; Liu, X.; Bielicki, J.M.; Levine, J.S. CO₂ deserts: Implications of existing CO₂ supply limitations for carbon management. *Environ. Sci. Technol.* **2014**, *48*, 11713-11720.
12. Northern Pipe Products. *AWWA C-900/C-905 Water Distribution Pipe*; Northern Pipe Products, Fargo, ND, 2015.
13. PA DEP. *Design and construction standards for centralized impoundment dams*; Pennsylvania Department of Environmental Protection, 2013.
14. US EPA. Technical development document for proposed effluent limitations guidelines and standards for oil and gas extraction. U.S. Environmental Protection Agency: Washington, DC, 2015.
15. Clark, C.E.; Han, J.; Burnham, A.; Dunn, J.B.; Wang, M. *Life-cycle analysis of shale gas and natural gas*; ANL/ESD/11-11; Argonne National Laboratory: Argonne, IL, 2011.
16. Dale, A.T.; Khanna, V.; Vidic, R.D.; Bilec, M.M. Process based life-cycle assessment of natural gas from the Marcellus shale. *Environ. Sci. Technol.* **2013**, *47*, 5459-5466.

17. Gilmore, K.R.; Hupp, R.L.; Glathar, J. Transport of hydraulic fracturing water and wastes in the Susquehanna River Basin, Pennsylvania. *J. Environ. Eng.* **2014**, *140*, Special issue: Environmental Impacts of Shale Gas Development, B4013002.
18. Mauter, M.S.; Palmer, V.R. Expert elicitation of trends in Marcellus oil and gas wastewater management. *J. Environ. Eng.* *140*, Special issue: Environmental Impacts of Shale Gas Development, B4014004.
19. Praxair. *Economical, efficient, effective: Using carbon dioxide for well fracturing*; Praxair, Inc: Danbury, CT, 2013.
20. McCollum, D.L.; Ogden, J.M. *Techno-economic models for carbon dioxide compression, transport, and storage & Correlations for estimating carbon dioxide density and viscosity*. Institute of Transportation Studies, University of California, Davis: Davis, CA, 2006.
21. NIST. Thermophysical properties of fluid systems. US Department of Commerce, National Institute of Standards and Technology, 2011.
22. Weidema, B.P. Ecoinvent data v.2.2. www.ecoinvent.org
23. Sonnad, J.; Goudar, C. Turbulent flow friction factor calculation using a mathematical alternative to the Colebrook-White equation. *J. Hydraul. Eng.* **2006**, *132*(8), 863-867.
24. King, C.W.; Webber, M.E. The water intensity of transportation. *Environ. Sci. Technol.* **2008**, *42* (21), 7866-7872.
25. US EPA. Stationary internal combustion sources. In *AP 42, Fifth Edition*; US Environmental Protection Agency: Washington, DC, 1996.
26. WV WRI. *Project overview: Water and waste stream study & Pits and impoundments study*. West Virginia Water Research Institute, 2013, Morgantown, WV.
27. ESRI. *ArcGIS 10.2*. Environmental Systems Research Institute: Redlands, CA, 2013.
28. Tao, Z.; Clarens, A. Estimating the carbon sequestration capacity of shale formations using methane production rates. *Environ. Sci. Technol.* **2013**, *47*, 11318-11325.
29. ANL. *GREET Model*. Argonne National Laboratory, Argonne, IL, 2014.
30. NETL. *NETL life cycle inventory data- Marcellus shale water treatment*. U.S. Department of Energy, National Energy Technology Laboratory, 2011.
31. Cipolla, C.L.; Lolan, E.P.; Erdle, J.C.; Rubin, B. Reservoir modeling in shale-gas reservoirs. *SPE Reserv. Eval. Eng.* **2010**.
32. Kang, S.M.; Fathi, E.; Ambrose, R.J.; Akkutlu, I.Y.; Sigal, R.F. Carbon dioxide storage capacity of organic-rich shales. *SPE Journal*, **2011**.
33. Reynolds, M.M.; Ku, R.Y.S; Vertz, J.B.; Stashko, Z.D. First field application in Canada of carbon dioxide separation for hydraulic fracture flow back operations. Proceedings of the SPE Unconventional Resources Conference Canada, Calgary, Alberta, Canada, Nov 5-7 2013.
34. Burke, L.H.; Nevison, G.W. Improved hydraulic fracture performance with energized fluids: A Montney example. Proceedings of the CSPG/CSEWG/CWLS GeoConvention, Calgary, Alberta, Canada, May 9-11 2011.
35. Mazza, R.L. *Production verification tests: Final report- Phase I*; DE-AC21-90MC26025; U.S. Department of Energy, National Energy Technology Laboratory: Canton, OH, 2003.

36. Lillies, A.T.; King, S.R. Sand fracturing with liquid carbon dioxide. Proceedings of the Production Technology Symposium, Hobbs, NM, USA, Nov 8-9 1982.
37. Ribeiro, L.H.; Sharma, M.M. Fluid selection for energized fracture treatments. Proceedings of the SPE Hydraulic Fracturing Technology Conference, The Woodlands, TX, USA., Feb 4-6 2013.
38. Frieauf, K.E.; Sharma, M.M. Application of a new compositional model for hydraulic fracturing with energized fluids: A south Texas case study. Proceedings of the SPE Hydraulic Fracturing Technology Conference, The Woodlands, TX, USA, Jan 19-21 2009.
39. The Linde Group. *Energized solutions: The EOR & IOR (E-I-OR) of energized fluids for hydraulic fracturing*; Linde North America, Inc.: Murray Hill, NJ, 2015.
40. Mazza, R.L. *Production verification tests: Final report- Phase II*; DE-AC21-90MC26025; U.S. Department of Energy, National Energy Technology Laboratory: Canton, OH, 2003.
41. Mazza, R.L. *Field testing & optimization of CO₂/sand fracturing technology*; DE-AC21-94MC31199; U.S. Department of Energy, National Energy Technology Laboratory: Canton, OH, 2004.
42. Staub, J. The growth of U.S. natural gas: An uncertain outlook for U.S. and world supply. Presented at the 2015 EIA energy conference, Washington, D.C., USA, Jun 15 2015.
43. EIA. (2015). US Energy Information Administration. Updated geologic maps provide greater detail for Marcellus formation.
44. Soeder, D.J. Porosity and permeability of eastern Devonian gas shale. *SPE Formation Eval.* **1988**.
45. Engelder, T. Capillary tension and imbibition sequester frack fluid in Marcellus shale gas. *Proc. Natl. Acad. Sci. USA.* **2012**, *109*(52), E3625.